DISSERTATIONES GEOPHYSICALES UNIVERSITATIS TARTUENSIS
22

DISSERTATIONES GEOPHYSICALES UNIVERSITATIS TARTUENSIS
22

OBSERVATIONS OF OZONE, POLAR STRATOSPHERIC CLOUD AND WATER VAPOUR PROFILES IN THE ARCTIC

RIGEL KIVI

TARTU UNIVERSITY
PRESS

This study was carried out at the Arctic Research Centre of the Finnish Meteorological Institute and at the Institute of Environmental Physics, University of Tartu.

The dissertation was admitted on April 4, 2007, in partial fulfillment of the requirements for the degree of Doctor of Philosophy in physics (environmental physics), and allowed for defence by the Council of the Department of Physics, University of Tartu.

Supervisors: Prof. Esko Kyrö, Arctic Research Centre, Finnish Meteorological Institute, Finland

Dr. Kalju Eerme, Tartu Observatory, Tõravere, Estonia

Opponents: Dr. Piia Post, Institute of Environmental Physics, University of Tartu

Dr. Antti Arola, FMI Kuopio, Finland

Defence: May 29, 2007, at the University of Tartu, Estonia

ISSN 1406–0310
ISBN 978–9949–11–581–5 (trükis)
ISBN 978–9949–11–582–2 (PDF)

Tartu Ülikooli Kirjastus
www.tyk.ee
Tellimus nr. 135

CONTENTS

1. LIST OF ORIGINAL PUBLICATIONS

1. Kivi, R., E. Kyrö, A. Dörnbrack, T. Birner (2001), Observations of vertically thick polar stratospheric clouds and record low temperature in the Arctic vortex, *Geophys. Res. Lett*., 28(19), 3661–3664, 10.1029/2001GL013187.
2. Kivi, R., E. Kyrö, T. Turunen, T. Ulich, and E. Turunen (1999), Atmospheric trends above Finland. Part II. Troposphere and stratosphere, *Geophysica*, 35, p. 71–85.
3. Kivi, R., E. Kyrö, T. Turunen, N. R. P Harris, P. von der Gathen, M. Rex, S. B. Andersen, and I. Wohltmann (2007), Ozonesonde observations in the Arctic during 1989–2003: Ozone variability and trends in the lower stratosphere and free troposphere, *J. Geophys. Res*., 112, D08306, doi:10.1029/2006JD007271.
4. Kyrö, E., R. Kivi, T. Turunen, H. Aulamo, V. V. Rudakov, V. Khattatov, A. R. MacKenzie, M. P. Chipperfield, A. M. Lee, L. Stefanutti, F. Ravegnani (2000), Ozone measurements during the Airborne Polar Experiment: Aircraft instrument validation, isentropic trends, and hemispheric fields prior to the 1997 Arctic ozone depletion, *J. Geophys. Res*., 105(D11), 14599–14612, 10.1029/2000JD900038.
5. Dörnbrack, A., M. Leutbecher, R. Kivi, and E. Kyrö (1999), Mountain wave induced record low stratospheric temperatures above Northern Scandinavia, *Tellus*, 51A, p. 951–963.
6. Vömel, H., M. Rummukainen, R. Kivi, J. Karhu, T. Turunen, E. Kyrö, J. Rosen, N. Kjome and S. Oltmans (1997), Dehydration and sedimentation of ice particles in the Arctic stratospheric vortex, *Geophys. Res. Lett*., 24, 795–798.
7. Rummukainen, M., Laurila, T. and Kivi, R. (1996), Yearly Cycle of Lower Tropospheric Ozone North of the Arctic Circle, *Atm. Env*., vol 30, 1875–1885.
8. Kivi, R., E. Kyrö, L. Rontu, A. Dörnbrack, M. Müller, C. Wedekind, H.Wille, B. Stein, V. Rizi, G. Redaelli, V. Mitev, R. Matthey, J. Rosen, L.Stefanutti, and M. Del Guasta (1999), On occurrence of type II PSCs over Northern Finland as observed by Lidar and balloon-borne sondes. In: Mesoscale processes in the stratosphere, Brussels, Belgium, 143–147.
9. Kivi, R., E. Kyrö, A. Dörnbrack, and T. Birner (2003), Polar stratospheric cloud observations in northern Finland during the recent winters, In: Proc. Sixth European Symposium on Stratospheric Ozone, (N. R. P. Harris, G. T. Amanatidis, J. G. Levine, editors), p. 245–249.
10. Stein, B., C. Wedekind, H. Wille, F. Immler, M. Müller, L. Wöste, M. del Guasta, M. Morandi, L. Stefanutti, A. Antonelli, P. Agostini, V. Rizi, G. Readelli, V. Mitev, R. Matthey, R. Kivi, E. Kyrö (1999), Optical classification, existence temperatures, and coexistence of different polar strato-

spheric cloud types, *J. Geophys. Res.,* 104(D19), 23983–23994, 10.1029/1999JD900064.
11. Deuber B., A. Haefele, D. G. Feist, L. Martin, N. Kämpfer, G. E. Nedoluha, V. Yushkov, S. Khaykin, R. Kivi, H. Vömel (2005), Middle Atmospheric Water Vapour Radiometer (MIAWARA): Validation and first results of the LAPBIAT Upper Tropospheric Lower Stratospheric Water Vapour Validation Project (LAUTLOS-WAVVAP) campaign, *J. Geophys. Res.,* 110, D13306, doi:10.1029/2004JD005543.
12. Kivi, R., A. Dörnbrack, E. Kyrö, V. Mitev, V. Rizi, and M. Müller (2000), Ice PSCs above northern Finland: Observations and mesoscale meteorological model simulations, Proc. of the Quadrennial Ozone Symposium, Hokkaido University, Sapporo, 481–482.
13. Kivi, R., E. Kyrö, A. Dörnbrack, M. Müller, H. Wille, B. Stein, V. Mitev, R. Matthey, L. Stefanutti, M. Del Guasta, and V. Rizi (2000), Observations of stratospheric temperatures, ozone and aerosols above northern Finland in the winter of 1998/99, Proceedings 5th European Workshop on Stratospheric Ozone (N. R. P. Harris, M. Guirlet and G. T. Amanatidis, editors), 169–172.
14. Kivi, R., E. Kyrö, and T. Turunen (1999), Long-term meteorological monitoring activities at Sodankylä and trends of the recent decade, In: Proceedings of Annual Conf. of Geophys. Soc. of Finland, 95–100.
15. Kivi, R., E. Kyrö, and T. Turunen (2004), Stratospheric ozone observations at Sodankylä during 1989–2003, in Ozone, Volume 1, Proc. of the Quadrennial Ozone Symposium, Edited by Chr. Zerefos, University of Athens, Greece, 377–378.
16. Kivi, R., Kyrö, E., Dörnbrack, A. (2004), Observations of polar stratospheric clouds at Sodankylä, Finland, in Ozone, Volume 2, Proc. of the Quadrennial Ozone Symposium, Edited by Chr. Zerefos, University of Athens, Greece, 982–983.
17. Kivi, R., E. Kyro, A. R. MacKenzie, V. V. Rudakov, V. V. Khattatov, M. P. Chipperfield, A. M. Lee, G. O. Braathen, H. Gernandt, I. S. Mikkelsen, and M. Molyneux (1998), APE/POLECAT transport studies: ozonesondes during APE, Proc. 4th Europ. Workshop on Polar Strat.Ozone, 201–204.
18. Kivi, R., E. Kyrö, C. Wedekind, L. Rontu, A. Dörnbrack, B. Stein, H.Wille, V. Mitev, R. Matthey, J. Rosen, N. Kjome, V. Rizi, G. Redaelli, B. Lazzarotto, B. Calpini, M. Del Guasta, M. Morandi, L. Stefanutti, P. Agostini, A. Antonelli, M. Rummukainen, T. Turunen, J. Karhu (1998), SAONAS activities at Sodankylä in winter 1996/1997. Proc. 4th Europ. Workshop on Polar Strat.Ozone, 135–138.
19. Rosen, J. M., N. T. Kjome, N. Larsen, B. M. Knudsen, E. Kyrö, R. Kivi, J. Karhu, R. Neuber, I. Beninga (1997), Polar stratospheric cloud threshold temperatures in the 1995–1996 arctic vortex, *J. Geophys. Res.,* 102(D23), 28195–28202, 10.1029/97JD02701.

20. Rao T. N., S. Kirkwood, J. Arvelius, P. von der Gathen, R. Kivi (2003), Climatology of UTLS ozone and the ratio of ozone and potential vorticity over northern Europe, *J. Geophys. Res.,* 108 (D22), 4703, doi:10.1029/ 2003JD003860.
21. Christensen, T., Knudsen, B., Streibel, M., Andersen, S., Benesova, A., Braathen, G., Claude, H., Davies, J., De Backer, H., Dier, H., Dorokhov, V., Gerding, M., Gil, M., Henchoz, B., Kelder, H., Kivi, R., Kyro, E., Litynska, Z., Moore, D., Peters, G., Skrivankova, P., Stubi, R., Turunen, T., Vaughan, G., Viatte, P., Vik, A., Gathen, P. and Zaitcev, I (2005)., Vortex-averaged Arctic ozone depletion in the winter 2002/2003, *Atmospheric Chemistry and Physics*, Vol. 5, 131–138.
22. Müller, M., R. Neuber, G. Beyerle, E. Kyrö, R. Kivi, L. Wöste (2001), Non-uniform PSC occurrence within the Arctic polar vortex, *Geophys. Res. Lett.,* 28(22), 4175–4178, 10.1029/2001GL013799.
23. Larsen, N., Knudsen, B., Svendsen, S., Deshler, T., Rosen, J., Kivi, R., Weisser, C., Schreiner, J., Mauerberger, K., Cairo, F., Ovarlez, J., Oelhaf, H. and Spang, R. (2004), Formation of solid particles in synoptic-scale Arctic PSCs in early winter 2002/2003, *Atmospheric Chemistry and Physics*, Vol. 4, 2001–2013.
24. Suortti, T., J. Karhu, R. Kivi, E. Kyrö, J. Rosen, N. Kjome, N. Larsen, R. Neuber, V. Khattatov, V. Rudakov, V. Yushkov, H. Nakane (2001), Evolution of the Arctic stratospheric aerosol mixing ratio measured with balloon-borne aerosol backscatter sondes for years 1988–2000, *J. Geophys. Res*., 106(D18), 20759–20766, 10.1029/2000JD000180.
25. Del Guasta, M., Morandi, M., Stefanutti, L., Balestri, S., Kyrö, E., Rummukainen, M., Kivi, R., Rizi, V., Masci, F., Stein, B., Wedekind, C., Mielke, B., Immler, F., Matthey, R., Mitev, V. and Douard, M., 1998. Lidar Observation of Spherical particles in a 65 deg cirrus observed above Sodankylä, *J. Aerosol Science*, Vol. 29, No. 3, 357–374.
26. Høiskar, B., Dahlback, A., Vaughan, G., Braathen, G., Goutail, F., Pommereau, J.-P., Kivi, R. (1997), Interpretation of ozone measurements by ground-based visible spectroscopy — a study of the seasonal dependence of airmass factors for ozone based on climatology data, *J. Quant. Spectrosc. Radiat. Transfer*, 57, p. 569–579.
27. Vömel, H., H. Selkirk, L. Miloshevich, J. Valverde-Canossa, J. Valdés, E. Kyrö, R. Kivi, W. Stolz, G. Peng, J. A. Diaz (2007), Radiation Dry Bias of the Vaisala RS92 Humidity Sensor, *J. Atmos. Oceanic Technol*., in press.
28. Vömel, H., V. Yushkov, S. Khaykin, L. Korshunov, E. Kyo, R. Kivi (2007), Intercomparisons of stratospheric water vapour sensors: FLASH-B and NOAA/CMDL frost point hygrometer, *J. Atmos. Oceanic Technol*., in press.

2. MAIN ARGUMENTS PROPOSED TO BE DEFENDED

1. The long-term and interannual variability of Arctic ozone profiles is explained based on the most recent understanding of processes influencing ozone variability. It is found that in the stratosphere ozone amounts correlate highly with proxies for the stratospheric circulation (100 hPa eddy heat flux averaged over 45–70º N), polar ozone depletion (the calculated volume of polar stratospheric clouds combined with the effective equivalent stratospheric chlorine) and with tropopause height. At altitudes between 50 and 70 hPa, chemical polar ozone depletion accounted for up to 50% of the March ozone variability. Negative trends in the lower stratosphere prior to 1997 can be attributed to the combined effect of dynamical changes (changes in large-scale transport of ozone and synoptic-scale meteorological processes affecting the ozone distribution through horizontal advection and the vertical displacement of the isentropes), impact of aerosols from the Mt. Pinatubo eruption and to winters of relatively large chemical ozone depletion. Since 1996–1997 the observed increase in lower stratospheric ozone can be attributed primarily to changes in synoptic-scale dynamical processes and the stratospheric circulation. In the free troposphere, a statistically significant increase of $11.3 \pm 1.8\%$ over 15 years is observed which also maximizes in the January-April period ($16.0 \pm 3.1\%$ over 15 years). Modelling suggests that this could be related to the effects of changes in the Arctic Oscillation.
2. Assessment of the electrochemical concentration cell (ECC) ozonesondes was performed, motivated by the need to homogenize the ozonesonde measurements. According to intercomparison measurements, the ozonesonde data agree with the near-simultaneous lidar data within 0–5% in the altitude range of 15–30 km and within 5–10% above an altitude of 30 km. The agreement with total column measurements by a Brewer ground-based spectrophotometer is within 2–3%. The average Brewer/sonde ratio was 1.004 ± 0.01, the respective ratio from the AURA satellite-borne Ozone Monitoring Instrument (OMI) measurements (OMI/sonde) being on average 0.989 ± 0.017. This close agreement with the reference instruments suggests that the new sonde systems may not require normalization. In addition to these measurements, a comparison between stratospheric aircraft-borne electrochemical sensors and the balloon-borne sensors was conducted. These comparisons, made in the Arctic stratospheric vortex, showed an average difference of $5.7 \pm 2.8\%$. Dual sonde flights of the EN-SCI and SPC types of ECC ozonesondes were made. These are the two ECC sonde types used in ozonesonde networks. The dual sonde flights suggest that in the stratosphere the relative differences between these sondes are less than

2%. For these flights the SPC type of sondes used a 1% potassium iodide (KI) sensing solution, while the EN-SCI sondes used a 0.5% KI sensing solution. The absolute differences in the troposphere are similar to those measured in the stratosphere. A series of ozonesonde test flights was performed during the years 2002–2006. These data were used to develop altitude-dependent corrections for the thermistor positioning and for the solution strength. The latter two corrections could be applied prior to the sonde profile normalization, which is based on total ozone measurements by other well-established instruments. It was found that the thermistor correction is of the order of 3% in the stratosphere above 150 hPa and between 1 and 3% below the 150 hPa level, decreasing linearly with decreasing altitude in the troposphere. As the average of a series of test flights, it was found that the use of a standard 1% KI sensing solution for both sonde types leads to a 2–8% positive bias between the EN-SCI and SPC ozonesondes, depending on the altitude region.

3. Series of observations of polar stratospheric clouds (PSCs) and corresponding observations of water vapour profiles in the Arctic lower stratosphere were performed during the winters of 1994/1995–2005/2006. These included unique observations of stratospheric ice clouds and near-simultaneous dehydration/rehydration processes in the Arctic lower stratosphere. Firstly, the measurements analyzed here contribute to our knowledge of PSC optical properties and formation processes, and secondly they provide valuable information on the actual water vapour distribution within the polar stratospheric vortex and in the vicinity of the vortex in the lower stratosphere, as well as contributing to an understanding of the processes affecting the fine-scale distribution of water vapour. The ice PSC measurements that were studied here in detail are among the very rare documented formation events of such clouds in the Arctic vortex, in contrast to the Antarctic stratospheric vortex. It has therefore been a scientific challenge to analyze and understand the meteorological conditions that favor local cooling in the stratosphere and the subsequent formation of water ice polar stratospheric clouds. It has been found that the Scandinavian mountains and even the orography of Greenland can cause local cooling that leads to PSC formation far downstream of the mountains, as detected by the aerosol backscatter sondes and lidar measurements over northern Finland. This work also includes technological challenges, because conventional sounding techniques are unable to measure the very low concentrations of water vapour found in the stratosphere. Water vapour has a strong impact on the Earth's climate system; it is therefore of interest not only to use sonde techniques to understand the water vapour distribution and the processes underlying this, but also to involve the data in a longer-term study. Here mean water vapour profiles inside and outside the vortex are calculated for the winters of 2002/2003 to 2005/2006 on a monthly basis,

providing a first insight into the interannual variability, and showing clear differences between the average profiles inside and outside the vortex. According to these measurements the outside-vortex measurements display the water vapour mixing ratio values typically between 4–5 ppmv in the lower stratosphere, while the inside vortex water vapour mixing ratio is between 5 and 7 ppmv. An important question is whether or not stratospheric water vapour is increasing, as is seen in mid-latitude measurements. If such trend also exists in the polar stratosphere, it would mean further cooling of the lower stratosphere and a larger potential for the formation of polar stratospheric clouds. All this would lead to a delay in the recovery of the polar stratospheric ozone. The first years of the sonde observations in the Arctic therefore comprise important material for future trend studies.

3. INTRODUCTION

Stratospheric ozone depletion has been one of the major areas of atmospheric research since the discovery of the Antarctic ozone hole [*Farman et al*., 1985]. Since then, several field campaigns have been performed both in the Antarctic and Arctic (see *World Meteorological Organization* [1994, 1999, 2003, 2007] and the numerous references therein for an overview of the scientific progress). In addition to the field campaigns, new stations with regular ozone programs were established in the European and Canadian sectors of the Arctic during the late 1980s. This thesis work is mainly based on observations made at Sodankylä, Finland (67.4° N, 26.6° E). The ozonesonde data from this station comprise one of the two longest continuous ozonesonde data series from the European sector of the Arctic [*Kivi et al*., 1999a]. Stratospheric in situ aerosol measurements at Sodankylä started in the year 1994 [*Kivi et al.,* 2001] and stratospheric water vapour profile measurements in 1996 using light-weight balloon-borne sensors [*Vömel et al*., 1997; *Kivi et al.,* 2007b]. The author has been personally involved in the measurements of stratospheric aerosols and water vapour at Sodankylä since the beginning of these measurements there. In recent years the focus has been on the assessment of ozonesonde performance and the analysis of long-term ozone measurements in order to evaluate the effects of the Montreal Protocol on the changes in the ozone layer. This work has been done in the framework of the EC-funded Chemical and Dynamical Influences on Decadal Ozone Change (CANDIDOZ) project, and was recently completed [*Kivi et al*., 2007a]. In addition to the data from Sodankylä, all available long-term ozonesonde datasets from the Arctic have been included in the study of ozone profile changes.

Long-term changes in ozone profiles are primarily important to the Earth's UV shield, but they are of considerable climatic interest, too. The latter is because ozone is also a greenhouse gas whose radiative forcing is dependent on its vertical distribution. A decrease in stratospheric ozone leads to cooling tendency, while an increase in tropospheric ozone leads to net positive radiative forcing [*Houghton et al.,* 2003]. Tropospheric ozone also indirectly affects the climate change depending on the concentrations of nitrogen oxides, as it controls the oxidation capacity of the troposphere. Despite its importance, there are only a few regular measurement programs of ozone profiles in northern high latitudes that have sufficient length and measurement frequency for long-term data studies [*Staehelin et al*., 2001].

Information about long-term changes in stratospheric and tropospheric ozone over northern high latitudes has been for the most part based on ozonesonde observations from northern Canada. *Logan et al.* [1999] reported a decrease of ozone over Resolute, Canada, between 1970 and 1996 at all profile levels during all seasons using statistical regression models that included the effects of changes in solar radiation and the quasi-biennial oscillation. A long-term ozone

decline over Resolute was also reported by *Fioletov et al.* [1997] and *Randel and Wu* [1999]. *Tarasick et al.* [1995] and *Oltmans et al.* [1998] found negative trends in tropospheric ozone over Canada from 1980 to 1993. A recent study by *Tarasick et al.* [2005] reports a change towards an increase of ozone at Canadian stations for the 1991–2001 time-period at levels below 63 hPa. The reported increase in stratospheric ozone since the mid 1990s should have influenced trends in the troposphere, because stratospheric ozone is an important source of tropospheric ozone in the Arctic [e.g., *Oltmans et al.,* 1981]. While a Northern hemispheric increase in tropospheric ozone has been reported based on data from mid-latitudes [*Vingarzan*, 2004], and Canadian high-latitude sites [*Tarasick et al.*, 2005], it is not known what changes have occurred in ozone profiles over larger regions in high northern latitudes, including Northern Europe and Greenland.

The ozonesonde stations in the European sector of the Arctic and Greenland were established in 1988/89 [*Kyrö et al.*, 1992] after the discovery of the Antarctic ozone hole [*Farman et al.*, 1985]. Of these new stations, Sodankylä (67.4º N) and Ny-Ålesund (78.9º N) have operated regularly since then, performing at least one ozone sounding per week, while Scoresbysund (70.5º N) and Lerwick (60.1º N) have data gaps in years the 1990–1992. At present, the length of the dataset from European and Greenland stations is over 15 years.

The first part of the thesis focuses on an analysis of the interannual variability and trends in Arctic ozonesonde profiles, using an ensemble dataset from seven sonde stations in Northern Europe, Greenland and Canada, located between 60º N and 82º N and having regular measurements from 1989 to 2003. The measurements and analysis presented here substantially increase the available information on recent trends in Arctic stratospheric and tropospheric ozone. Special emphasis is put on the data from winter/springtime-period, since this is the season of largest variability both on interannual and longer time-scales. The Arctic winter is also the period when sondes provide unique data, even in the lower stratosphere, as these measurements do not depend on solar light.

An important data quality issue with ozonesondes is related to the fact that each flight uses a different instrument. Both the sonde's manufactured quality and its preparation and operation can influence the consistency of the datasets. At Sodankylä, a series of sonde comparison flights was performed in order to investigate the effect of thermistor positioning in the ozone box and the significance of the concentration of the sensing solution for the two main electrochemical concentration cell (ECC) sonde types. The results allow the application of altitude-dependent corrections to the profile data, thus improving the consistency of the dataset without offsetting the profiles by using the standard correction factors for total ozone. It is important for long-term data records, but also for ozonesonde campaign networks, to minimize any deviations arising from different operational procedures at individual stations.

A detailed assessment of the newest ozonesondes using the most up-to-date ground equipment and radiosonde technology was performed in the spring of 2006, involving comparisons with ground-based lidar and five spectrophotometers. In addition, balloon sonde observations were compared to aircraft measurements in the winter of 1996/1997. The first-ever campaign involving the M55 Geophysica stratospheric aircraft for scientific use was conducted at Rovaniemi (Finland), and provided a unique opportunity to obtain high-resolution information on the ozone distribution in the vicinity of the Arctic stratospheric vortex. In this work the aircraft measurements are compared to the sonde measurements using the technique of mapping the observed ozone in potential vorticity/ potential temperature space.

The main motivation for the ozone analysis done within the thesis work (presented in Chapter 4) has been the need to quantify and to understand the long-term changes in the Arctic ozone profiles. In addition to the statistical analysis of the sonde data (Chapter 4.2), this part of the work (ozonesonde analysis) also includes a thorough assessment of ozonesonde data quality, leading to the homogenization of the ozonesonde data. For these reasons, instrumental intercomparisons done during the different field campaigns are discussed in detail. This involves dual and multiple sonde field tests performed over several years, as well as comparisons with other instruments available to the author: ground-based, aircraft-borne and space-born. Although all the instrument comparisons cannot be used for ozonesonde data homogenization, they are discussed here, because they provide additional information on sonde data quality. These results will be important for similar long-term data studies to be conducted in the future. The field tests of spring 2006 suggest that the new sonde systems may not require normalization, in contrast to the sondes used in the data analysis covering the time-period of 1989–2003.

In the second part of the thesis (Chapter 5), Arctic observations of stratospheric aerosols and water vapour are presented, based on the measurements made at Sodankylä from winters in the period 1994/1995 to 2005/2006. Stratospheric aerosols are directly related to the ozone depletion through heterogeneous reactions on the aerosol particles. Stratospheric humidity has an influence on the ozone depletion by affecting both the formation temperature of polar stratospheric clouds (PSCs) and the polar vortex temperatures themselves [*Kirk-Davidoff et al*., 1999]. Finally, all aspects of the work presented here are related to the climate change issue, as climate change is influenced by changes in ozone, aerosols and water vapour [*IPCC*, 2003].

The actual quantity of stratospheric water vapour in the Arctic is an important parameter not only for ozone chemistry, but also to infer the radiative budget and the resulting vertical motion inside the polar vortex. During the winters of 2002/2003–2005/2006, accurate measurements of stratospheric water vapour were performed at Sodankylä using in situ balloon-borne instruments. These measurements have contributed to a knowledge of the actual water

vapour distribution in the polar stratospheric vortex and in the vicinity of the vortex in the lower stratosphere, as well as to an understanding of the processes affecting the fine-scale distribution of water vapour.

This part of the thesis work (in Chapter 5) includes a description of the instrumentation used; a summary of the polar stratospheric cloud observations at Sodankylä; three detailed case studies on the occurrence of water ice polar stratospheric clouds in the Arctic; and finally a discussion on the long-term aspects of the PSC and water vapour observations.

The observations of water ice PSCs are of special interest, because ice PSC formation can cause a significant removal of water vapour from the stratosphere. At Sodankylä, ice PSCs as well as the Antarctic-like dehydration processes have been observed using in situ observational techniques. Furthermore, in the winter of 2004/2005, both dehydrated and rehydrated water vapour layers were observed in connection with ice PSC formation. In situ observational techniques are ideal for such case studies, because they provide profiles with a high vertical resolution. In addition, measurements of PSCs and lower stratospheric water vapour also have a climatological value, due to the lack of similar satellite-borne long-term observations. The thesis work also provides the first insight into the interannual variability of inside- and outside-vortex water vapour profiles in the Arctic.

4. OZONE IN THE LOWER STRATOSPHERE AND FREE TROPOSPHERE

4.1. Long-term and short-term ozone profile variability

Several chemical and dynamical factors have to be taken into account in order to explain long-term changes and interannual variability in polar ozone. In addition to the quasi-biennial oscillation (QBO) and solar cycle, whose influence is well established in statistical analyses of ozone [e.g., *WMO*, 2003], in this work a few additional phenomena are considered. Ozone builds up in the Arctic lower stratosphere during winter and early spring as a consequence of poleward and downward transport. Ozone transport is related to planetary wave activity. The stronger the wave activity, the more ozone is transported towards high latitudes. At the same time the adiabatic heating of air leads to higher stratospheric temperatures and thus a smaller potential for chemical ozone depletion [*Weber et al.*, 2003; *Andersen and Knudsen*, 2002]. Previous studies have used the vertical component of the Eliassen-Palm flux or eddy heat flux as a measure of ozone transport by the residual circulation [*Fusco and Salby*, 1999; *Randel et al.*, 2002; *Weber et al.*, 2003; *Ma et al.*, 2004; *Hadjinicolaou et al.*, 2002].

Ozone is destroyed by catalytic cycles during winter/spring and also in summer, although different cycles dominate during different seasons. In winter/spring, ozone depletion is caused primarily by the ClO dimer and ClO+BrO cycles. A pre-requisite for winter/spring ozone depletion is the formation of polar stratospheric clouds (PSCs) at temperatures below about 195K [*Solomon*, 1999; *WMO*, 2003]. *Rex et al.* [2004] reported high correlation between the mean volume of polar stratospheric clouds (VPSC) and mean end-of-winter column ozone depletion. However, because the results in *Rex et al.* [2004] were derived under conditions of near-constant stratospheric halogen loading, and because changes in equivalent effective stratospheric chlorine (EESC) also modulate polar ozone depletion, VPSC * EESC is used here as a proxy for heterogeneous ozone depletion.

Another parameter to consider in the context of chemical changes is the background aerosol. In the Arctic, background aerosol concentrations were significantly increased 2–3 years after the volcanic eruption of Mt. Pinatubo in 1991 [e.g., *Suortti et al*., 2001]. This led to an increase in ozone depletion due to heterogeneous reactions [*Solomon*, 1999], and influenced stratospheric transport and dynamics [*Solomon et al.*, 1996].

The vertical distribution of ozone is also influenced by changes in the horizontal transport and convergence/divergence of the air. Tropopause pressure or altitude can be used as a proxy for these dynamical processes [e.g., *Bodeker et al.,* 1998; *Weiss et al.*, 2001]. In an earlier study, the tropopause effect has been discussed by *Dobson and Harrison* [1926] in the context of daily variations of total ozone.

Hoinka et al. [1996] and *Steinbrecht et al.* [1998] used tropopause pressure and height to explain changes in monthly and seasonal ozone observed over Germany. *Bodeker et al.* [1998] found that ozone trends at Lauder, New Zealand, showed a significant dependence on tropopause height changes. *Weiss et al.* [2001] applied tropopause pressure in the regression model to explain trends observed over Switzerland. *Wohltmann et al.* [*2005*] introduced the integrated equivalent latitude proxy (EL), which is able to simulate short-term variability related to vertical displacement of isentropes and horizontal isentropic advection in the lower stratosphere. Compared to the earlier proxies, EL models physical process more directly. Some studies have also pointed out the correlation between the Arctic Oscillation (AO) or North Atlantic Oscillation (NAO) and total ozone [*Appenzeller et al.*, 2000; *Weiss et al.*, 2001; *Thompson and Wallace*, 1998]. These climate variables are defined via wintertime sea surface pressure measurements [*Thompson and Wallace*, 1998] and mainly influence ozone dynamically.

Ozone in the free troposphere is controlled by vertical exchange with the stratosphere, vertical mixing in troposphere, long-range transport within the troposphere and in situ chemical processing. *Simmonds et al.* [2004], *Vingarzan* [2004] and *Tarasick et al.* [2005] have reported an increase in tropospheric ozone in northern latitudes. The cause of tropospheric ozone changes has been attributed to changes in downward transport of stratospheric ozone, [*Oltmans*, 1981; *Logan*, 1985], in situ ozone production from methane [*Fusco and Logan*, 2003] and reactions of volatile organic compounds (VOC) with natural NO_x [*Dibb et al.*, 2003], as well as long-range transport of ozone from distant pollutant sources [*Marenco et al.*, 1994; *Wang et al.*, 1998; *Vingarzan*, 2004]. Recently *Lamarque and Hess* [2004] reported that the Arctic Oscillation index correlates with both modelled and observed tropospheric ozone over Northern America and Central Europe.

Ozonesondes are usually flown 1–2 times per week. However, an example of daily ozonesonde launches from March 22–April 14, 2006 at Sodankylä is presented in Figure 1. A large amount of day-to-day variability is evident, especially during the first half of the measurement series. The observed variability is linked to dynamical variability in the troposphere and stratosphere. In the troposphere, high pressure system events over northern Finland were interrupted several times, as indicated by the changes in ozone concentration at altitudes of 4–10 km and fluctuations in the dynamical tropopause. In Figure 1 the dynamical definition of the tropopause is based on a value of 2 potential vorticity units (1 PVU=10^{-6} m^2 Ks^{-1} kg^{-1}), similar to *Hoor et al.* [2004]. The meteorological data used here is from the European Centre for Medium-Range Weather Forecasts (ECMWF) operational analyses. The dynamical tropopause follows the ozone changes in the upper troposphere and lower stratosphere more closely than does the thermal tropopause [*WMO*, 1957]. In two cases (March 29 and April 2, 2006), a tropopause fold was sampled by the ozonesondes down to an altitude of 4 kilometres. In the historical dataset of over 1000 ozone soundings,

less than 10% have sampled tropopause fold associated with the vicinity of the jet stream.

Stratospheric profiles indicate filamentary structures associated with differential advection. This statement is based on backward trajectory calculations. Some ozonesondes sampled vortex filaments of very high ozone content (for example the profile obtained on March 25 and March 26, 2006), while others have captured filaments of low-latitude origin (for example the profile obtained on March 26, 2006). Due to ozone transport in the stratosphere and fluctuations of the tropopause, column ozone varied between 430 and 500 DU during the given period. During the winter of 2005/2006, vortex ozone depletion was of the order of 10% [*Goutail, private communication*] due to the early break-up of the polar stratospheric vortex. Thus most of the observed profile variability is indeed due to the dynamical variability. Lack of heterogeneous ozone depletion and on the other hand a stronger-than-usual residual circulation led to unusually high values of stratospheric ozone over northern high latitudes during spring 2006. At Sodankylä, 20% higher values of ozone partial pressure between 200 hPa and 50 hPa were observed compared to the climatological mean for the same time-period (March 22 to April 14) over the years 1989–2003.

4.2. Long-term ozonesonde datasets in the Arctic

Altogether 5572 individual soundings were available for this study. The stations involved are located between 60.1º and 82.5º N (Table 1). The stations selected are those having regular sounding programs at high latitudes in the northern hemisphere. The best data coverage for Arctic stations is during the winter period, thanks to frequent campaign activities [*von der Gathen et al.*, 1995; *Rex et al.*, 2004]. The data coverage at each station is shown in Table 2 (soundings per month per station and averages). Table 3 presents the fraction of soundings that were made inside the Arctic vortex during the winter/spring period between November and April; an average of 48% of all profiles were obtained inside the Arctic vortex, with peak frequencies in January (62%) and February (60%). The Arctic vortex was defined as being 2 degrees inside where the PV gradient in equivalent latitude exceeded 0.8 PVU/degree (see *Karpetchko et al.* [2005] for details).

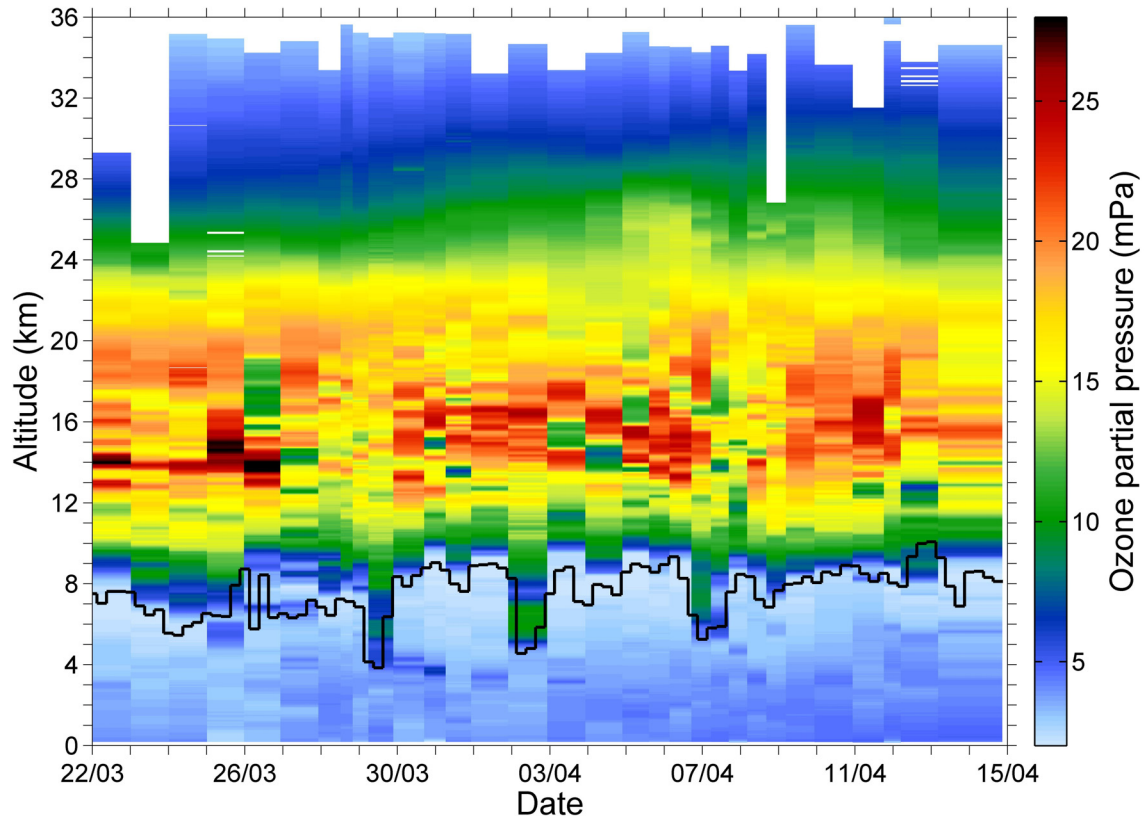

Figure 1. Sequence of 31 ozonesonde profiles obtained between March 22 and April 14, 2006. The black solid line marks the altitude of the dynamical tropopause based on a value of 2 potential vorticity units (1 PVU=10^{-6} m^2 K s^{-1} kg^{-1}); missing data due to telemetry breaks or levels above the altitude of balloon burst are indicated in white.

Table 1. Coordinates of sounding stations and starting year of regular ECC sonde observations

Station	Country	WMO number	Latitude	Longitude	Data record
Resolute	Canada	24	74.7º N	95.0º W	1979-
Alert	Canada	18	82.5º N	62.3º W	1987-
Sodankylä	Finland	262	67.4º N	26.6º E	1989-
Ny-Ålesund	Svalbard	89	78.9º N	11.9º E	1989-
Lerwick	UK	43	60.1º N	1.2º W	1992-
Eureka	Canada	315	80.0º N	85.9º W	1992-
Scoresbysund	Denmark	717	70.5º N	22.0º W	1993-*

* additional data in February–May 1989 and November 1991–April 1992

Table 2. Data coverage per station per month

	J	F	M	A	M	J	J	A	S	O	N	D	Year
Sodankylä	151	139	136	76	69	60	61	65	61	68	70	92	1048
Ny-Ålesund	154	137	172	119	75	53	72	48	54	58	76	124	1142
Scoresbysund	81	77	71	51	45	37	46	41	44	43	41	58	635
Alert	91	88	73	56	60	52	50	51	54	58	53	59	745
Resolute	76	62	54	43	39	37	38	32	34	39	43	50	547
Lerwick	126	141	108	50	28	18	19	27	23	23	49	112	724
Eureka	115	99	96	43	41	40	36	41	41	41	49	89	731
all	794	743	710	438	357	297	322	305	311	330	381	584	5572

Table 3. Data coverage per station per month, percentage of profiles obtained inside the polar vortex. The polar vortex is defined as being 2 degrees inside where the PV gradient in equivalent latitude exceeded 0.8 PVU/ degree (*Karpetchko et al.* [2005] provide a detailed description of the method)

	J	F	M	A	M	J	J	A	S	O	N	D	Nov–Apr
Sodankylä	55	60	51	20	3	0	0	0	0	0	16	40	45
Ny-Ålesund	90	86	67	32	1	0	0	0	0	3	49	65	67
Scoresbysund	58	61	51	6	2	0	0	0	0	0	22	34	43
Alert	86	86	56	25	0	0	0	0	0	7	45	73	66
Resolute	58	55	43	14	0	0	0	0	0	3	33	42	43
Lerwick	18	19	11	4	4	0	0	0	0	0	2	11	13
Eureka	65	61	55	28	0	0	0	0	0	0	41	46	53
all	62	60	49	21	1	0	0	0	0	2	30	43	48

4.3. ECC ozonesonde: measurements, corrections and comparisons

4.3.1. Sonde equation

All stations considered here have used electrochemical concentration cell (ECC) ozonesondes during the time-period under consideration. The ECC ozonesonde is used to obtain an ozone density profile with a high vertical resolution from the ground to typically up to 35 km. The sondes are extremely valuable during the dark time of the year in the polar region, because most of the other measurement techniques use sunlight to obtain an ozone retrieval. Sondes are also the only long-term source of ozone data in the free troposphere. In recent years, sondes have been used extensively during satellite-borne sensor validation campaigns and at polar latitudes during campaigns aiming to understand and quantify the polar stratospheric ozone loss.

ECC ozonesondes use a platinum electrode electrochemical cell sensor as described by *Komhyr et al.* [1986, 1995]. In the sonde a nonreactive gas-sampling pump forces the ozone molecules in the air into the sensor cathode chamber. An ozone molecule reacts with the iodide in the sensing solution to form an iodine molecule. The iodine molecule is converted back to iodide and simultaneously two electrons of charge flow through the cell's external circuit. Thus the sensor's output current is proportional to the uptake rate of ozone in the sonde cathode chamber.

The ozone partial pressure is calculated using the following formula:

$$P_{O3}=4.308\times10^{-4}(i-i_b)t\times T\times PC\times C, \quad (1)$$

where PO3 is the ozone partial pressure in millipascals, i is the cell output current in microamperes, i_b is the cell background current, t is the flow rate in seconds per 100 cm^3 of air flow, T is the air temperature in the sonde pump in K, PC is the pump flow-rate correction, and C is a correction factor. The correction factor in most cases is not altitude-dependent and is known as the "normalization factor". However, within this work altitude-dependent empirical corrections for the thermistor positioning and for the solution strength were also developed. The latter corrections could be applied prior to the sonde profile normalization, which is based on total ozone measurements by other well-established instruments.

4.3.2. ECC sonde types and the sensing solutions

There are two manufactures of ECC ozonesondes: the Science Pump Corporation, Camden, New Jersey (SP sondes) and the EN-SCI Corporation, Boulder, Colorado (ES sondes). The ozonesondes have been interfaced to Vaisala RS-80 radiosondes at the European stations, and during 1993–2003 at the Canadian stations also. During the period 1989–1993 the Canadian stations used VIZ radiosondes [*Tarasick et al.*, 2005]. Thorough post-flight quality assurance of the sonde data is needed, because of the variable practices and sonde types used at different sites in different time-periods. This post-flight quality control of individual ozone profiles was started using a computer program that checks each measured profile for technical problems such as gaps, low bursts, excessive noise or anomalous box temperatures. Potential problems identified by the software are checked by careful visual inspection by an experienced technician. In terms of further data homogenization, the two main issues are the changes in sonde sub-types and the changes in operational practices at any given station. Laboratory comparisons [*Smit et al.*, 2000; *Smit and Sträter*, 2004] have shown that small (order of 5%) differences exist between SPC and EN-SCI manufactured ozonesondes, which may depend on the time-period they were manufactured. In addition, the composition of the potassium iodide (KI) sensing solution used in the sensor cell will produce differences of similar magnitude.

The standard sensor solution is a 1% KI buffered solution as given by *Komhyr* et al. [1995] and the Science Pump Manual [*Science Pump Corporation*, 1996]. The *EN-SCI Corporation* [1996] recommends using a 0.5% KI buffered sensor solution. However, several stations have continued to use the standard 1% KI solutions, even when changing from SP to ES sondes. The influence of the KI solution on ES ozonesondes is such that ES sondes yield a better agreement with the reference total ozone measurements when using the 0.5% KI solution than when using the standard 1% KI solution. In addition, different sub-types of ozonesondes using different preparation procedures have been compared to a laboratory reference, revealing altitude-dependent differences [*Smit et al.*, 2000].

Since 2006, all the ES sondes flown at Sodankylä have used the 0.5% KI buffered sensor solution (sondes shown in Figure 1). The ozonesondes were interfaced to Vaisala RS-92 SGP radiosondes with a digital OIF-92 interface. The ozonesonde payloads were flown by TA1200 rubber balloons. The Vaisala DigiCORA Sounding System MW31 was used to receive and process radiosonde data, including ozone sensor data processing and GPS altitude retrievals. For double soundings EN-SCI interface boards V2D with an extension board were used interfaced to Vaisala RS80 radiosondes.

4.3.3. Dual sonde flights

During the thesis work a series of dual sonde payloads were flown at Sodankylä. An example of the dual ozonesondes flown on April 7 and April 11, 2006 is shown in Figure 2. Both payloads included an ES sonde using a 0.5% KI sensing solution and a SP sonde using a 1% KI sensing solution. Sondes from different production batches were also used. Both profiles were transmitted by the same telemetry system and in both cases the same pump corrections were applied. Figure 2 presents the absolute values of ozone partial pressure, as well as the relative difference obtained from the flights. The dark solid line is the smoothed value of the high vertical resolution data, indicating good agreement between the SP and ES sondes in the stratosphere (the difference is of the order of 2%). Below the tropopause much larger differences are obtained (between 4 and 7% relative difference), with SP sondes showing relatively higher values. The light-grey lines in the background indicate the differences in the un-smoothed data; the variability is partly caused by differences in sensor response times. The total column ozone from the ES sonde flights is 9 DU lower (by 2%) for the ES/SP pair. For another pair of sondes the total column ozone is identical. The latter agree with Brewer data to within 0.7–0.9%. For the first dual flight there is no reference total column from the Brewer, because the balloon flight started at 20:32 UT.

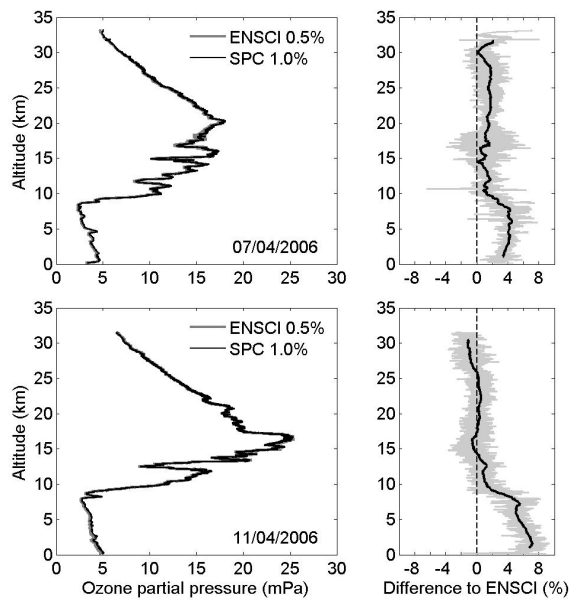

Figure 2. Dual sonde flights in April 2006. "Difference to ENSCI" is calculated as (SP-ES)/ES.

Between May 2003 and March 2005 a total of 18 dual sonde flights were performed. In each payload at least one pair of ENSCI/SPC manufactured sondes was flown. The results are shown in Figure 3. In total 9 dual soundings were obtained with the ES and SP type of sensors both using the standard 1% KI sensor solution, and another 9 double soundings with the ES sensor using a 0.5% KI solution and the SP using a 1% KI solution. Comparison with local Brewer spectrophotometer measurements of total ozone shows that the best agreement is achieved by using a 0.5% KI solution for the ES ozone sensors, while for SP sensors the standard flights allow the development of a correction algorithm that can be applied to those ES profiles that have been obtained using the standard 1% KI sensing solution. According to the comparison flights, the percentage difference between the ozone profiles obtained by ES vs. SP ozonesondes, if both are using the standard 1% KI sensing solution, ((ES−SP)/SP), can be approximated by the following polynomial:

$$\Delta O_3 = 5.56\times10^{-3} z^3 - 2.02\times10^{-2} z^2 + 0.308z + 1.36, \quad (2)$$

where z is the altitude in kilometres.

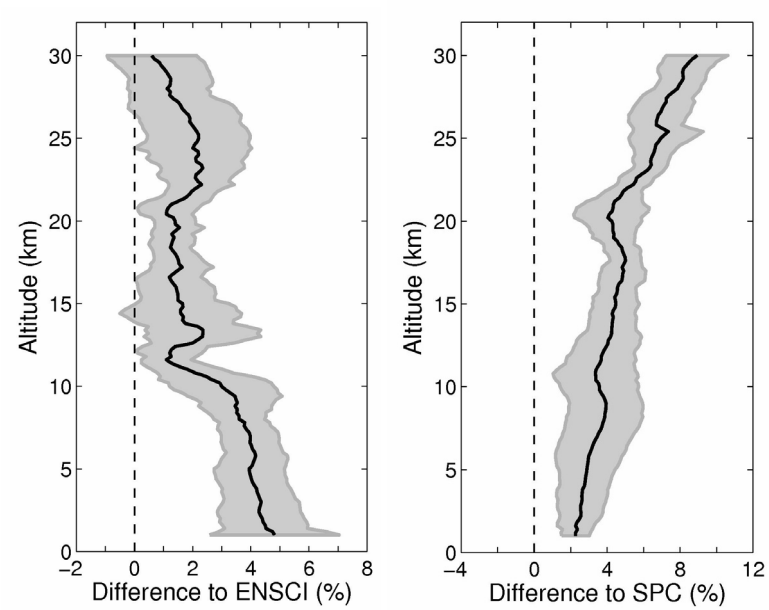

Figure 3. Average difference between ES and SP ozonesondes using different sensor solutions from 18 dual flights, ± one standard deviation (shaded area). Left: ES sondes using a 0.5% KI buffered sensor solution, SP sondes using a 1% solution. Difference to ENSCI is calculated by ((SP1.0-ES0.5)/ ES0.5). Right: ES and SP sondes both using the standard 1% KI sensor solution. Difference to SPC is calculated by ((ES1.0-SP1.0)/ SP1.0).

Recently the World Meteorological Organisation-sponsored Balloon Experiment on Standard Operating procedures for ozonesondes (BESOS) has carried out activities aiming to standardize operational procedures and investigate the differences between ES and SP ozonesondes [*Deshler et al., paper in preparation,* 2007]. Results from the BESOS experiment are expected to become available in the near future and will contribute to data homogenization procedures.

4.3.4. Thermistor correction

In the newest type of SP and ES sondes the thermistor is mounted in the pump in order to determine the temperature of the volume of gas in the pump cylinder. However, in earlier models the temperature was measured at the cathode inlet tube close to the pump. The difference between these temperatures, which will introduce differences into the final ozone data, can be significant in the stratosphere. This was confirmed by a series of thirteen test flights at Sodankylä. In the data presented here an empirical correction formula (below) derived from these flights was used to correct for the changes in thermistor positioning.

$$C=\begin{cases} -0.0144\times\ln P+1.1064 & \text{if } P > 165 \text{ hPa} \\ 1.033 & \text{if } P \le 165 \text{ hPa} \end{cases} \qquad (3)$$

In this thesis the above correction has been made to data at Sodankylä, Ny-Ålesund and Scoresbysund, as the required metadata were available. In the Sodankylä case an additional data correction was used to remove an inconsistency in pump efficiency corrections. This concerned data obtained between October 1994 and January 1995, when older pump corrections were used due to a change in the data processing software. For this study the profiles were recalculated using the same standard pump corrections for all Sodankylä files.

4.3.5. Data homogenization based on total ozone

To complete the data homogenization a reference total ozone dataset was formed using the three well-known satellite datasets covering the corresponding periods. From January 1989 to May 1993, measurements by the Total Ozone Mapping Spectrometer (TOMS) version 8 data (Nimbus-7 TOMS) are used, while from May 1993 to November 1994 TOMS version 7 data from Meteor-3 TOMS are used. From June 1995 to June 2003 GOME WFDOAS (Global Ozone Monitoring Experiment total ozone retrieved using the weighting function differential optical absorption spectroscopy) algorithm Version 1.0 data are used [*Weber et al.*, 2005]. The Meteor TOMS data were set to the level of the TOMS v.8 dataset using a short overlap period with the Nimbus TOMS. This data homogenization was needed due to a small latitude-dependent positive bias (from 2 to 5% over the given stations) between Meteor TOMS v.7 and Nimbus TOMS v.8 data. Finally, a bias between TOMS version 8 and GOME WFDOAS version 1 data [*Weber et al.*, 2005] was removed using overlapping measurements in 1997–2000. The TOMS data were set to match the data of GOME WFDOAS especially to remove the differences at low solar elevations (more than 5%). The resulting reference dataset was then used to assess the data quality history using the ozone correction factor time series as illustrated in Figure 4. The correstion factor or "normalization factor" [*Logan et al.,* 1994; *Bodeker et al.,* 1998] is the ratio of reference instrument total ozone to the total ozone integrated from the ozonesonde profile supplemented with the residual ozone if the balloon burst altitude was 20 hPa or higher. The latter supplement was obtained from the recently-updated climatology for estimating the amount of ozone above balloon burst altitude [*McPeters et al.*, 2007]. Correction factors shown here refer to the dataset that has already been homogenized taking into account known corrections as described above. Figure 4 suggests that, even after these altitude-dependent corrections, there remain shifts in correction factor statistics that tend to persist for relatively long periods. Possible reasons include changes in manufactured lots, sonde subtypes or operational procedures. The overall consistency would therefore improve if the wintertime sonde data, for which there are generally no reference measurements, could also be corrected with the average correction coefficient of neighbouring seasons. Analysis of the datasets of 1989–2003 suggest that these kinds of corrections are justified, while the most recent data may not need corrections due to improvements in sonde preparation procedures; also the telemetry systems have become more reliable [*Kivi et al.,* 2007c]. It should be noted that the recent experiment made at Sodankylä in spring 2006 suggests that these corrections may not be needed for sondes that have been prepared according to the most recent methods. Improvements in manufacture quality and data processing systems also result in significantly less errors in the final profile retrievals.

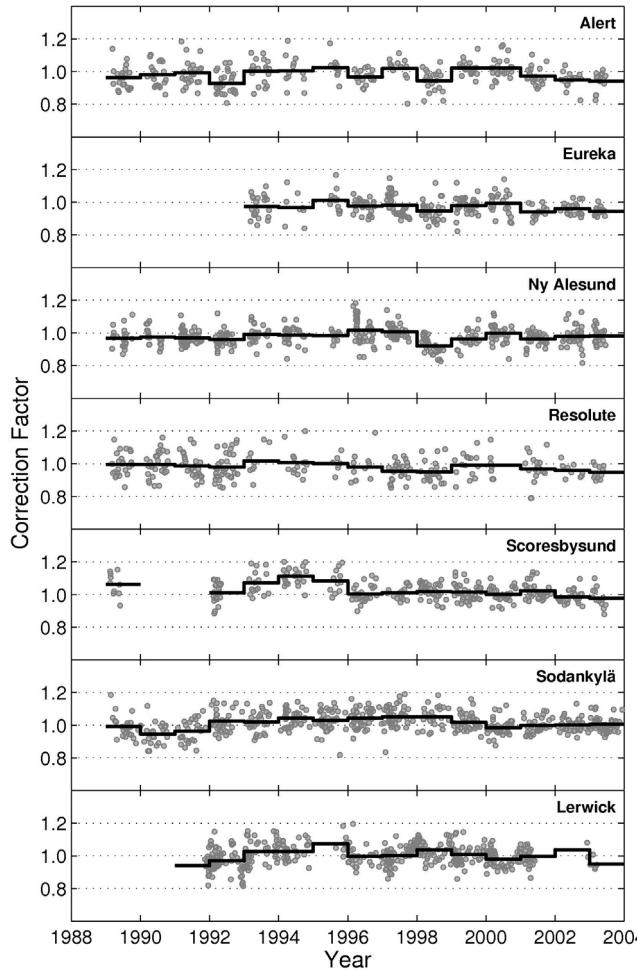

Figure 4. Correction factors for individual high-latitude sonde stations. From upper panel down: Alert, Eureka, Ny-Ålesund, Resolute, Scoresbysund, Sodankylä, Lerwick. Annual mean correction factors are shown by a solid line.

4.3.6. Comparison with other ozone instruments

4.3.6.1. Lidar versus ozonesonde measurements

Measurements from the recent campaign are used here in order to assess the performance of the ozonesondes in 2006. The campaign, the Sodankylä Total Ozone Intercomparison and Validation Campaign, was conducted from March 20 to May 4, 2006 aiming first to compare space-borne and ground-based ozone

measurements under conditions of low solar elevation and high values of total ozone during the Arctic late winter/spring; secondly it was intended to improve understanding of the performance of the ground-based instruments.

The ground-based instruments included ozonesondes, five Brewer spectrophotometers, two Dobson instruments, two differential ozone absorption spectrometers (DOAS), a SAOZ (Systeme d'Analyse par Observation Zenitale) spectrophotometer, and an ozone lidar. During the intensive phase of the campaign (March 22 – April 14, 2006) ozonesondes were launched daily, synchronized with the observations of the Ozone Monitoring Instrument (OMI) on board the AURA satellite and with lidar observations. In addition, during the campaign dual flights of the two balloon-borne electrochemical concentration cell (ECC) ozone sensors that are most commonly used in ozonesonde networks were performed. The NASA Goddard Space Flight Center (GSFC) mobile lidar system measures stratospheric ozone using the differential absorption lidar (DIAL) technique [*McGee et al.,* 1991, 1993, 1995]. It serves as the standard instrument of the Network for the Detection of Atmospheric Composition Change (NDAAC).

Recently *Liu et al.* [2006] showed that ozonesondes flown during the years 1996–1999 have large biases at several stations, including high-latitude stations, when compared to GOME satellite measurements [*Liu et al.,* 2006, their Figure 6]. The ECC sondes flown during the March-April 2006 campaign are similar to those flown during previous years; however, there are recent improvements in sonde preparation practices that should reduce measurement errors. This allows improved estimates in ozone profiles and also in the estimates of total ozone column based on the ozonesondes.

Direct comparison between ES ozonesonde and lidar profiles was made on March 28, 30 and April 7, 2006 (Figure 5). The payload of the April 7 flight also included an SP sonde, the data of which agreed with the ES sonde data to within 2%, as shown in the previous section. During the March 28 flight the differences between the ES sonde and lidar profiles are less than 5% over the altitude range of 15 to 30 km, the difference increasing to 10% higher up. Roughly the same magnitude of differences is obtained during the sonde flight of April 7. On March 30 the average differences are 5% higher in the same altitude range, which may be partly caused by the strongly laminated structure of ozone on that occasion, something not resolved by lidar retrievals. The comparisons are also influenced by balloon drift and balloon altitude calculations.

During the 1st and 2nd flights, the balloon altitude calculation is based on an RS92 radiosonde, while during the 3rd flight (on April 7) an RS80 radiosonde was used in the dual ozonesonde system. All the RS92 radiosondes flown during the campaign had a built-in GPS system; for RS80 radiosondes, a separate GPS unit was employed. Unfortunately the GPS unit on flight 3 failed at altitudes above 25 km. Therefore the comparisons with lidar data shown are

based on pressure altitude calculations. In the case of flight 1 and 2 with RS92 sondes, the altitude differences between pressure altitude and GPS altitude were less than 30 m, and were thus not significant for the lidar comparison (though the use of GPS altitude slightly improves the agreement above 30 km). During the 3rd flight, the balloon altitude calculation had an offset of 200 m at an altitude of 25 km. Due to the failure of the GPS system in the sonde payload, it was not possible to obtain GPS altitudes higher than 25 km. A simple extrapolation suggests an altitude offset of the order of 400 m, which would reduce the relative difference between the lidar and sonde profiles in this case above 25 km.

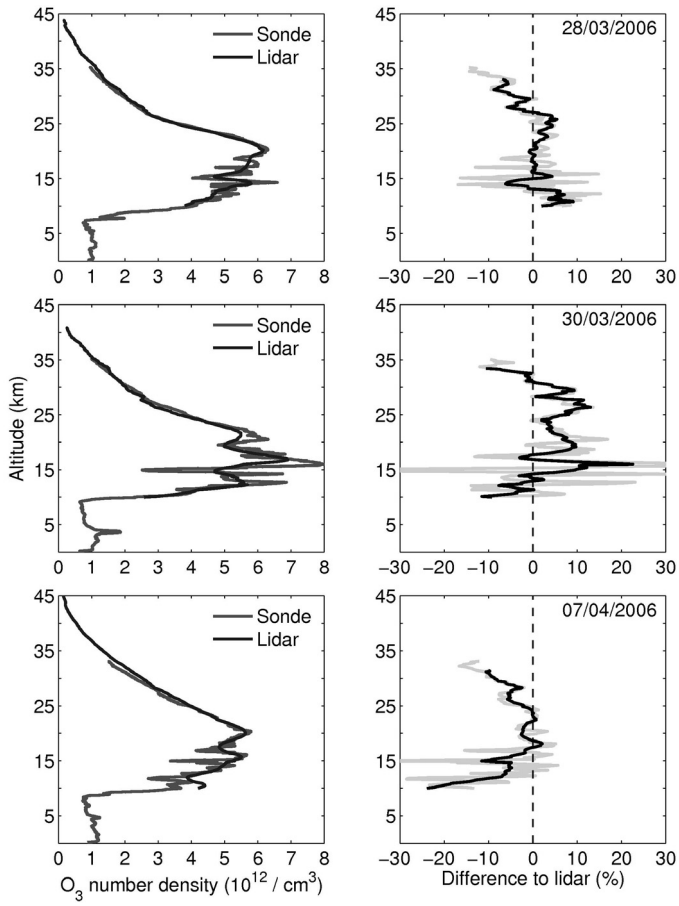

Figure 5. Near-simultaneous observations of ozone profiles by lidar and ES sondes. In the right-hand panel the grey line in the background represents a direct comparison, while the black line corresponds to the same type of altitude averaging for both lidar and sonde data.

In order to estimate possible pressure altitude errors in the stratosphere for a larger dataset, pressure altitude and GPS altitude differences were calculated for all ozonesonde flights during the comparisons (shown in Figure 6). These comparisons suggest that the average difference is less than 10 m up to an altitude of 15 km, from where it starts to deviate, becoming 50 m at an altitude of 35 km (the pressure altitude has generally having a negative bias). In an extreme case, the difference at 35 km was as great as 250 m with a positive bias, which may be related to a pressure sensor error. The RS80 pressure altitude (Figure 6, right panel), taking an average of 30 flights, has a larger standard deviation at 25 km; however there are not enough data at altitudes between 25 and 35 km to estimate the average and standard deviation in this altitude range.

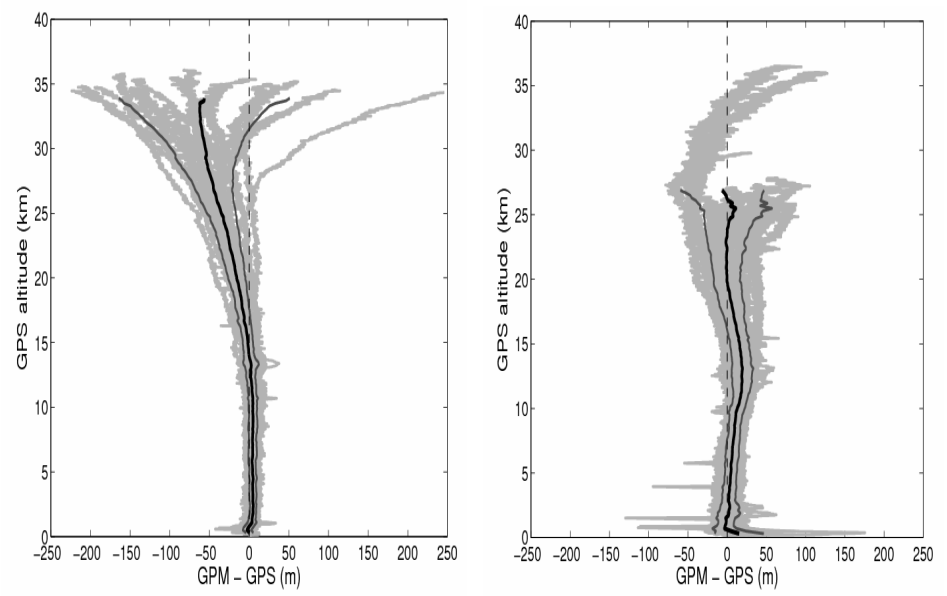

Figure 6. Left panel: Absolute difference between pressure altitude and GPS altitude (m) based on 30 RS-92 flights on an ozonesonde payload during the time-period March 22 – April 14, 2006. Right panel: Absolute difference between pressure altitude and GPS altitude (m) based on 30 RS-80 flights during the time-period 2002–2006.

4.3.6.2. Brewer or OMI versus the ozonesonde

The Ozone Monitoring Instrument (OMI) is an imaging spectrometer on board the AURA satellite launched in 2004. It measures in the spectral range between 270 and 500 nm. OMI provides relatively high spatial resolution. From the radiance spectra measured by OMI, total columns of ozone can be derived. During early 2006, two algorithms were used to derive the total column of ozone: the NASA TO3 algorithm and the DOAS algorithm by KNMI. The Very Fast Delivery (VFD) products developed by FMI and KNMI were also available.

During March-April 2006 three double monochromator and two single monochromator Brewers instruments were operated at Sodankylä. The double Brewers were as follows: #185 (the European standard instrument), #171 (from the NASA Goddard Space Flight Center), #085 (the World Standard instrument). The single Brewers were #037 (the Brewer located permanently at Sodankylä) and #039 (owned by Environment Canada). This allowed the establishment of statistical corrections for the single Brewers. The main problem with single Brewers is the stray-light issue, which is significant at high solar zenith angles (SZA). The simultaneous measurements by 5 Brewers allowed the derivation of empirical stray-light corrections for the single Brewers. Thus Brewer #037 data can be considered to be as accurate as the best estimate of total ozone from ground-based observations. The same corrections were also applied to the historical data of Brewer #037. This instrument has been continuously operational at Sodankylä since 1989.

On average excellent agreement between Brewer #037 and the total ozone from ES ozonesondes was observed (ratio Brewer/sonde = 1.004 ± 0.013) during the measurement campaign. The Brewer data were corrected for the stray-light error and synchronized with the timing of the balloon launches. Only direct sun (DS) measurements were used during clear sky time-periods. The OMI data were based on the TO3 algorithm. For OMI data, the corresponding ratio (OMI/sonde) shows an average value of 0.989 ± 0.017. If the measurement days were selected when both instruments provided data (16 measurements), the ratios were similar: Brewer/sonde = 1.008 ± 0.013 and OMI/sonde = 0.992 ± 0.017. These results are presented in Table 4 along with information on sonde serial numbers and column ozone calculated from the sonde data. The Brewer data are not shown if near-simultaneous DS measurements were not possible due to cloudiness.

Table 4. Summary of the ozone soundings made during the March–April 2006 campaign. The ES sondes (type z) used the 0.5% KI solution and the SP sondes (type 6a) the 1% KI solution.

Launch time	Serial number	Max_alt (km)	Max_alt (hPa)	Measured (DU)	Total (DU)	Brewer/ sonde	OMI/ sonde
22-03-06 11:15	z10656	29.3	10.6	411.4	455.0	1.001	1.000
23-03-06 11:13	z10662	24.8	22.1	365.2	452.6	1.023	0.990
24-03-06 11:14	z10659	35.2	4.4	448.5	470.6	1.000	0.951
25-03-06 11:15	z10658	34.9	4.6	477.3	500.5	0.996	0.975
26-03-06 09:45	z10657	34.2	5.1	415.7	443.6	0.978	0.964
27-03-06 08:55	z10655	34.8	4.8	422.7	448.5	1.033	0.991
28-03-06 09:27	z10661	33.4	5.9	407.7	437.6	1.023	1.003
28-03-06 13:01	z10654	35.6	4.2	423.6	449.5	0.990	
29-03-06 00:29	z10649	35.2	4.5	417.2	441.4		
29-03-06 08:46	z10660	35.0	4.7	447.7	474.7	1.001	0.986
30-03-06 08:01	z10644	35.2	4.7	446.0	469.5	0.998	0.995
30-03-06 23:30	z10645	35.2	4.7	415.5	440.4		
31-03-06 11:00	z10653	35.2	4.8	416.5	443.5		0.984
01-04-06 07:47	z10650	33.2	6.6	415.2	448.3		0.981
02-04-06 09:55	z10648	34.7	5.2	467.8	496.9	0.976	
03-04-06 09:00	z10652	33.4	6.4	394.3	428.0	1.029	1.019
04-04-06 09:50	z10647	34.2	5.5	412.9	442.2		1.001
05-04-06 07:15	z10636	35.3	4.7	405.9	431.2	1.003	1.005
05-04-06 19:00	z10651	34.6	5.3	444.5	472.7		
06-04-06 09:31	z10638	34.5	5.4	452.0	481.1		0.977
06-04-06 22:45	z10641	34.3	5.7	471.0	500.5		
07-04-06 10:10	z10639	34.6	5.4	415.4	449.2	1.021	1.014
07-04-06 20:32	6a17355	33.3	6.6	387.3	427.0		
07-04-06 20:32	2z3283	33.3	6.6	381.2	418.3		
08-04-06 09:17	z10637	34.2	5.8	433.4	469.0		0.975
08-04-06 21:05	z10642	26.8	18.1	375.2	452.5		
09-04-06 10:01	z10643	35.6	4.7	465.9	493.9		0.983
10-04-06 09:11	z10646	33.6	6.4	456.7	494.1	1.003	0.995
11-04-06 10:02	6a19454	31.5	9.2	440.4	490.9	1.005	1.009
11-04-06 10:02	1z10640	31.5	9.2	438.1	489.8	1.008	1.011
12-04-06 00:16	2z3639	36.6	4.2	450.3	474.8		
12-04-06 07:15	z10665	33.8	6.3	416.9	454.1	1.002	0.942
13-04-06 23:31	z10667	34.6	5.5	402.3	428.2		
19-04-06 11:31	z10666	33.4	6.6	380.8	419.3	1.001	0.981
27-04-06 09:49	z10663	35.4	5.2	329.4	358.7	1.008	1.015
28-04-06 10:32	z10664	34.6	5.8	347.8	381.8	1.009	1.000
03-05-06 12:37	z10669	36.0	5.0	361.3	388.6	0.989	
Average		33.8	6.5	417.9	451.9	1.004	0.990
st dev		2.4	3.6	35.3	33.0	0.015	0.019

4.3.6.3. Residual ozone amount above the balloon-burst altitude

The residual ozone amount above the balloon-burst altitude is one of the uncertainties in estimating column ozone from sondes, as different methods can result in 10–20 DU differences [*Thompson et al.,* 2003]. It is a common practice either to assume the constant mixing ratio measured at the balloon-burst altitude [*Claude et al.,* 1986] or, alternatively, to use climatological estimates based on satellite measurements [*McPeters et al.*, 1997; *McPeters et al.*, 2007]. In order to provide a reliable estimate of residual ozone based on a constant mixing ratio from an individual flight, a balloon should ascend to at least 17 hPa [*Claude et al.*, 1986] or even 15 hPa [*EnSci*, 1997]. While 15–17 hPa is around the mean maximum altitude of Arctic balloon flights, 32 flights out of 37 reached ceilings of at least 6.6 hPa (33.2 km) during the campaign (Table 4). Relatively high balloon ceiling statistics give one a good opportunity to compare different methods of estimating residual ozone. Five such methods were examined:

1. the standard method, which assumes a constant mixing ratio (CMR) as obtained at the balloon-burst altitude

2. a residual estimate from the add-on table of the updated climatology (LLM climatology) by *McPeters et al.* [1997, 2007]. The value for each sounding was interpolated according to time of the month and latitude.

3. Sonde station climatology to estimate the column from the sonde burst (if at least as high as at 32 hPa) to 10 hPa. The remaining column above 10 hPa was obtained from the LLM climatology (CLLM method). This is similar to the method proposed by *Bodeker et al.* [1998].

4. similar to the previous method, but the residual above 10 hPa was based on the 15-year ozonesonde CMR climatology (CCMR method).

5. combination of method 1 and 4: if the sonde balloon burst above 10 hPa, CMR was used (34 flights out of 37 flights during the campaign), otherwise the CCMR method was applied (3 flights).

The results for the campaign period and also for a longer period of measurements are shown in Figure 7. Here the longer period of measurements covers the sonde data series from 1989 to 2003, which have been previously homogenized using altitude-dependent corrections. For comparison, data from March–April is shown (220 flights). The CCMR and CLLM methods give almost identical results: therefore, only the CCMR results are shown. The method 5 results are shown in Table 4, but not in Figure 7, because for the campaign period they are dominated by the CMR results, while for the 1989–

2003 time-period this method would reduce significantly the number of data points due to lower balloon burst altitudes. Thus the method is only needed to create the best estimate of total ozone from the sondes during the campaign, but not for the multi-year analysis. The CMR method yields better agreement with Brewer and OMI measurements, probably because in spring 2006 ozone levels were anomalously high compared to climatology; secondly, sondes had no problems at higher altitudes near the balloon burst, such as is as often seen in historical data due to the pump efficiency issue and evapouration of the sensing solution. For the multiyear analysis, the best agreement with the Brewer is obtained if the climatological CCMR method is used. At 10 hPa and higher all methods yield similar results. The difference between LLM and CCMR is significant only during the December–April period, as LLM climatology involves zonal means, and longitudinal differences are significant only in the winter/spring season. A minor part of the differences between the CCMR and LLM methods is also related to different averaging periods: LLM climatology is based on the years 1988–2002 and CCMR climatology on the period 1989–2003. Due to the actual year-to-year variability, the standard deviations of the estimates shown in Figure 7 are largest if the CMR method is used. In Figure 7b the standard deviations are larger than those for the campaign dataset. This is linked to the fact that, for longer time series, Brewer daily means were used instead of the near-simultaneous Brewer measurement; secondly, the campaign measurements benefit from the recent improvements in quality of the sondes, preparation procedures, radiosonde technology and ground equipment. They indeed show that it is possible to obtain total column estimates from ozonesondes that agree closely with the reference instrument. The normalization procedure [e.g., *Logan et al.*, 1994, 1999] or other corrections therefore become unnecessary, providing that the sondes reach at least 10 hPa and there are no anomalies in the upper part of the profiles.

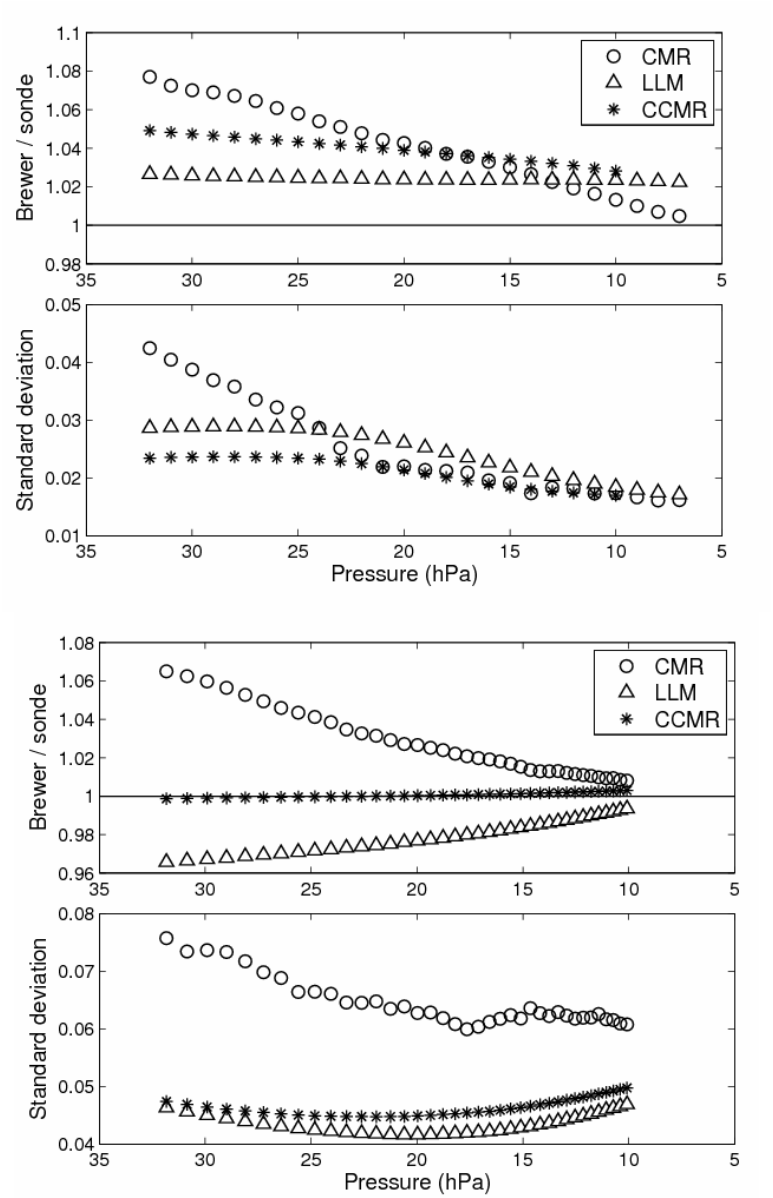

Figure 7. Altitude dependence of Brewer/sonde total ozone ratio depending on the method used for residual estimation based on the Sodankylä data a) for the campaign period and b) for the homogenized time series of 1989–2003. Only data from March-April is involved. Brewer measurements are DS measurements obtained within 1.5 hour of the sonde reaching 50 hPa, having a standard deviation of 5 measurements of 2.5 DU or less. The DS measurements are interpolated to the sonde time. Please see text for the explanation of the abbreviations used to describe the residual ozone methods.

4.3.6.4. Aircraft observations with a modified ECC sonde

During the winter of 1996/1997 the aircraft observations of ozone were made by the Russian stratospheric aircraft M-55 Geophysica. The campaign, the Airborne Polar Experiment (APE) from Rovaniemi (Finland) was the first scientific campaign ever made involving this high-flying aircraft [*Kivi et al.,* 1998a]. In situ measurements of ozone by the aircraft were performed by the ECOC instrument, which is the electrochemical concentration cell used on the Geophysica [*Kyrö et al.,* 2000]. Ozone data for the same air masses as sampled by Geophysica is also available from the network of balloon-borne ozonesondes (Figure 8). Balloon-borne ozonesondes provide additional information on the vertical structure of the ozone layering that is complimentary to the mostly horizontal information obtained by Geophysica's sensors.

Ozonesonde data was obtained from 36 stations, which belonged to the OSDOC (Ozone Soundings as a tool for Detecting Ozone Change) network in the winter of 1996/1997 [*Kivi et al.,* 1998a]. The sonde data underwent careful quality checks. Three main tools were used. First was the visual inspection of data for large gaps, low bursts and other major problems. Secondly, a comparison of the integrated ozone with the best total ozone value available from a set of reliable and validated instruments, i.e. Dobson, Brewer, SAOZ, Earth Probe TOMS, and Adeos TOMS was made. As the third tool, inspection was carried out for possible outliers in the potential vorticity (PV)- potential temperature (θ) binned sounding data. Generally the performance of the sonde network was good. The average correction factor, or the ratio of the local or satellite total ozone observation to the integrated sonde total ozone, was 1.00 ± 0.07. This result from the sonde network supports the results by *Komhyr et al.* [1995] that the ECC sonde accuracy in the stratosphere is of the order of ± 5%.

The aircraft-borne ECOC data was grouped in PV, θ bins of size of 4 PVU by 5 K, (1 PVU = 10^{-6} K m^2 kg^{-1} s^{-1}). The PV values were obtained from the European Centre for Medium-Range Weather Forecasts (ECMWF) analyses at 12 UT. Most APE flights occurred reasonably close to 12 UT. The nominal θ levels were centred at 435, 440, …, 475 K. The final bin centres were displaced from the nominal values to the actual means determined from the flight trajectory. For each flight the potential vorticity on the 435 K and 475 K potential temperature levels was obtained directly from the ECMWF analyses. For levels in between these, the PV bin centres were interpolated using the fact that potential vorticity varies in the vertical as $\theta^{9/2}$ [*Lait*, 1994]. Based on experience with the ECMWF fields, this simple interpolation rule was, apart from sharp laminae cases, able to give the PV bin centres to within ± 1 PVU of the analyzed values. The same bin centres and sizes were used in subsequent analyses of the ozonesonde data. In order to gather enough sonde data, soundings occurring within ± 5 days from each Geophysica flight day were included in the analysis. The cooling rate at the time and altitudes of the APE mission was of the order of 1 K/day, leading to a +20 ppb/day change in ozone

mixing ratios [*Knudsen et al.*, 1998]. Diabatic effects during a period of five days are thus not negligible but, on the other hand, two factors reduce the errors arising from diabatic subsidence. First, sonde data were collected both before and after each APE flight, so that the bin average in time occurs close to the flight day and second, chemical ozone loss will reduce the positive trend on an isentrope. The ± 5 day temporal bin size can therefore be considered as an acceptable compromise between gathering enough sonde data and avoiding biases arising from downward diabatic motion in the arctic wintertime lower stratosphere.

The data and results are illustrated in Figure 9, where the ECOC sounding profiles obtained during ascents and descents of the aircraft are plotted as a function of potential temperature (dots). In the second panel the dive to the tropopause during the flight of January 7 is also shown. Each dot in the ECOC ozone profile represents one data sample. In the same panels the contemporaneous and co-located ozone soundings from Sodankylä are presented, too (solid lines). Also shown are the ozone concentrations from the SLIMCAT model following the Sodankylä balloon trajectory on December 31st (open rectangles) and the (PV, θ) bin averages analyzed from the sonde network (filled rectangles). Because of air traffic control regulations, the Sodankylä

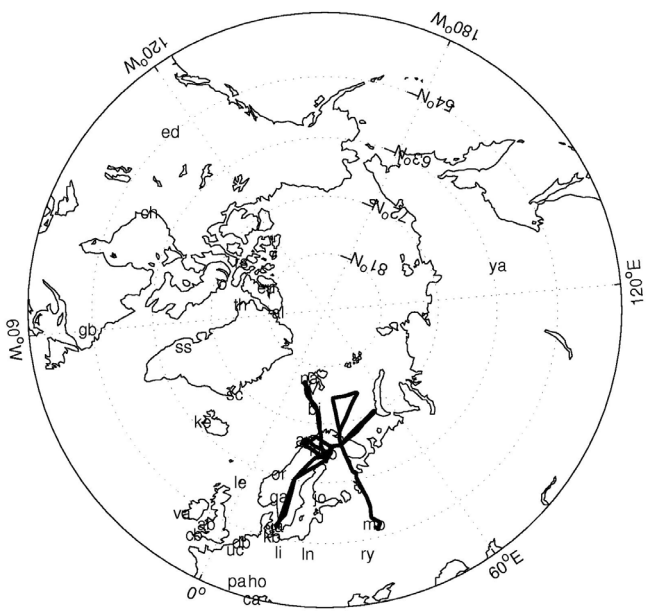

Figure 8. Geophysica flight paths between December 23rd, 1996 and January 16th, 1997, and the locations of sonde stations.

ozone soundings were never made exactly coincident with Geophysica overpasses, but sometime between the take-off and landing. In some cases two soundings are available from Sodankylä on the same day, because a sonde campaign was running in parallel with the APE campaign. Although the whole height of the Sodankylä ozone soundings is plotted in each panel, it should be noted that a direct comparison with the ECOC data can only be done at tropospheric altitudes, when the two instruments were geographically reasonably close. At Geophysica's cruising altitudes, a comparison is only obtained from the OSDOC sondes, which are co-located with the ECOC instrument in (PV-θ) space.

The average ozone mixing ratio for each bin was calculated from OSDOC data and ECOC data and the comparison was performed on the bin averages. In Table 5 the results are summarized for each flight. Bins averaged over less than 3 ozone soundings and less than 10 ECOC data points were neglected. The results in Table 5 are given as mean and the standard deviation of the differences of (PV-θ) bin averages. On all flights the difference between ECOC and OSDOC data is negative but not statistically significantly so, due to the large variability. Taking all the bin-averages from all the flights (the total number of selected levels is 57) gives the result that the ECOC measures lower (–5.7 ± 6.8%) mixing ratios compared to ozonesondes. However, there is a significant difference between the results obtained from early flights in December and from the later part of the campaign such that the variability becomes much smaller in January. This behaviour is understandable, considering that sonde data of December were scant, resulting in a poor sample of (PV-θ) bins in conditions of a weak and less homogeneously mixed vortex. For the inside-vortex measurements, the comparison gives similar average results with, however, much less scatter (–5.7 ± 2.8%).

Table 5. Summary of the calculated difference between ECOC and sonde measurements for each individual flight in percent; for all flights and for the inside-vortex flights of January 1997.

	ECOC- sondes, relative difference ± standard deviation	Number of PV-θ bins used in analysis
961223	–10 ± 5	9
961229	–7 ± 12	7
961231	–3 ± 9	9
970107	–8 ± 4	8
970109	–3 ± 6	12
970114	–4 ± 1	9
All flight days	–5.7 ± 6.8	54
Flights inside vortex (January 1997)	–5.7 ± 2.8	26

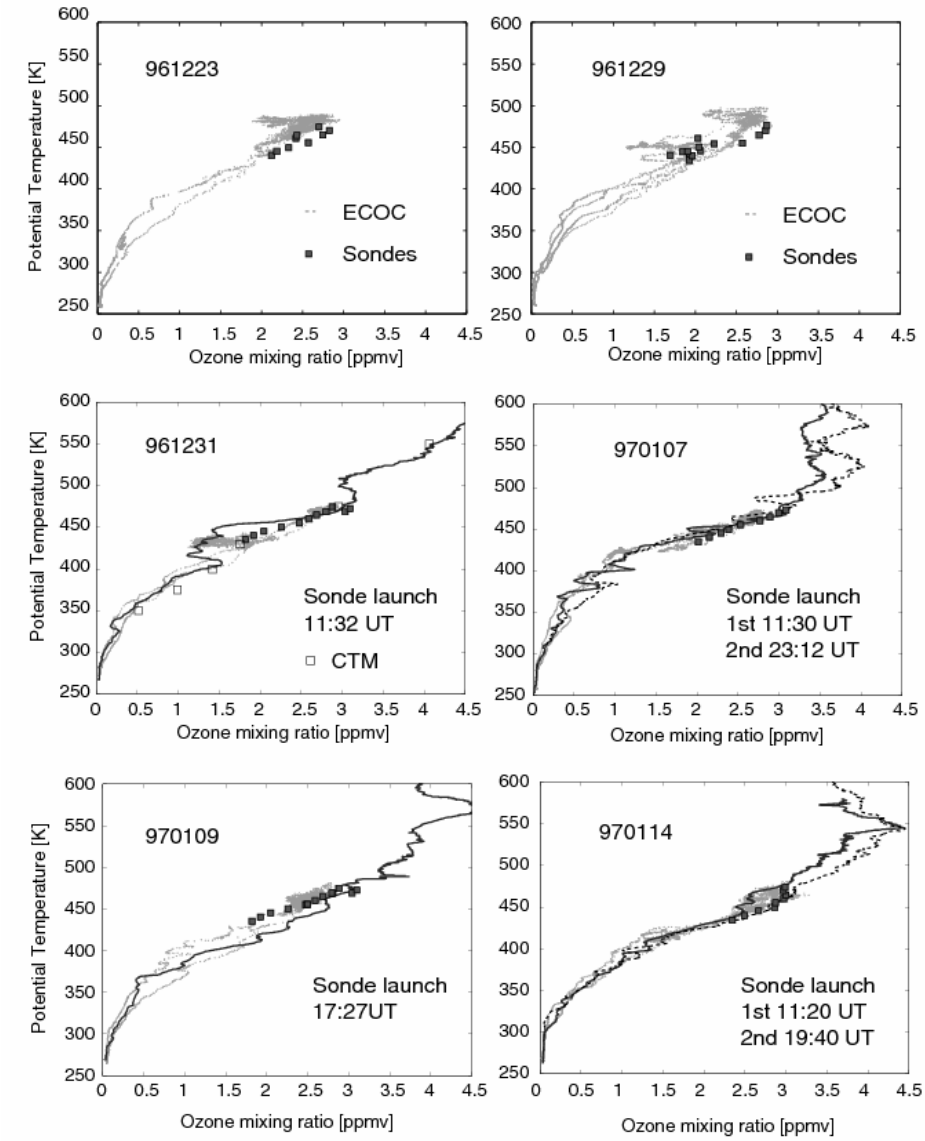

Figure 9. ECOC vertical ozone profile (dots), (PV, θ) - bin averages analyzed from the balloon-borne sonde network (filled rectangles), CTM output for the flight of December 31st, 1996 (open rectangles) and vertical profiles of balloon-borne measurements of ozone by a sonde launched at Sodankylä (solid line). If available for the corresponding flight day, a 2nd balloon-borne sonde profile from Sodankylä is included (dashed line).

4.4. Statistical analysis of ozonesonde data

4.4.1. Monthly mean profiles

Monthly mean ozone profiles and standard deviations up to an altitude of 10 hPa in 1 km vertical layers were calculated for each individual station and as a mean of all station data. These extend earlier climatologies of Arctic ozone [*Taalas and Kyrö*, 1992; *Logan*, 1994; *Logan et al.*, 1999; *Fortuin and Kelder*, 1998; *Rao et al.*, 2003] by using a longer ozonesonde record for the stations in the European Arctic. Standard deviations at all stations are largest in the stratospheric data during the winter-spring months, which is the season of main interest here. This analysis highlights the climatological layered structure in ozone partial pressure found in the lowermost stratosphere and related to the quasi-isentropic transport of low-ozone air from low latitudes [*Reid et al.*, 2000]. In high-latitude ozonesonde data, a mean secondary maximum between the tropopause and about 150 hPa altitude is evident in summer (May-August) profiles. This is in contrast to mid-latitude ozonesonde data, which shows that in monthly averages the frequency of high-ozone layers above the tropopause decreases to almost zero in the summer [*Logan et al.*, 1999].

The ensemble dataset includes data from all stations and thus shows lower variability than the individual station data. This ensemble dataset is used in the analyses presented later in the thesis because the observed changes are consistent from station to station.

4.4.2. Long-term behaviour of total ozone

Figure 10 shows the monthly total ozone deviations from the 1979–1988 mean TOMS version 8 data for the year-round 1989–2003 ozonesonde measurements (smoothed and unsmoothed). The period of satellite measurements was selected in order to put the sonde data of 1989–2003 into a longer-term context. The sonde data are the monthly means of the ozonesonde ensemble dataset. The TOMS data of 1979–1988 used in the calculation of the deviations are the monthly averages for the sonde locations (overpass data). The figure suggests that for the sonde dataset (the region of 60–82º N) the long-term minimum in total ozone is not as well-defined as in the case of the global average, where a minimum in the year 1993 becomes evident [*Fioletov et al.*, 2002]. The long-term minimum in total ozone according to the annual sonde data is in 1996 (318 DU), as is the long-term minimum of mean January-April seasonal data (324 DU). In total ozone almost as low values are obtained in 1997: 320 DU as the yearly average and 343 DU in the January-April season. These low values are in agreement with the observed significant ozone depletion in the Arctic lower stratosphere in 1996 and 1997. The largest monthly deviations (grey background line in Figure 10) from the 1979–1988 monthly mean values are

observed during the January–April period. For comparison, the March–September satellite observations for the years 1979–2003 (TOMS version 8 and GOME WFDOAS version 1 datasets) over given sonde locations each year are also shown. The TOMS data are the average of the overpass data, while the GOME WFDOAS data are taken from the nearest grid point for each ozonesonde station. These March-September averages cannot reveal the large negative deviations observed in the winter months; however, they are in reasonable agreement with the smoothed values of the sonde dataset.

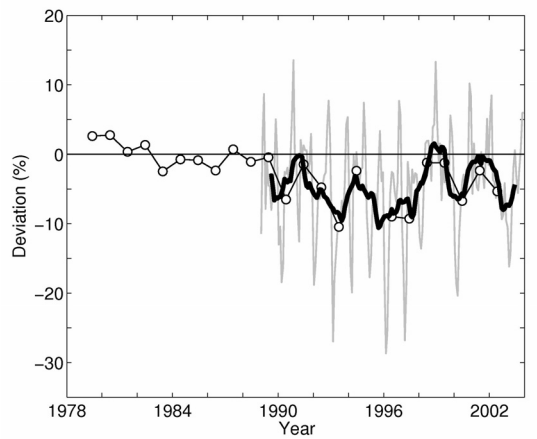

Figure 10. Monthly deviations of total ozone from sondes (1989–2003) in comparison to the 1979–1988 mean using TOMS version 8 satellite data (grey line in the background). Also shown are the smoothed values of the monthly ozonesonde data (thick black line) and the combination of TOMS version 8 and GOME WFDOAS version 1 data of the period 1979–2003 as mean March-September deviations from the 1979–1988 period (thin black line with circles).

4.4.3. Multiple regression model

The ozonesonde time series and the time series of the explanatory variables discussed in the previous section were used in a multilinear regression analysis to study the contributions of the predictors to interannual variability and trends in ozone profiles, with emphasis on January-April ozone data. In the model the proxies are based on a priori knowledge, each representing some known physical process. The model includes the following terms:

$$Y_L = b1_L \cdot TP + b2_L \cdot HTF + b3_L \cdot VPSC^* + b4_L \cdot aerosol + c_L + e_L, \qquad (4)$$

where Y_L refers to the layer average ozone density of the month or season of analysis, $b1_L..b4_L$ are the coefficients of the explanatory variables, c_L is a constant term representing the climatological layer average over the fitted period, and e_L is the residual. The explanatory variables and their data sources are as follows:

1) TP is the average tropopause height calculated from the sounding profiles using the WMO definition of the thermal tropopause [*WMO*, 1957], a proxy for the influence of dynamical changes connected to pressure systems.
2) HTF is the eddy heat flux at 100 hPa averaged over 45–70º N and accumulated from January to March in the seasonal analysis, a proxy for ozone transport by the meridional circulation. Here the dataset for calculating HTF is the ERA-40 re-analysis of the European Centre for Medium-Range Weather Forecasts (ECMWF) covering the period 1989-June 2002 [*Uppala et al.*, 2004]. From then on the operational analyses by ECMWF (T213 L60) are used.
3) VPSC* is defined as the product of VPSC and EESC. VPSC is the volume of temperatures below the equilibrium temperature of nitric acid trihydrate T_{NAT}, here averaged between the 400 K and 550 K isentropic levels and integrated over the November-March period; it is used as a proxy for polar heterogeneous chemistry. The meteorological data is the same as used for the calculation of the HTF data. The altitude range was set to correspond to *Rex et al.,* [2004], as most of the ozone depletion has been observed in the given altitude range during the time-period 1989–2003 (see also Figure 1 in *Rex et al.*, [2004]). The EESC estimates are provided by the NASA Goddard Space Flight Center [*Newman et al.*, 2006] and are similar to the Antarctic EESC data. WMO scenario A1, mean age-of-air 5 years, width of age-of-air spectrum 2.5 years and a bromine scaling factor of 50 are used. Some model runs used the linear trend term or the EESC to estimate the anthropogenic influence on ozone trends.
4) "Aerosol" is a proxy for aerosol loading due to volcanic eruptions, which is the aerosol backscatter ratio obtained in the altitude region of 200–100 hPa from the Arctic aerosol sonde stations during the years 1989–2000 from *Suortti et al.* [2001]. This altitude range was originally chosen in order to avoid including PSC backscatter in the statistics of background aerosol backscatter ratio. The aerosol sonde dataset is described in detail in *Suortti et al.* [2001].
5) Arctic Oscillation indices (AO) were used in an alternative model instead of the TP term similar to *Weiss et al.* [2001]. AO represents the sea surface monthly Arctic oscillation indices obtained at http://www.cpc.ncep.noaa.gov/.

QBO and solar flux terms [e.g., *WMO*, 2003] were not included in the model, as in the dataset neither of these proxies significantly added to the overall explanatory power of the model. The probable explanation for is that the interannual variability seen in the QBO is already explained by other terms in the model, and changes in solar radiation should have a significant effect only at

relatively high altitudes for the ozonesondes. The model residuals were tested for autocorrelation using the Durbin-Watson test [e.g., Neter, 1996] and found to be insignificant. The likely reason is that the time step in the model is one year, and the ozone 'memory' is believed to reset every year at the start of the ozone build-up period [*Fioletov et al.*, 2002].

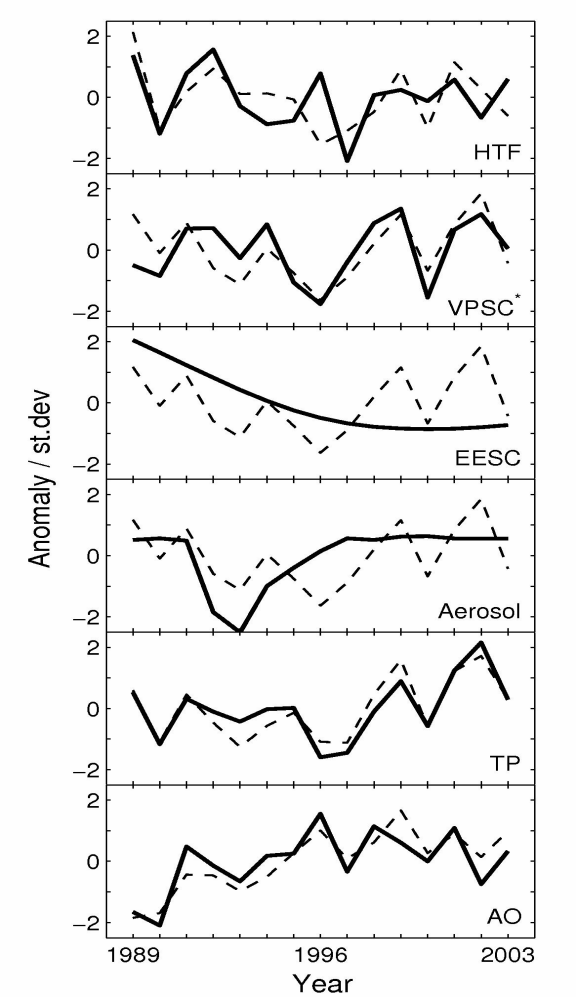

Figure 11. Time development of the model terms in the January-April season (solid lines) and ozone column data (dashed lines) expressed as anomaly/standard deviation. Starting from the upper panel: the ozone columns in the upper panel are from the layer L4 (40–10 hPa) together with the HTF data; VPSC*, EESC and Aerosol terms overlay the ozone layer L3 (150–40 hPa); the TP term overlays the ozone layer L2 (tropopause-150 hPa); the AO proxy overlays the layer L1 (surface-400 hPa). The model terms are scaled with −1.0 in the lowermost 5 panels.

The contribution of the individual variables to the regression model was also tested by using a forward stepwise regression method [*Milton and Arnold*, 1995] and the March total ozone time series from the Brewer spectrophotometer #037 daily observations made at Sodankylä since 1989. This data examination led to the conclusion that 80% of the year-to-year variability in March total ozone in 1989–2003 above Sodankylä can be explained by three variables: the tropopause altitude, the eddy heat flux at 100 hPa averaged over 45–70º N, and the ozone depletion approximated by the volume of polar stratospheric clouds. A similar model was applied to ozonesonde profiles. In order to improve the profile model, two explanatory variables were added: the Arctic aerosol backscatter data as a proxy for volcanic aerosol load and the Arctic Oscillation as an alternative to the TP term in the troposphere. In the model the TP, HTF and AO terms can be seen as dynamical terms, while the VPSC* and Aero terms are more closely linked to chemical processing.

The ozone profiles are analyzed in approximately 1 km layers between the surface and 9.8 hPa. The different proxy time series along with the layer ozone data are presented in Figure 11 for the January-April (JFMA) time-period. The selected ozone layers (shown in the background by the dashed line in Figure 11) are expected to correlate with the given proxy data. The three four-month seasons are chosen because the monthly trends and the underlying physical reasons for the changes are similar during these selected four-month periods. An additional reason is that, in the case of the ozone soundings, monthly data suffers from a relatively low sampling rate. The acronyms used later in the text are JFMA (corresponding to the January-April time-period), MJJA (May-August) and SOND (September-December). Generally, station-specific results are not reported, except in the case of significant differences between the station data and the ensemble data.

4.4.4. Interannual variability and trends in ozone profiles

The explanatory power R^2 [*Milton and Arnold*, 1995] of the regression model described above is shown in Figure 12. On average the model explains from 62 to 95 percent of variability in the January-April ozone profiles on average, depending on the altitude. The TP and HTF terms alone explain between 60% (at 150 hPa) and 90% (at 250 hPa) of the variability in the stratosphere. However the model is more complete when the Aerosol and VPSC* terms are included, improving the overall explanatory power (rightmost dark solid line in Figure 12). A small part of the variability (up to 12 percent) in the troposphere is due to the correlation with terms explaining stratospheric ozone variability; however, most of the variability in the tropospheric model is explained by the AO term: its explanatory power R^2 is 60–65% for the troposphere up to an altitude of approximately 400 hPa. The results suggest that in the dataset during the January-April season changes in AO play a major role regarding

tropospheric ozone variability. This result is in agreement with the findings by *Lamarque and Hess* [2004].

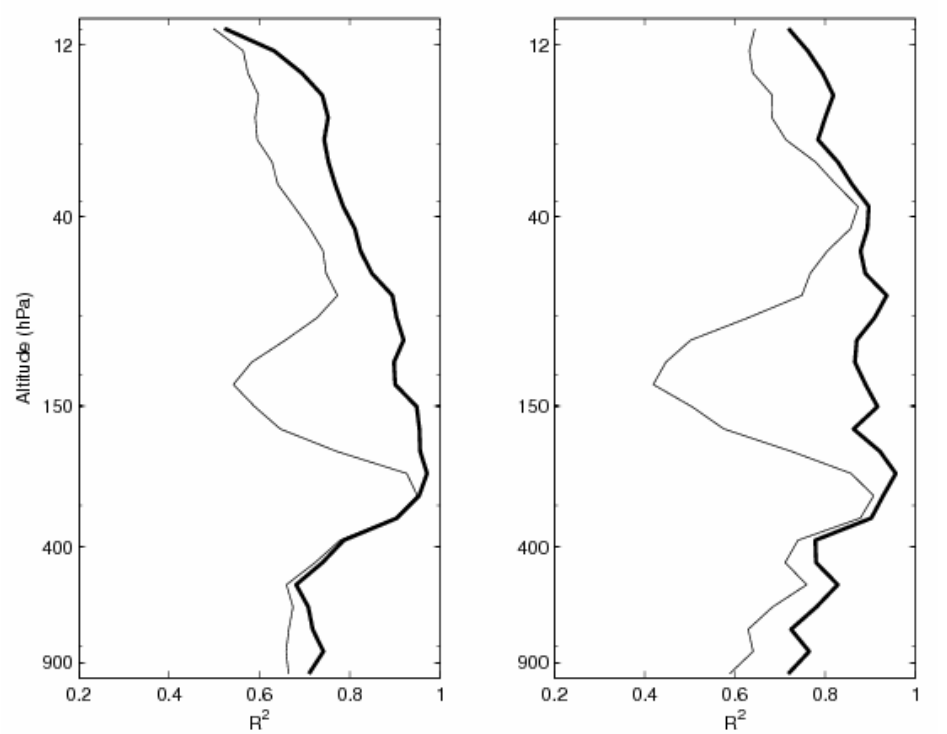

Figure 12. Explained variance in the model regarding January-April ozone profiles (left panel) and the March ozone profiles (right panel). Two cases are shown: the model including dynamical variables only (thin line), and with the additional VPSC* and aerosol terms (black solid line).

Figure 13 presents the observed profile anomalies for January-April of each individual year and additionally provides an estimate of the contribution of individual proxies to the model fit (shown as a dashed line). Large negative deviations in the ensemble dataset are found in the years 1992, 1993, 1995, 1996, 1997 and 2000, while positive deviations are evident in 1989, 1991, 1999, 2001, 2002 and 2004. The quality of the statistical model is tested by comparing the ozonesonde measurements for JFMA 2004 with profiles for the same period that are calculated using the model coefficients found for the previous period 1989–2003 together with the meteorological data from the 2004 winter. The good agreement between the reconstructed and observed ozone in 2004 supports the contention that the major variables regulating the JFMA ozone variability are included in the model. The same kind of model fit regarding March anomalies

yields better results in years 1989 and 2003. This is probably because the four-month period includes a larger amount of internal variability both in observed ozone and proxy data, at least during winters/springs such as 1989 and 2003. Otherwise the March anomalies (both observed and reconstructed) are very similar to the mean JFMA profile anomalies. Thus March alone is a good indicator of the changes observed throughout the season January-April. No a priori information about the expected altitude ranges of the explanatory variables was used in the fit, and it was therefore remarkable that the regression yields altitude distributions of the coefficients that are in agreement with the dynamical and chemical considerations. The regression model suggests that the negative anomalies in 1992 and 1993 can be attributed to the aerosol term in the model, while the observed anomalies in 1996 and 2000 can be attributed to the combined effect of TP and VPSC*. The TP term seems to especially dominate in the years 1997, 2002, and 2004. The VPSC* term in the multiple regression is most pronounced during 1989, 1990, 1995, 1996 and 2000. The HTF term makes a substantial contribution to the anomaly fit in most of the years during 1989–1997. The interdependence of the model terms was tested by calculating the variance inflation factor VIF [*Neter et al.*, 1996]; the critical value that would lead to exclusion of one of the terms was never reached. Yet, some of the variability with a maximum at 50–70 hPa that can be attributed to the VPSC* term is already explained by the variance in the TP term. Indeed, the correlation between the TP in JFMA and the VPSC* term was found to be +0.69 with a statistical significance of 99%. During the same season the correlation between the HTF term and TP is –0.37 and between the HTF term and the VPSC* term –0.19.

Figure 14 presents time series of observed and modelled ozone in the 3 seasons, expressed as anomalies around the layer mean value. For comparison between seasons, the vertical scale of the layer anomalies is kept constant. In both the troposphere and stratosphere the largest changes on both interannual and longer time-scales are found in the January-April period. The model suggests that in the troposphere the variability of JFMA ozone is related to the AO changes. In the stratosphere a significant increase in ozone between the tropopause and 40 hPa is observed since 1996–1997; this can primarily be attributed to the changes in the TP term in the model. The observed changes between 40 and 10 hPa can be attributed to the changes in both the HTF and the TP terms. The decrease in stratospheric ozone prior to 1996–1997 cannot be explained by changes in TP and HTF only. In fact, it is the inclusion of the Pinatubo aerosol term that significantly improves the model fit. Between the tropopause and 40 hPa both VPSC* and TP terms have significant explanatory power, but the combination of the TP and aerosol terms results in a better model fit than the combination of the VPSC* and aerosol terms. This is probably because the VPSC* effect is most significant in the March profiles, while here 4 months of data are fitted, and the data also include profiles obtained outside the stratospheric vortex.

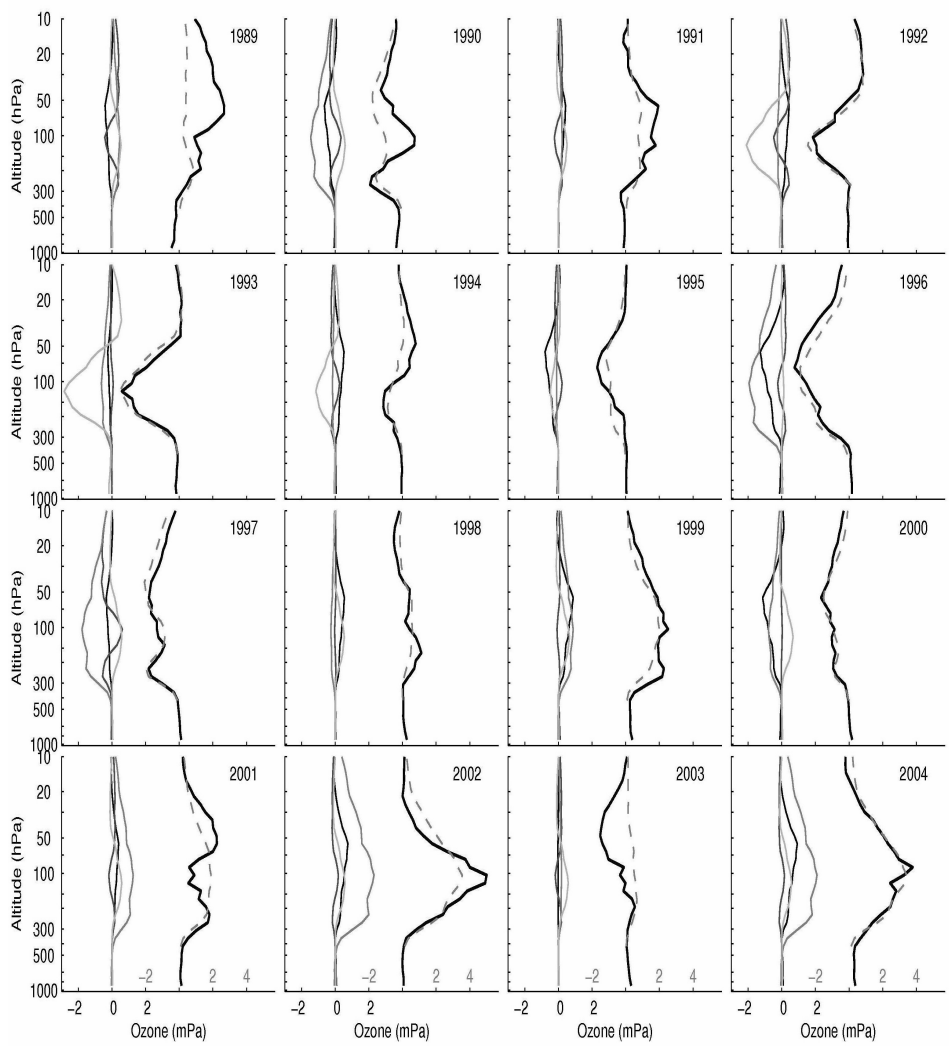

Figure 13. Anomalies in January-April ozone profiles: observed (black continuous line) and regression model fit (dashed line). Also shown are the contributions to the variability by individual terms on each subplot. The shades of the grey colour represent the individual terms, from light grey to dark grey in the following order: Pinatubo aerosols (light grey), tropopause term, eddy heat flux at 100 hPa and the volume of polar stratospheric clouds (dark grey).

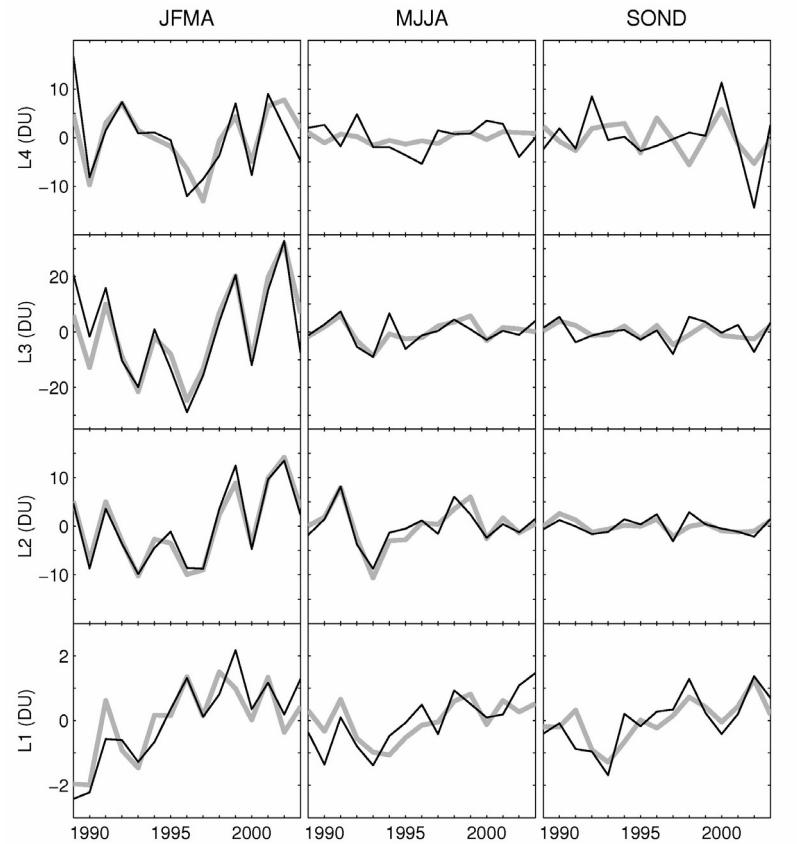

Figure 14. Time series of anomalies of observed seasonal ozone in layers L1-L4 (solid black line) and model fit (grey line). Layers L1-L4 are shown in increasing order starting from the bottom row.

Figure 15 presents the observed trends over two time-periods with a vertical resolution of about 1 km. The trends are calculated directly from the observations using a linear trend as the only variable in the model. In the stratosphere, significant negative trends at all levels are found in JFMA for 1989–1997: the trends vary between –2 and –2.5% per year depending on the altitude (Figure 14a). There are no definite trends in the stratosphere during other seasons. During the period ending in 2003 (Figure 15b) there is an increase in JFMA ozone in the altitude range from the tropopause to 50 hPa. The latter is in agreement with increasing trends in total ozone observed over mid-latitudes during the period 1994–2003 and modelled over high latitudes [*Hadjinicolaou et al.*, 2005]. The profile trends also indicate a significant increase in tropospheric ozone from the surface to about 400 hPa.

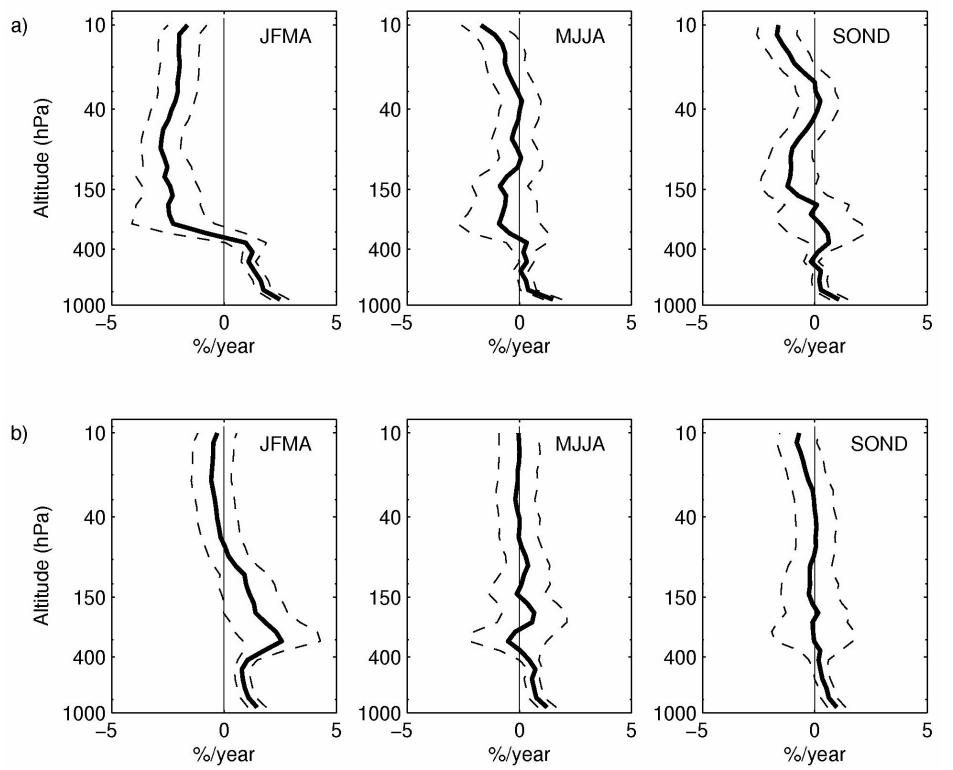

Figure 15. Observed seasonal profile trends ± one standard deviation over two time-periods: a) 1989–1997 and b) 1989–2003.

In order to characterize the influence of changing the end year to the JFMA trend, observed trends were calculated by varying the ending year of the trend period from 1995 to 2003 (Figure 16). The observed tropospheric ozone increase remains significant at the 95% significance level (indicated by the white crosses) regardless of the chosen time-period. In the stratosphere, significant changes (a negative trend) are observed up to 1998 depending on the altitude region. Finally, Table 6 summarizes the observed seasonal and yearly trends in the four layers L1-L4 as defined above. In addition, the table shows the trends for 3 time-periods to highlight the change in the Arctic total ozone trends in the mid-1990s. The results are given for the ensemble dataset. Consistent results are also obtained if stratospheric trends are calculated at each station separately. However, the time-series of tropospheric ozone for 1989–1994 show lower values at Resolute and Alert (northern Canada) than in the European sector of the Arctic (Sodankylä and Ny-Ålesund). In the time-period 1996–2003, these differences are much smaller, leading to similar tropospheric trends during the latter period.

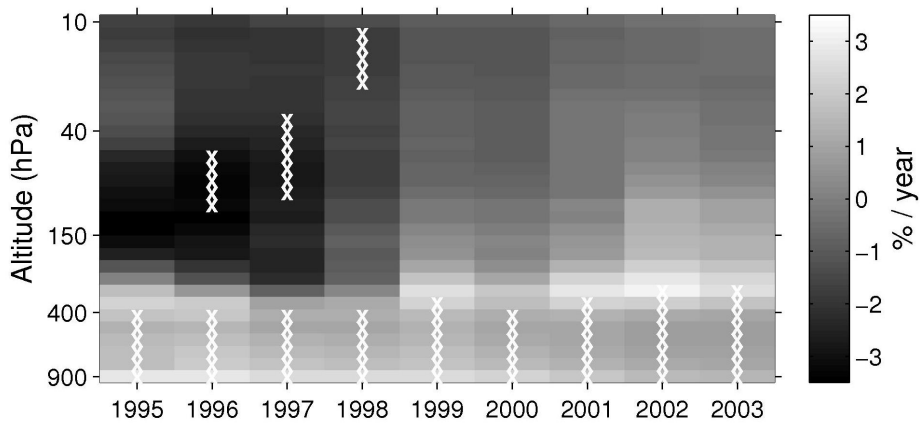

Figure 16. Grey-colour-coded observed seasonal trends for JFMA in %/year units evenly distributed in 30 vertical layers between 900 hPa and 9.8 hPa. The ending year of the trend period varies from 1995 to 2003; the starting year is set to 1989. "X" marks a layer and time-period that corresponds to statistically significant trends at the 95% confidence level.

Table 6. Observed seasonal trends in ozone in layers L1–L4 in %/year ± standard deviation for 3 time-periods. Only significant trends at the 95% confidence level are shown. The layers are: L1 = surface to 400 hPa, L2 = tropopause to 150 hPa, L3 = 150 to 40 hPa and L4 = 40 to 10 hPa

	L1	L2	L3	L4
JFMA(89-03)	1.14±0.23	1.71±0.96	*	*
MJJA(89-03)	0.73±0.15	*	*	*
SOND(89-03)	0.57±0.19	*	*	*
YEAR(89-03)	0.81±0.13	0.69±0.50	*	*
JFMA(89-96)	2.27±0.46	-1.99±1.62	-3.20±1.02	-1.87±1.11
MJJA(89-96)	0.68±0.47	*	*	-1.18±0.31
SOND(89-96)	*	0.80±0.64	*	*
YEAR(89-96)	1.09±0.36	*	-1.53±0.58	-1.18±0.54
JFMA(96-03)	*	4.93±2.63	3.32±2.04	1.63±1.19
MJJA(96-03)	0.81±0.34	*	*	*
SOND(96-03)	*	*	*	*
YEAR(96-03)	0.34±0.30	1.34±1.26	1.25±0.78	*

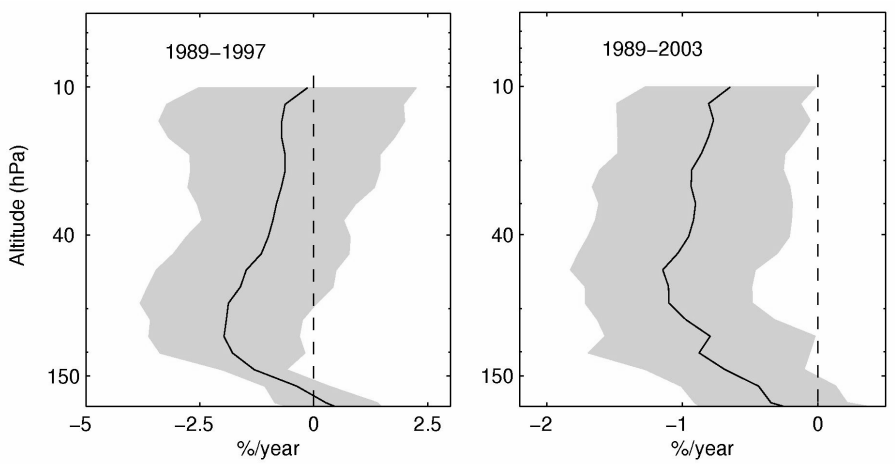

Figure 17. Linear "remaining" trend component in %/year for two time-periods, 1989–1997 (left panel) and 1989–2003 (right panel). The model includes the influence of natural variability (TP, HTF, Aerosol term) and a "remaining" linear term to represent the anthropogenic influence on ozone trends. The shaded area corresponds to the 95% confidence limits.

In order to estimate the "remaining trend" term, presumably caused by anthropogenic influences, the model was run including the proxies for natural variability (HTF, TP and the aerosol term) and a trend term, similar to the approach by *Weiss et al.* [2001] and *Brunner et al.* [2006]. These results are shown in Figure 17 for two time-periods: 1989–1997 and 1989–2003. The linear "remaining" trend for the earlier period (1898–1997) is of the order of −1 to −2 %/year in the lower stratosphere (altitude dependent, the average between 150 and 40 hPa being −1.7 %/year) for the first time-period and varies between −0.7 and −1.1%/year for the second time-period, 1989–2003 (layer average is −1.0 %/year). If the trend term in the model is replaced by the Arctic EESC term, a very similar influence for the first period is obtained, but a somewhat smaller one compared to the linear trend term (around −2 mPa/ppb between 150 and 40 hPa) for the time-period ending in year 2003. Regardless of the choice of the EESC or the trend term, the model assigns about the same amount of change (about 1/2) to the TP term. For the time-period since 1996 the model suggests that the dynamical terms provide the main contribution to the observed increase.

4.4.5. Relationship between ozone and the explanatory variables

4.4.5.1. Tropopause altitude

The TP term is highly correlated with all stratospheric ozone layers in JFMA, with values of –0.91 between the tropopause and 150 hPa, –0.84 between 150 hPa and 40 hPa and –0.68 between 40 and 10 hPa. The correlation with the total ozone column is –0.91. The correlations are statistically significant at the 99% level. Figure 18 confirms that the correlation decreases with altitude as expected [*Vaughan and Price*, 1991; *Weiss et al.*, 2001], but is still significant in the upper layer of 40–10 hPa. The strongest correlations are found in JFMA, but during the other seasons the TP term is also highly correlated with ozone in the lowermost stratosphere. A more process oriented alternative to the TP term is the integrated equivalent latitude proxy (EL) as proposed by *Wohltmann et al.* [2005, 2007]. The EL proxy can be understood as the dynamically-driven ozone content, here calculated for the altitude range between 340–725 K. The benefit of this approach is that one can separate contributions from vertical displacement of the isentropes and horizontal isentropic advection, the two dynamical processes affecting ozone in the lower stratosphere. According to the findings in this work the correlations between stratospheric ozone and the EL proxy are largely driven by the vertical component. The correlation with the horizontal component of the proxy is weak. Thus the vertical displacement term plays the key role in the interannual variations of the lower stratospheric ozone in the dataset, while the effect of variability in horizontal advection is found to be small in the Arctic. The vertical component of the EL proxy closely follows the long-term tropopause changes and also the changes in stratospheric ozone in JFMA shown in Figure 14. Thus, in the Arctic, the dynamical trend in lower stratospheric ozone derived from correlations with tropopause height is driven by changes in the vertical displacement of the ozone profile. Since these correlations are more likely to hold on longer time-scales than the correlations between horizontal advection and tropopause height, the use of TP as a proxy for total ozone in the Arctic is better justified than it is in mid-latitudes.

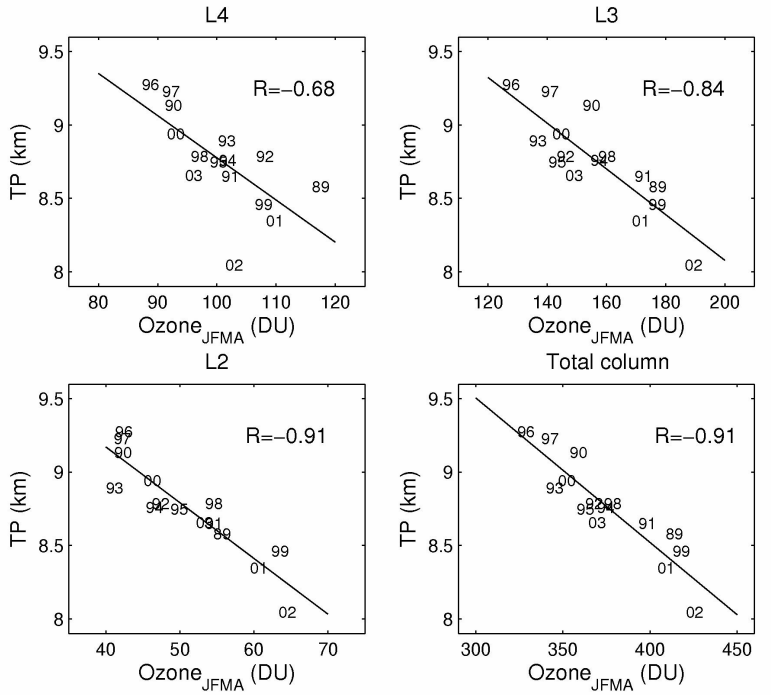

Figure 18. Correlation between monthly ozone columns in the stratospheric layers of up to 150 hPa (L2), 150–40 hPa (L3), 40–10 hPa L4), total column ozone and the mean tropopause altitude of the January-April time-period.

4.4.5.2. Eddy heat flux

Here the eddy heat flux (HTF) at 100 hPa is averaged over 45–70º N based on meteorological analyses and used as a proxy for ozone transport by the meridional circulation. The approach is similar to the one used by *Weber et al*. [2003], though here the analysis additionally includes information about the vertical structure of ozone and data for January-April. It is found that there is a strong correlation between the HTF and stratospheric ozone during most Arctic winters, and March stands out as the month of the highest such correlations. The correlation between February HTF and March ozone is highly significant: 0.73 in case of total ozone, 0.81 for the layer 40–10 hPa, 0.59 for the layer 150–40 hPa and 0.66 from the tropopause to 150 hPa. Figure 19 presents the correlations for the layer 40–10 hPa and the total column. The correlations are statistically significant at the 99.9% level. In a similar way January ozone is strongly correlated to the HTF in the preceding month: R=0.67 for total ozone, R_{L2}=0.77, R_{L3}=0.65 and R_{L4}=0.57.

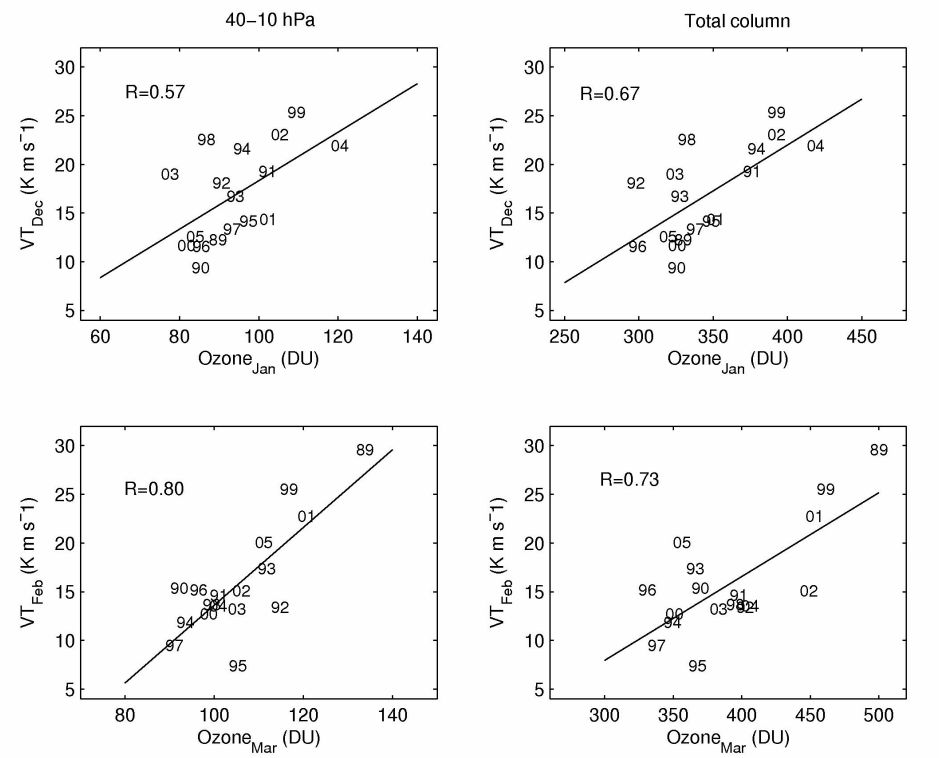

Figure 19. Upper two panels: Correlation between January ozone columns (10–40 hPa layer and total column) and mean eddy heat flux of the preceding month at 100 hPa averaged over 45–70º N. Lower two panels: Correlation between March ozone columns (10–40 hPa layer and total column) and mean eddy heat flux of the preceding month at 100 hPa averaged over 45–70º N.

4.4.5.3. The Arctic Oscillation

During JFMA the AO term is negatively correlated with ozone in the troposphere with R=–0.83, which is statistically significant at the 99.99% level. In comparison to the other terms for JFMA, the AO remains the most prominent explanatory variable in the troposphere. In the published literature, the AO relationship to total ozone has been related to changes in tropopause altitude [*Thompson et al.*, 2000]. It is proposed that, for example, a negative AO index represents a weak vortex, which is accompanied by a low tropopause. *Brönnimann et al.* [2000] came to similar conclusions as they reported a significant correlation between the AO and total ozone in Arosa during winter months. In contrast, no significant correlation between the AO and stratospheric ozone for northern high latitudes is found, although there is a strong relationship between

AO and tropospheric ozone. Possibly changes in the AO index can be understood in the context of changes in large-scale transport, thus indicating a change towards more frequent transport from distant pollutant sources of ozone and its precursors and secondly, changes in transport from the stratosphere to the troposphere. Such an interpretation is supported by tropospheric ozone model results presented by *Lamarque and Hess* [2004]. The observed ozone increase at the surface and in the free troposphere during the recent period of observations is also in line with earlier studies [*Simmonds et al.*, 2004; *Vingarzan*, 2004; *Tarasick et al.*, 2005].

4.4.5.4. Volume of polar stratospheric clouds

The correlation between the VPSC* term and ozone in the 150–40 hPa layer in JFMA is negative and significant at the 99% confidence level with R=-0.68. In 1995, 1996, 1997 and 2000 anomalously low ozone was observed in layer L3, corresponding to the high VPSC* values during the same winters. In Figure 20 the altitude profile of the coefficient of the VPSC term from the March soundings inside the polar vortex is presented. Integrating the whole profile gives a total depletion potential of 2.6 DU/10^6 km^3. If the altitude range is limited to 125–25 hPa, corresponding to *Rex et al.* [2004], the integration yields 2.2 DU/ 10^6 km^3. This value is very close to the depletion potential obtained from their ozonesonde analysis. The VPSC influence peaks at 50–70 hPa, and the term explains on average up to 50% of the interannual variability in the ensemble dataset in March. This corresponds to observed anomalies in ozone partial pressure of up to 4 mPa.

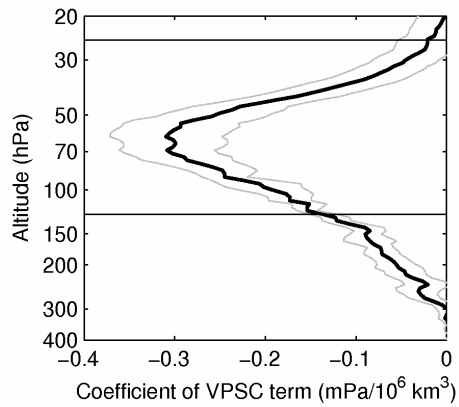

Figure 20. The altitude profile of the coefficient of the VPSC term calculated from the soundings made inside the polar vortex in March.

5. POLAR STRATOSPHERIC CLOUDS AND WATER VAPOUR

5.1. Introduction

According to the current understanding of lower stratospheric ozone depletion, polar stratospheric cloud (PSC) particles provide the major portion of the aerosol surface for heterogeneous chlorine activating reactions, especially during periods when volcanic aerosol loading is low [*WMO*, 1999]. PSCs are observed in cold regions of the lower polar stratosphere. Low temperatures trigger the activation of inert chlorine species on the surface of polar stratospheric cloud particles by complex heterogeneous reactions [*Solomon,* 1999]. PSCs consist of water ice particles (PSCs of type II), of solid nitric acid trihydrate ($HNO_3 \cdot 3\ H_2O$ - NAT; PSCs type Ia), or of liquid supercooled ternary solutions ($HNO_3/H_2SO_4/H_2O$ - STS; PSCs type Ib). For a given mixing ratio of water vapour and nitric acid, PSCs can exist if the local temperature falls below one of the threshold values $T_{NAT} > T_{STS} > T_{ICE}$ [*Hanson and Mauersberger,* 1988]. The actual formation process, however, is still a matter of debate [*Peter,* 1997; *WMO,* 1999]. The greater the region occupied by PSC particles, the greater the probability of large-scale ozone reduction in spring. Indeed, low Arctic springtime ozone levels were observed during cold stratospheric winters [*Rex et al.,* 1997]. Low temperatures inside the vortex are related to weak planetary wave forcing [*Coy et al.,* 1997; *Newman and Nash,* 2000].

During the winters of 1995/1996–2004/2005 field campaigns involving ground-based lidar and balloon-borne sonde measurements were undertaken at Sodankylä. During these campaigns systematic measurements of stratospheric profiles of ozone and aerosols were conducted; during some of the winters, in situ measurements of stratospheric water vapour were made. A large proportion of measured polar stratospheric cloud data has been analyzed with respect to the microphysical aspects of the particles, e.g. by *Stein et al.* [1999] and *Rosen et al.* [1997]. Especially PSC type I observations, which form the majority of observations, have been studied systematically. The less common PSC type II events in the Arctic have been reported e.g. by *Vömel et al.* [1997], *Kivi et al.* [1998b], *Dörnbrack et al*. [1999], *Kivi et al.* [2000a], *Kivi et al.* [2001], *Müller et al.* [2001], *Kivi et al.* [2004b] and *Maturilli and Dörnbrack* [2006].

In the absence of condensation, the stratospheric water vapour abundance is controlled by photochemistry and dynamics. Vertical transport from the troposphere in the tropics provides an important source of stratospheric water vapour, limited by freeze-drying at the cold tropical tropopause [*Brewer*, 1949]. In the upper stratosphere, methane oxidation acts as the primary water vapour source within the stratosphere [*Abbas et al*., 1996; *Michelsen et al.,* 2000], generally leading to an increase of water vapour from the lowermost strato-

sphere to the stratopause. The general circulation accumulates trace gases including water vapour by descent within the polar vortex. Thus the downward transport in the polar vortex leads to higher water vapour amounts in the vortex than those at the source regions. Consequently, a horizontal gradient across the vortex edge arises in the lower stratosphere with higher mixing ratios inside than outside the vortex. The actual quantity of stratospheric water vapour in the Arctic is an important parameter not only for ozone chemistry, but also for inferring the radiative budget and the resulting vertical motion inside the polar vortex. During the winters of 2002/2003–2005/2006 accurate measurements of stratospheric water vapour were performed at Sodankylä using in situ balloon-borne instruments. These measurements have contributed to the knowledge of the actual water vapour distribution in the polar stratospheric vortex and in the vicinity of the vortex in the lower stratosphere, as well as to an understanding of the processes affecting the fine-scale distribution of water vapour.

5.2. Instruments

The ground-based lidar used during the years 1996–1999 was assembled around a Nd:YAG laser with detection at 355, 387, 532 and 1064 nm, allowing a determination of the ratio between the total backscatter coefficient and the pure molecular one (backscatter ratio) at 532 nm, 355 nm and 1064 nm, and the depolarization ratio at 532 nm. The lidar and its subsystems are described in detail by *Matthey et al.*, [1997]. Balloon-borne backscatter sondes [*Rosen and Kjome*, 1991] were flown during the period 1994–2006, some of them near simultaneously with the lidar measurements [*Kivi et al*., 1998b, 1999c]. The sondes measure aerosol backscatter at wavelengths λ = 490 and 940 nm with an average vertical resolution of 30 m [*Rosen and Kjome,* 1991]. The backscatter ratio R_λ is defined as the ratio of total (i.e., aerosol and molecular) to the molecular backscatter. Pressure, temperature, ozone density, and tropospheric relative humidity are measured simultaneously. The instrument signal noise relevant for the measurements is of the order of 1%. The aerosol color index CI, defined by $(R_{940}-1)/(R_{490}-1)$, serves as a rough estimate of particle sizes, and allows one to distinguish between liquid (CI < 6) and solid (CI > 9) particles [*Larsen et al.,* 1997].

Water vapour was measured by a balloon-borne frost point hygrometer developed by the National Oceanic and Atmospheric Administration/ Climate Monitoring and Diagnostics Laboratory (NOAA/CMDL) [*Oltmans*, 1985, *Vömel et al.*, 1995]. This instrument measures the temperature of a cryogen-cooled chilled mirror which maintains a small and constant layer of water ice. Therefore, the temperature of the air passing through the sensor equals the frost-point temperature of H_2O. By applying the formula for the saturation water pressure p_{sat} over a plane ice surface, the water vapour mixing ratio q_{H2O} can be

estimated. The overall accuracy of the instrument is stated to be better than 10% [*Vömel et al.*, 1995]. The temperature profiles were measured by Vaisala RS 80 sensors. Their accuracy is ± 0.5 K and the data were recorded every 2 s ($\Delta z \approx$ 8 m during a typical ascent of the plastic balloons used during the winter campaigns).

Recently, a new instrument has been developed that can be flown on small meteorological balloons, and is suitable for polar process studies in the stratosphere as well as for long-term trend studies. This instrument, a cryogenic frost point hygrometer (CFH), is currently built at the University of Colorado and is in part based on the earlier NOAA/CMDL frost point hygrometer. The new CFH sensor uses the same basic principle as the NOAA sensor: a frost layer on a gold coated mirror that is optically measured and kept constant through a feedback system. The absolute accuracy of the CFH instrument depends on altitude, and ranges between 3% in the lower troposphere to less than 10% in the middle stratosphere at 28 km. A full description of the CFH design and measurement characteristics is given by *Vömel et al.* [2007c].

At Sodankylä the first flights of the CFH instrument were made during the LAPBIAT Upper Tropospheric Lower Stratospheric Water Vapour Validation Project (LAUTLOS-WAVVAP) campaign in February 2004 [*Deuber et al.,* 2005; *Karpechko et al.*, 2007, *Vömel et al.,* 2007a; *Suortti et al.,* 2007]. Since then the instrument has been improved, and the new version of the instrument was flown at Sodankylä between December 2005 and December 2006. In total the author has employed eight flights using the improved version of the instrument. Up to December 2006 another light-weight water vapour instrument (the Fast Lyman-alpha Stratospheric Hygrometer of the Central Aerological Observatory) was flown during four flights in a dual balloon payload with the CFH instrument for comparison purposes. In general both instruments have shown good agreement and very similar small-scale vertical layering of water vapour in the Arctic lower stratosphere, in most cases related to differential advection.

5.3. Observations

At Sodankylä both aerosol-profiling instruments (the lidar and the sondes) were deployed during the cold events in the Arctic stratosphere when, according to stratospheric forecasts, PSCs were expected. In addition, temperature profiles from regular radiosondes, available every 12 hours, were used to plan the balloon-borne instrument launches. Table 7 summarises the aerosol backscatter sonde launches during the period 1996–1999.

Table 7. Summary of aerosol backscatter balloon-borne soundings

Date	Launch time UTC	Burst level [hPa/km]	PSCs at altitudes [km]	Max scattering ratio at 940 nm in PSC/ altitude [km]	minimum temperature [deg C]/ altitude [km]
960214	16:58	14.5/ 26.2	16–20, 22–23	8/ 19.2	–85.5/ 22.6
960217	23:20	17.2/ 25.1	15–17, 22–22.6	4.4/ 15.5	–82.3/ 20.2
960303	19:04	16.3/ 25.9	17–20	6.1/ 18.4	–82.2/ 20.1
960327	20:02	19.5/ 25.1	no PSC	–	–72.0/ 19.1
970105	19.14	15.5 / 26.1	24–26	nan/ 25.2	–82.5/ 24.8
970107	23.13	14.9 / 26.2	23.5–25.9	8.2/ 25.3	–82.8/ 23.9
970114	19.40	13.9 / 27.0	23.7–25.2	4.9/ 24.5	–86.0/ 24.1
970119	18.36	15.8 / 25.8	20.5–21, 23.2–24	19.7/ 20.9	–90.2/ 23.2
970122	19.06	13.1 / 27.1	21.5–27	352/ 26.3	–91.9/ 26.3
970316	19:40	14.0/ 27.2	no PSC	–	–70.4/ 16.6
971216	14:08	12.5/ 27.5	20–24	102.6/ 21	–88.4/ 23.2
980124	17:15	13.3/ 27.0	20–22	5.0/ 21.2	–83.5/ 21.7
980126	17:51	16.9/ 25.3	20–21.5	16.9/ 20.4	–85.6/ 23.6
980319	18:52	17.6/ 25.8	no PSC	–	–72.1 / 22.2
990126	21:20	12.9/ 27.6	no PSC	–	–72.9/ 23.1
990220	1:35	15.2/ 26.4	no PSC	–	–78.6/ 23.7

During the winter campaigns of 1994/1995 and 1996/1997 (the cold Arctic stratospheric winters) observations were made of 40 different PSC of type I and in two cases (during January 22–23, 1997), PSC of type II were detected by the lidar system [*Kivi et al*., 1998b; *Stein et al*., 1999]. In winter 1997/1998 another PSC type II event was observed by the lidar system: on December 16, 1997, the lidar measured an ice PSC at an altitude of 22–23 km for a duration of 2 hours in the presence of record low December temperatures for this altitude. Some of the PSC type II events are likely to be not detected by the ground-based lidar, because of the presence of thick tropospheric clouds preventing the remote sensing by the laser beam. Balloon-borne techniques were used on such occasions. In the following sections, individual case studies of PSC type II events are presented. Balloon-borne observations were made during all of these events; in the first case study, in addition, the temporal development of the particle backscatter measured by the lidar is presented.

5.3.1. Ice PSC observation in January 1997

One of the most spectacular PSC measurements was made both by lidar and sondes in January 1997. On 22 January 1997 one of the lowest stratospheric

temperature in more than 40 years of observations was recorded, when a radiosonde launched at Sodankylä achieved the minimum temperature of 178.6 K at an altitude between 25 and 26 km.

Lidar measurements on January 22nd detected ice PSCs between 1:30 and 4:00 UT around 23 km of altitude: in the 532 nm channel the backscatter ratio was 30–50, with a depolarization ratio around 12%. The second PSC of type II with similar optical characteristics was detected about 24 hours later between 25 and 27 km of altitude, lasting for approximately 3 hours. The structure of this PSC was less homogeneous, and it was superimposed by layers of PSC type Id, according to the classification by *Stein et al*. [1999]. The second PSC was also sampled by a balloon-borne backscatter sonde, which reached the PSC altitude at approximately 21 UT on January 22nd. The highest backscatter ratios were reached at an altitude of 25–26.5 km, in the 490 nm channel the peak value was 30, while the depolarization was about 20% throughout the whole altitude range of the PSC layers. The lidar measurement, which started at 20 UTC on January 22nd, detected a PSC type Id in the same altitude range. This difference may be explained by the different locations of the measurements, because of the sonde drift of about 200 km downwind of Sodankylä. However, the lidar profile obtained at 1:30 on January 23rd shows similar values at the altitude of the highest backscatter, taking into account differences in the wavelengths used by the instruments (Figure 21).

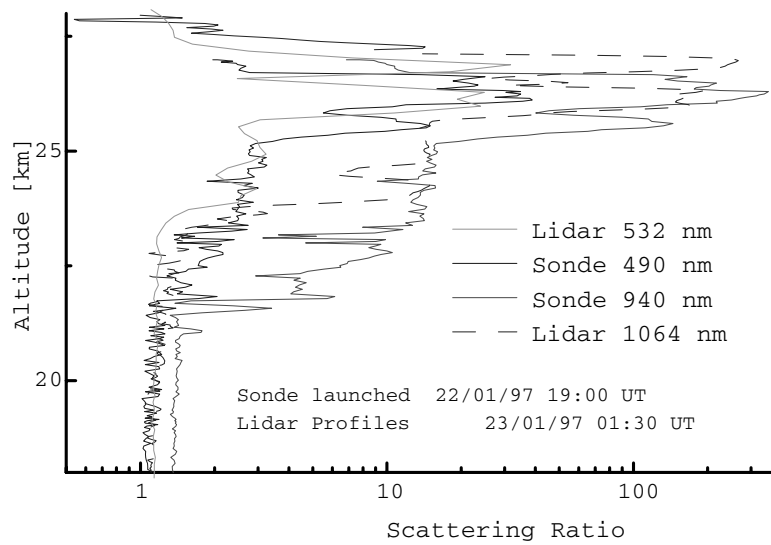

Figure 21. Aerosol backscatter profiles by a ground-based multiwavelength lidar and balloon-borne sonde launched at Sodankylä during the PSC type II event on January 22–23, 1997.

The lidar observations are shown in Figure 22. The “dark” areas on the plot indicate high backscatter ratios, corresponding to cells of ice particles within the cloud. These cells can be of different scales and are superimposed by other particles, which are not in the ice phase. The meteorological fields were not adequately resolved by synoptic-scale meteorological analysis; a special setup of a mesoscale model (MM5) was therefore needed, as described in detail in *Dörnbrack et al.* [1999]. MM5 is a non-hydrostatic meteorological model developed by National Center for Atmospheric Research (NCAR) [*Dudhia*, 1993]. Both the vertical cross sections (Figure 23) and the horizontal sections (Figure 24) by the model are shown corresponding to the timing of the lidar observations.

The MM5 simulation showed good agreement with the observations at the altitude of the lowest temperatures, showing that mesoscale cooling in a mountain wave may reach up to 13 K. In Figure 25 a comparison of the measured temperature profile with the mesoscale model MM5 simulation is shown. The record low temperatures at an altitude of 26 km due to orographic forcing were captured by the model simulations. Due to the drift of the balloon and the large horizontal temperature gradients, the model profile was calculated to correspond to the actual balloon profile. Furthermore, the location of the eastern mesoscale temperature anomaly, simulated by the model 200 km downwind of Sodankylä agrees with the balloon-borne backscatter observation of the PSCs in that region.

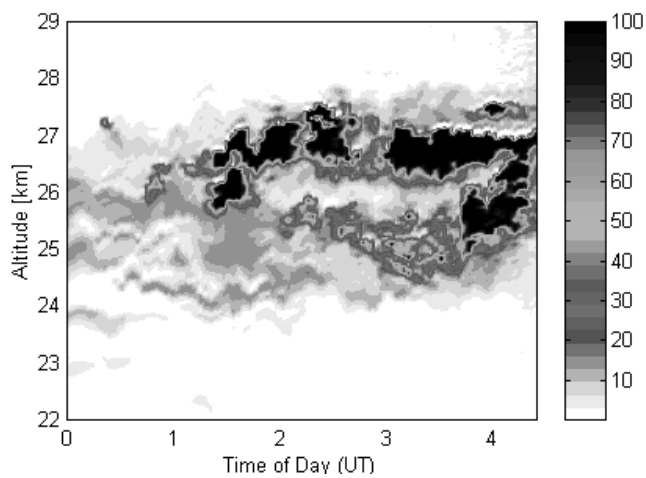

Figure 22. Ice PSC observed above a ground-based lidar station at Sodankylä, Finland on 23 Jan 1997. The color bar indicates the aerosol backscatter ratio at 1064 nm, the time resolution is 3.3 minutes and vertical resolution is 15 m.

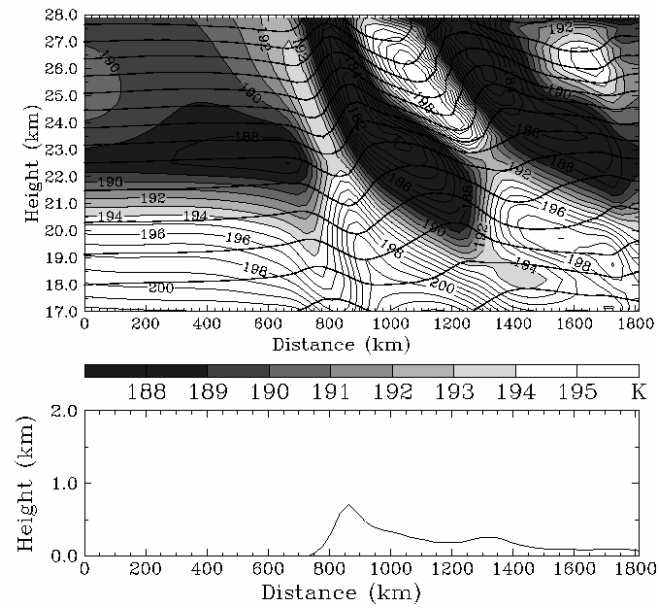

Figure 23. Mesoscale meteorological model MM5 simulation showing vertical structure of temperature and potential temperature (thick lines) fluctuations associated with the mountain wave event of 22–23 Jan 1997. Bottom: terrain height along the section.

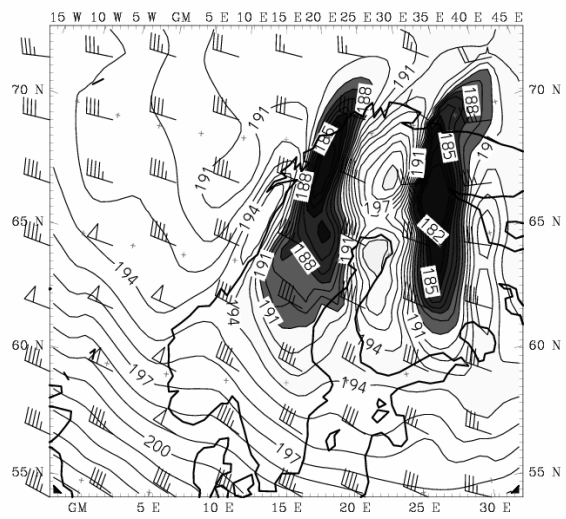

Figure 24. Temperature and winds on the 600K potential temperature surface for 22/01/1997, 12 UTC simulated by the model MM5.

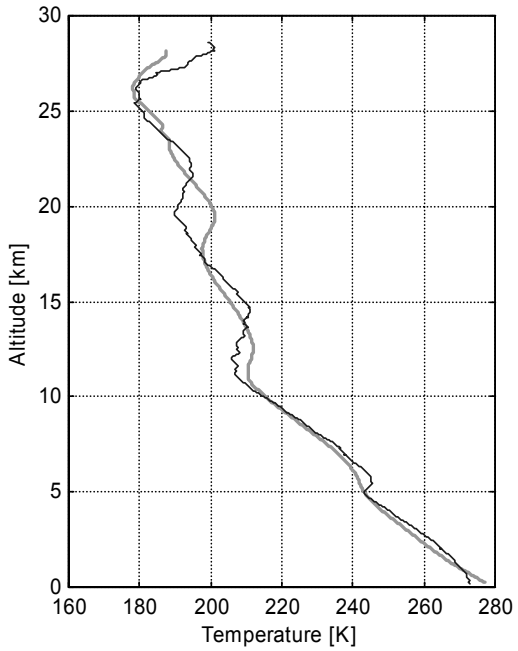

Figure 25. Observed and simulated (by MM5) temperature profile on Jan 22, 1997 12 UT at Sodankylä during the mountain wave event which caused the record low temperatures of 178.6 K at an altitude of 26 km: high-resolution radiosonde (solid line) and model temperature along the actual balloon trajectory (dashed line).

The same event was also simulated using a version of the Finnish Meteorological Institute of the High Resolution Limited Area Model HIRLAM [*Rontu*, *private communication,* 1998]. The HIRLAM model showed development on January 22nd 1997 of a second cold region about 500 km downstream of the mountains with minimum temperatures of 184 K at the 15 hPa level, while the minimum temperatures on a synoptic-scale were around 190 K (Figure 26).

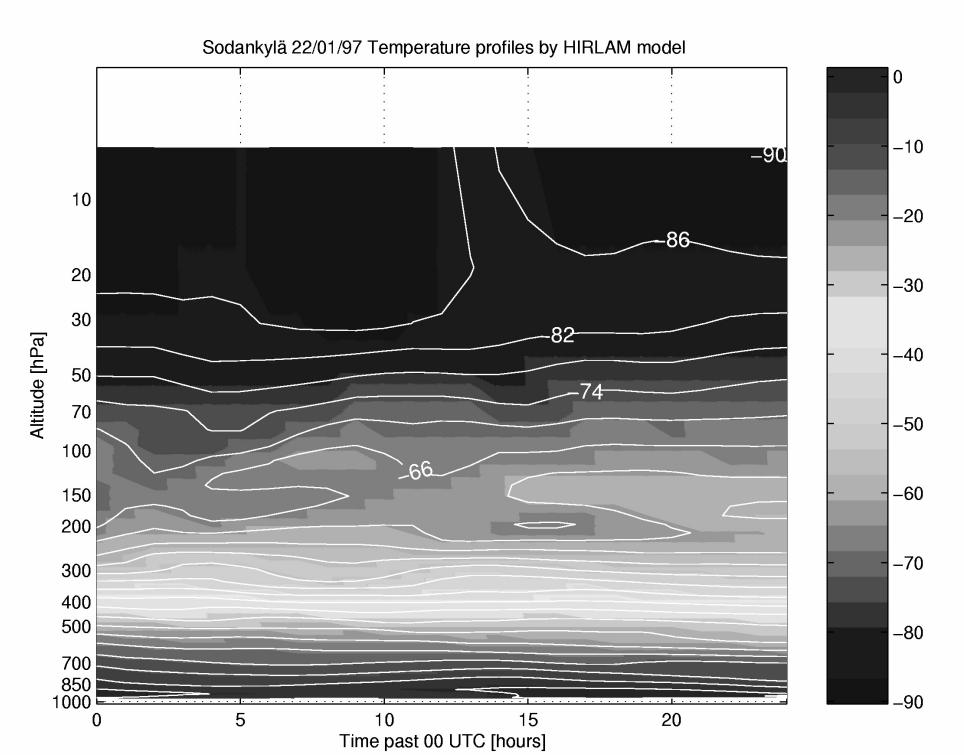

Figure 26. Mesoscale model (FMI-HIRLAM) simulation of the temporal development of the vertical distribution of temperature above Sodankylä for 24 h from January 22, 1997 00 UTC.

The models suggest that this PSC event can be interpreted as a consequence of adiabatic cooling along the isentropes induced by large-scale gravity waves influenced by the Coriolis force. Mountain-wave-induced PSCs are frequently observed at Kiruna near the Scandinavian mountain range [*Enell et al.*, 1999]. Airborne lidar measurements [*Wirth et al.,* 1999; *Dörnbrack and Flentje, private communication*, 2000] show that these PSCs may extend hundreds of kilometres downstream associated with a gradual decrease in cloud tops. Often another almost as massive ice cloud is found further downstream above northern Finland, revealing the same pattern.

5.3.2. Stratospheric ice clouds in January 2001

On 12 and 13 January 2001 backscatter sondes launched at Sodankylä detected an extraordinarily thick polar stratospheric cloud layer with a vertical extent of more than 8 km. On these days the polar vortex passed over northern Scandinavia. This provided synoptic-scale low stratospheric temperatures leading to the formation of both liquid and solid phase particles. Two days later, on 15 January 2001, a regular radiosonde measured a record low temperature of 176.7 K at an altitude of 25.2 km at the vortex edge. High vertical resolution radiosonde profiles and meteorological analyses indicated strong mountain wave activity on this day. This provides further evidence that the lowest temperatures in the Arctic lower stratosphere occur as a consequence of mountain-wave cooling under cold synoptic-scale background conditions.

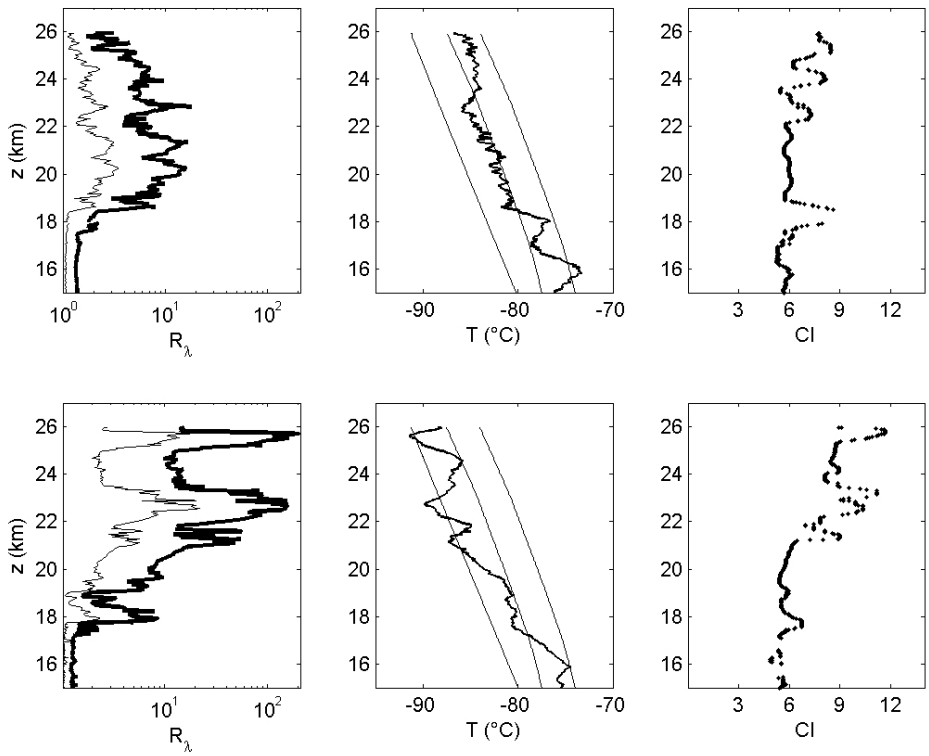

Figure 27. Left: Vertical profiles of backscatter ratio R_λ on 12 January 2001 at 17:40 UT (top) and 13 January 2001 at 17:52 UT (bottom) measured by balloon-borne backscatter sondes. Thick solid lines mark λ = 940 nm, thin lines λ = 490 nm. Middle: Corresponding temperature profiles. The threshold temperatures $T_{ICE} < T_{STS} < T_{NAT}$ are indicated by the straight solid lines. They have been calculated assuming a volume mixing ratio of 5 ppm for water vapour and a LIMS profile at 68° N for HNO_3 [*Carslaw et al.,* 1994]. Right: The aerosol color index CI = $(R_{940}-1)/(R_{490}-1)$.

On both 12 and 13 January a thick PSC layer was detected extending from an altitude of about 18 to 26 km (Figure 27). On 12 January, the backscatter ratios R_{940} and R_{490} fluctuated around 7 and 2, respectively. The color index was generally small (around 6). Between altitudes of 18 and 23 km the temperature dropped slightly below T_{STS}. Thus, the cloud layer was mainly composed of liquid droplets, most likely a STS. On 13 January, the stratosphere above 20 km cooled down by about 4 K and a pronounced stratification developed (Figure 27, bottom). The backscatter ratio R_λ for both λ increased dramatically in the cold layers (maximum values $R_{940} \approx 55$, 150, and more than 200 at altitudes of approximately 21.5, 22.5, and 25.5 km were obtained). The values of R_{490} were generally smaller, but increased significantly in the three layers as well. CI-values greater than 9 were found in all of the cold layers, which indicate the presence of water ice particles. Furthermore, the maximum R_λ-values correspond to regions with $T < T_{ICE}$.

In Figure 28a, the temperature profiles of the two backscatter sondes are shown together with a sequence of high vertical resolution radiosonde profiles in the period from 11 to 17 January. Temperatures below the frost point were measured during each sonde launch between 13 and 14 January. In the period shown, a remarkable rise and fall of the tropopause with a maximum to minimum difference of about 4 km occurred. During this event the tropopause reached its maximum height of about 13 km on 13 January at 18 UT. This value is more than 3 km larger than the long-term average tropopause level in January at Sodankylä.

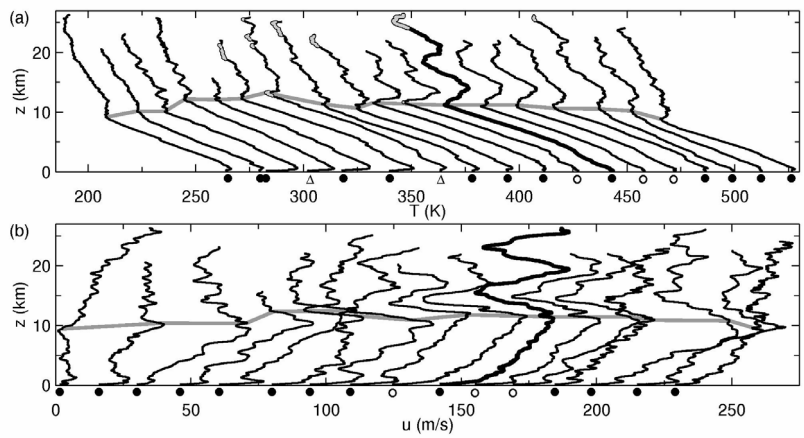

Figure 28. High vertical resolution profiles of temperature (a) and horizontal wind speed (b) measured by radiosondes launched at Sodankylä between 11 January 2001 at 12 UT and 17 January 2001 at 12 UT. Regular 12-hourly soundings are marked by full circles. Additional soundings (open circles) were launched on 15 January 2001 at 06 UT, 15 UT, and 18 UT (from left to right). The temperature profiles shown in Figure 26 are marked by triangles. Consecutive profiles are each shifted by (a) 15 K and (b) 15 m/s. The thick profile marks the January 15 launch at 12 UT. Grey segments indicate layers with temperatures below T_{ICE}, which is computed as in Figure 27. The grey horizontal thick lines show the tropopause height.

On 15 January 2001, a series of five radiosonde launches enabled the observation of large-amplitude stratospheric temperature fluctuations. The vertical temperature profiles are characterized by a nearly uniform tropopause level and a marked inversion above the tropopause (Figure 28a). However, the rising top of this inversion and the gradually growing stratospheric temperature fluctuations mark the stratospheric wave event. The largest temperature fluctuations on this day occurred at 12 UT. In this sounding, three stratospheric inversions of about +4 K/km (this corresponds to a Brunt-Väisälä frequency of $N \approx 2.6 \cdot 10^{-2}$ s^{-1}; $N=\sqrt{\{g/\Theta \, d\Theta/dz\}}$, where Θ is the potential temperature) alternate with layers where the temperature drops more than 23 K within 4 km ($N \approx 1.4 \cdot 10^{-2}$ s^{-1}). At the base of the highest inversion the sonde measured a record low temperature of 176.7 K at an altitude of 25.2 km (this is the lowest temperature in the 42-year database of regular radiosoundings at Sodankylä). During the night and the following day the wave amplitude diminished and the tropopause descended.

The amplification of the large-amplitude stratospheric temperature fluctuations occurred concurrently with a steady increase in the near-surface wind speed and the wind speed maximum near the tropopause (Figure 28b). There, maximum values of 50–55 m/s were attained on 14 to 15 January almost simultaneously with the stratospheric wave event. In the stratosphere, a wave-structured vertical profile of the horizontal wind speed gradually developed in a similar way as for the temperature.

Figure 29 explains the temporal evolution of the stratospheric and tropospheric flow by meteorological analyses during the considered period. In the troposphere, the track of an intensifying cyclone north of Greenland got deflected by a stable anticyclone (blocking high) extending from the Atlantic Ocean to central Europe (Figure 29, bottom). The evolving counter-rotating vortices caused a strong westerly flow over the Scandinavian mountain range after 13 January 2001. Furthermore, in the stratosphere, the polar vortex passed over northern Scandinavia in the period shown (Figure 29, top and middle). This advection of cold stratospheric air masses increased the temperature difference between the middle troposphere and lower stratosphere. Large values of this temperature difference are related to a high tropopause if tropospheric and stratospheric temperature gradients do not change essentially [*Zängl and Hoinka,* 2001]. Here, the temperature difference between the 5 and 15 km levels increased from 33 to 58 K (first and sixth profile in Figure 28a) between 11 and 13 January. This, and the extending anticyclone, can explain the unusual high and cold tropopause on the latter date. Accordingly, minimum temperatures (Figure 27, right) and a low value of integrated total ozone (25% below the mean for January, not shown) were measured above Sodankylä on this day.

As suggested by the ECMWF analyses in Figure 29, the polar vortex passed over northern Scandinavia in a period of only 5 days (top), accompanied by a significant synoptic-scale stratospheric temperature decrease between 11 and

13 January (middle). Thus, the temperature conditions conducive to the PSCs observed by the backscatter sondes were synoptically generated inside the polar vortex. Furthermore, the amplification of the backscattered signal is consistent with the decreasing temperature (increasing potential vorticity) above Sodankylä due to the passing vortex.

The observed depth of the cold layer can be explained by the rapid and undisturbed evolution of the polar vortex prior to the cold event. In the winter of 2000/2001 the polar vortex developed in a short, three-week period starting in late December. The vortex spun up quickly without significant perturbations due to planetary waves. The zonally-averaged meridional heat flux was low, and correlated strongly with minimum temperatures inside the vortex prior to the PSC observations. Thus, an unusual deep and cold layer could develop. The period considered remained the coldest event of the winter 2000/2001 above Sodankylä.

Optical in situ measurements can be used to estimate the chemical composition of cloud particles. The detected synoptic-scale PSCs are interpreted as mainly composed of STS droplets. Thin NAT layers are identified within the ternary PSC. Close to the inner edge of the polar vortex, thick layers of water ice particles were determined in the bulk of the PSC.

At Sodankylä, backscatter ratio profiles often exhibit a pronounced layering of increased R_λ like that of Figure 27. On January 13 this feature can be explained by small-amplitude gravity waves (less than 4 K) excited by the jet stream. Later on, between 14 and 16 January, large-amplitude stratospheric temperature fluctuations (Figure 28a) were caused by the nearly uniform flow over the Scandinavian mountain range (see geopotential heights in Figure 29, bottom). Since the flow was stationary for more than 12 hours, inertia gravity waves could propagate into the stratosphere during this time and cause vertically displaced isentropes at stratospheric levels far downstream of the mountains (see also [*Dörnbrack et al.,* 1999]). In addition, visual observations at Sodankylä confirmed the existence of wave-like PSCs on 15 and 16 January.

The stratospheric wave activity can be quantified by calculating the potential energy density $E_{pot}=0.5\cdot g^2/N^2\cdot\overline{[((T'/T_0)^2)]}$ from stratospheric temperature fluctuations T'. These T' are the deviations from a mean background profile T_0 determined by fitting a quadratic polynomial to the temperature profile in a 7 km altitude range starting 4 km above the tropopause. The overbar indicates the average over this range. Generally, the stratospheric wave activity increased significantly during the polar vortex passage (Figure 28). The highest energy density of $E_{pot} \approx 20$ J/kg is obtained for 15 January 12 UT, when the record low temperature was measured. This value is more than ten times larger than the climatological January average of E_{pot} at Sodankylä.

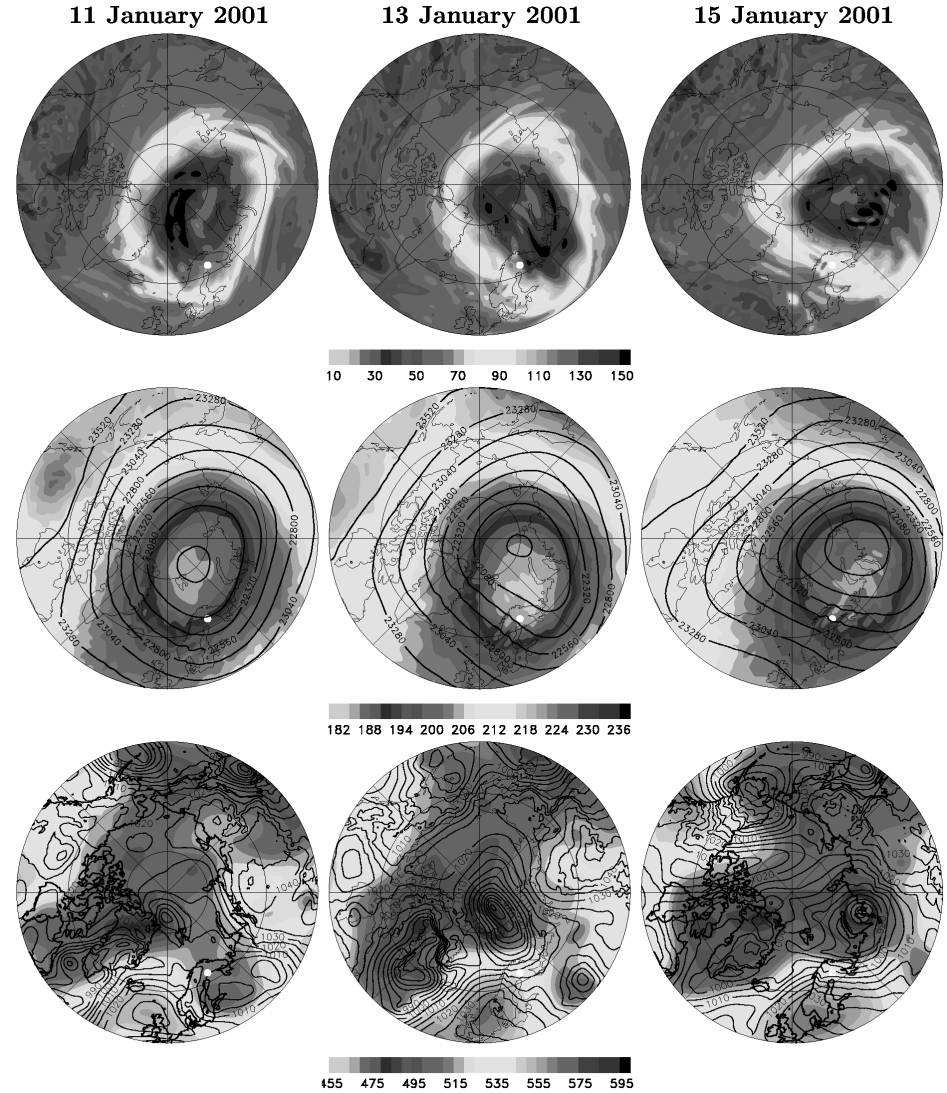

Figure 29. Tropospheric and stratospheric ECMWF analyses in a polar stereographic projection on 11, 13, and 15 January 2001 at 12 UT. Bottom: Mean sea level pressure (hPa, black lines) and geopotential height on 500 hPa (decametre, color shading). Latitude circles at 80˚ N and 60˚ N are plotted. The white spots mark the position of Sodankylä. Middle: Temperature (K) and geopotential height (m) on the 30 hPa surface. Top: Potential vorticity (10^{-6} K m^2 kg s^{-1}) at the 550 K isentropic surface.

At Sodankylä, PSCs between altitudes of 15 and 27 km have been observed during last decade, but in only one case was the detected PSC thickness similar

to that case [*Vömel et al.,* 1997]. The evolution of tropospheric weather systems enabled the excitation of inertia gravity waves at the Scandinavian mountain range. These mountain waves caused significant stratospheric temperature anomalies far downstream of their source: a radiosonde measured a record low temperature at the polar vortex edge.

In the relatively warm Arctic stratospheric winter of 2000/2001, the polar vortex was stable for only three weeks. The overall fraction of possible PSC area inside the vortex was not greater than in previous winters. However, vertically thick PSCs were detected inside the polar vortex in mid-January 2001.

5.3.3. Ice PSCs and stratospheric dehydration in January 2005

Temperatures in the Arctic vortex were exceptionally low in late January 2005. On 26 January 2005, a balloon-borne frost point hygrometer launched at Sodankylä detected layers of water vapour dehydration in an altitude range of 18–23 km. Beneath an altitude of 18.5 km a 1 km deep rehydrated layer was identified. Nearly simultaneous aerosol backscatter sonde measurements revealed the presence of stratospheric ice clouds. Meteorological analysis indicates ice-supersaturated regions produced by mountain waves at the edge of and inside the polar vortex. In contrast to the Antarctic vortex, previous observations of reduced stratospheric water vapour and ice particle formation have been relatively rare in the Northern Hemisphere, and there have been no previous reports on the possible rehydration of water vapour in the Arctic stratosphere.

Stratospheric dehydration, i.e., the large-scale removal of water vapour from the polar vortex, has been rarely observed in the Arctic. There are reports about particular events based on balloon-borne observations with different types of in-situ sensors [e.g., *Vömel et al.,* 1997; *Schiller et al.,* 2002]. Additionally, remote-sensing by the Microwave Limb Sounder (MLS) onboard the Upper Atmosphere Research Satellite (UARS) and by the Aura satellite allows a continuous monitoring of the northern hemispheric stratospheric water vapour distribution [e.g., *Herman et al.,* 2002; *Nedoluha et al*., 2003]. However, in contrast to the fine vertical resolution ($\Delta z = 10$ m) of the in situ measurements by balloons, the limb sounding gives vertical profiles of the water vapour mixing ratio q_{H2O} with Δz ranging between 3 and 5 km and covering a horizontal area of 200×200 km^2.

Based on the MLS data, *Jiménez et al.* [2006] recently reported a widespread dehydration (a 0.5 ppmv q_{H2O}-drop with respect to the vortex background value) during the exceptionally cold Arctic winter 2004/2005 [*Manney et al.*, 2006]. Dehydration between 12 and 20 km altitude was observed above the Atlantic Ocean, the Norwegian and Barents Seas south of Spitsbergen and north of

Scandinavia on three consecutive days (from 25 till 27 January 2005). The time-series of the areas of reduced q_{H2O} indicate two separated, coherent regions apparently propagating eastward (Figure 6 in *Jiménez et al.* [2006]). Based on reverse trajectory calculations the authors concluded that the water vapour depletion is due to large-scale condensation inside the cold Arctic vortex.

This is in accordance with the first appearance of a stratospheric ice cloud in the long-term record of the German lidar at Ny-Ålesund, Spitsbergen (78.9º N, 11.9º E) on 26 January 2005 [*Maturilli and Dörnbrack*, 2006]. The authors argued that the cloud formation and the associated H_2O-reduction was most likely due to the adiabatic cooling in the ascending branches of mountain waves locally excited by the flow past Spitsbergen.

Here the focus is on stratospheric observations by balloon-borne instruments launched at Sodankylä during the same period from 24 till 27 January 2005. The concurrent appearance of both stratospheric ice clouds and significant H_2O-reduction was observed. Additionally, the balloon-borne frostpoint hygrometer measured layers of water vapour increase with respect to the climatological mean inside the polar vortex.

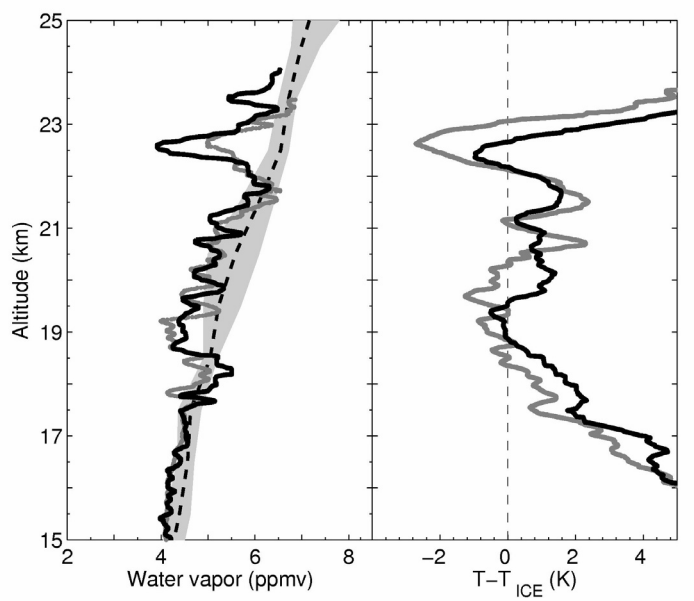

Figure 30. Frost point hygrometer q_{H2O} observations on 26 January 2005 (left panel). Balloon ascent data are shown in grey and descent data in black. The balloon was launched at 15:53 UTC. The average water vapour profile in winter 2004/2005 of all inside-vortex soundings is marked by the dashed line, their respective minimum and maximum values being sketched by the shaded area. The right panel presents $T-T_{ICE}$ for the 26 January 2005 sounding using the mean inside-vortex water vapour profile to calculate T_{ICE}.

Making use of operational T511/L60 European Centre for Medium Range Weather Forecast (ECMWF) analyses, the temperature history of the sampled air mass was analysed in order to find possible causes for the observed H_2O-profile. Estimates about the formation conditions of ice particles lead to hypotheses about the physical processes responsible for this event. Here the Sodankylä observations are discussed in the context of the dynamical processes occurring during the period considered.

Water vapour was measured by a balloon-borne frostpoint hygrometer described before. The frostpoint hygrometer was launched on 26 January 2005 at 15:53 UTC. The balloon burst at an altitude of 26.2 km at 17:36 UTC after drifting about 50.8 km southeast (147.5º) of Sodankylä. Both balloon ascent and descent q_{H2O} data are shown in Figure 30a. Between the altitude of 18.5 km (≈ 60 hPa) and 23.5 km (≈ 25 hPa) q_{H2O} was significantly reduced by up to 2 ppmv with respect to an average, undisturbed profile calculated from all inside-vortex observations of the winter 2004/2005. Below z = 18.5 km, the descent data revealed a slight increase in q_{H2O} by 0.5 ppmv in a 1 km deep layer. Collocated temperature measurements showed that the layers of reduced q_{H2O} corresponded to minimum temperatures close to or even below T_{ICE}; the strongest cooling was associated with the largest q_{H2O}-depletion near z ≈ 22.5 km (Figure 30b). The bulk of the depleted q_{H2O}-layer was characterized by strongly fluctuating temperatures close to T_{ICE}. In contrast, the region of increased q_{H2O} was associated with increasing values of T. The increased water vapour beneath an altitude of 18.5 km in a 1 km deep layer may be an indication of an enhancement of water vapour above the normal values due to the evaporation of falling ice particles. Previously the rehydration process has only been observed in the Antarctic [*Vömel et al.*, 1995]. There is another layer of enhanced water vapour at 21.5 km and some thinner layers in the 19–21 km region. The ice frost point T_{ICE} was calculated according to *Marti and Mauersberger* [1993] and assuming the undisturbed q_{H2O}-profile from observations. For a recent discussion about the accuracy of the frost point calculations see *Murphy and Koop* [2005].

The high backscatter values R_λ measured by the sonde launched at 21:06 UTC (i.e., about three hours after the q_{H2O} observations) indicated the existence of a polar stratospheric cloud (PSC) covering an unusually deep layer between altitudes of 16 and 25.5 km (Figure 31). Throughout this layer, $R_{940} > 5$, attaining $R_{940} \approx 30\ldots100$ in vertically thin ($\Delta z < 500$ m) layers at heights between 19 and 22 km. Their high backscatter ratios and CI > 10 indicate the presence of ice particles. This interpretation is supported by the corresponding layers of $T \leq T_{ICE}$. It is likely that the remaining part of the PSC layer consisted of solid particles, as CI was predominately larger than 9 and the temperatures were well below the existence temperature for nitric acid trihydrate (T_{NAT}). This fact is supported by nearly uniform cross-polarization values of 30% at λ = 490 nm at altitudes from 16 to 24 km.

Backscatter observations before and after that event (sondes launched on 24 January at 17:30 UTC and on 27 January at 18:55 UTC, respectively) revealed distinct states of the stratospheric air mass above Sodankylä. The bulk of the PSC observed on January 24 consisted predominantly of liquid particles ($R_{940} < 5$, $CI \leq 6$); only the upper and lower edges indicated the presence of solid particles ($CI \approx 9$), probably NAT, as $T < T_{NAT}$. However, the large R_λ values on 27 January resemble those observed one day before, i.e., the PSC consisted mainly of solid particles (Figure 31). Here, the ice particles with $R_{940} > 10$ are confined to a single layer between altitudes of 19 and 21 km corresponding to $T \approx T_{ICE}$.

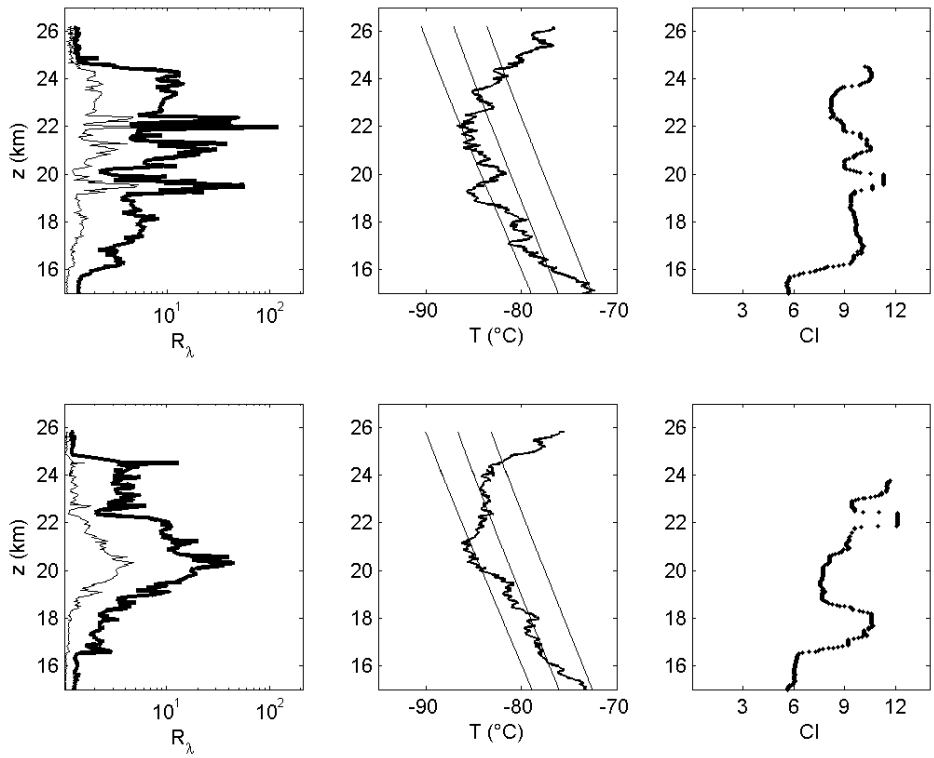

Figure 31. Left**:** Vertical profiles of aerosol backscatter ratio R_λ on January 26, 2005 at 21:06 UTC (top) and January 27, 2005 at 18:55 UTC (bottom) measured by balloon-borne backscatter sondes. Thick solid lines mark λ = 940 nm, thin lines λ = 490 nm. Middle: Corresponding temperature profiles. The threshold temperatures $T_{ICE} < T_{STS} < T_{NAT}$ are indicated by the straight solid lines. These are calculated assuming mean inside-vortex volume mixing ratios of water vapour and a LIMS profile at 68° N for HNO_3. Right: The aerosol color index $CI = (R_{940} - 1)/(R_{490} - 1)$.

Comparing the water vapour and backscatter observations of 26 January 2006, the strongest reduction in H_2O occurs above z = 22 km. Although $R_{940} \approx 10$, $T > T_{ICE}$ does not allow the existence of ice particles. Ice particle layers were predominantly observed at lower altitudes corresponding to layers of $T < T_{ICE}$. Here, water vapour was reduced in the mean by 0.5 ppmv. This region displayed the properties of a quasi-homogeneous mixed layer with fluctuating components of R_{940}, q_{H2O}, and CI.

In order to explore the temperature history of the sampled air mass, backward trajectories were launched from a box between 25 and 30º E and 65 and 68º N on 26 January 2005 at 18 UTC. The applied trajectory scheme [*Wernli and Davis*, 1997] was run with meteorological data provided by T511/L60 operational ECMWF data interpolated on a regular 0.5º×0.5º latitude-longitude grid every 3 hours (6-hourly operational analyses at meteorological standard times plus $t_0 + 3$ h and $t_0 + 9$ h predictions at the intermediate steps based on the deterministic forecasts initialized at t_0 = 00 UTC and t_0 = 12 UTC, respectively).

T_{ICE} was calculated by assuming water vapour values from ECMWF operational analyses (q_{H2O}^{ECMWF}). At 30 hPa, q_{H2O}^{ECMWF} varied between 3.4 and 5.1 ppmv, and at 50 hPa between 2.4 and 4.0 ppmv along the calculated trajectories. However, comparing q_{H2O}^{ECMWF} with the observed profile gives deviations of up to 1.5 ppmv. A similar dry bias was found during an international hygrometer intercomparison LAUTLOS in winter 2003/2004 at Sodankylä [*Deuber et al.,* 2007; *Kivi et al.,* 2007b]. Therefore, a constant value of 1.5 ppmv was added to the actual ECMWF data in order to fit the background value of q_{H2O}.

All backward trajectories passed over the Atlantic in the first 36 hours and crossed Greenland's east coast at about 76º N. The temperature of a good proportion of the air parcels released at both 30 and 50 hPa remained at or dropped below T_{ICE} during the first 30 hours. However, the most prominent cooling of the air parcels- by about 8 K (at 30 hPa) and 11 K (at 50 hPa)- occurred between 48 and 24 hours prior to the observation. Inspection of the pressure change along the trajectories suggests that this cooling was caused by large-scale adiabatic lifting of air parcels by an underlying tropospheric high-pressure system. The largest spread in values of $T - T_{ICE,}$ of up to 8 K between the trajectories, occurred when the air parcels passed Greenland's east coast, probably caused by temperature fluctuations induced by mountain waves.

The meteorological situation on 25 January 2005 at 18 UTC, 24 hours before the q_{H2O}-observation, was characterised by large-amplitude mountain waves along the east coast of Greenland with vertical displacements of the isentropes of up to 2000 m. Depending on the particular upstream conditions, they produced localized regions of $T - T_{ICE} < 0$ in the whole period from 25 January till 27 January 2005; an extreme event was a minimum temperature of 176.5 K at 30 hPa on 26 January 2005 at 12 UTC. In addition to these vertically-

propagating hydrostatic mountain waves the ECMWF analyses also resolved inertia-gravity waves which propagated horizontally away from Greenland's coast line. These waves generated stratospheric temperature anomalies protruding from the polar vortex above the Atlantic Ocean and the Norwegian Sea. Inspection of the location along the trajectory revealed that the air parcels were always located in these wave-generated regions of $T - T_{ICE} < 0$.

In order to investigate whether homogeneous freezing was responsible for the PSC formation, the ice saturation ratio $S_i = p_w/p_{sat}(T)$ was calculated, where p_w is the partial pressure of water vapour and p_{sat} is the saturation vapour pressure over a plane ice surface, calculated after *Sonntag* [1990] (see also *Murphy and Koop* [2005]) along backward trajectories. Furthermore, the freezing threshold saturation ratio S_{cr} for the homogeneous nucleation of ice crystals from supercooled aqueous solution droplets [*Koop et al.*, 2000] was computed, using the approximation by *Kärcher and Lohmann* [2002]. The ratio S_i/S_{cr} for all backward trajectories during the previous 36 h showed that the ECMWF analyzed temperature fluctuated slightly around 185 K at 30 hPa (22 km) and 188 K at 50 hPa (19 km). Although S_i was larger than 1, the ice saturation ratio S_i never exceeded the threshold S_{cr}. Air parcels released 3 h before and after 18 UTC at the same locations experienced a similar temperature history and $S_i/S_{cr} < 1$ all the time. S_i/S_{cr} had a maximum near the east coast of Greenland (0.90 and 0.96 at 30 and 50 hPa, respectively) and had values of about 0.7 over Scandinavia. The large spread of the S_i/S_{cr} values above the Greenland's coast line was caused by the mountain-wave induced stratospheric temperature anomalies resolved by the T511/L60 operational analyses.

Recent numerical simulations of the stratospheric temperature field above Greenland by *Leutbecher and Volkert* [2000] indicate that a broader spectrum of mountain waves is resolved by using a finer spatial resolution. In particular, rapidly vertically-propagating gravity waves can lower stratospheric temperatures by 10 -15 K [*Kivi et al.*, 1998b, 1999c; *Maturilli and Dörnbrack,* 2006]. These gravity waves with horizontal wavelengths of about 20 km were not resolved in the ECMWF analyses. Their additional contribution might have brought the local temperatures above Greenland's east coast well below T_{ICE} and, eventually, lead to conditions where $S_i/S_{cr} > 1$, large enough for homogeneous ice formation. Mesoscale numerical simulations of the flow over Scandinavia during this period showed no evidence of mountain waves reducing the stratospheric temperature locally above northern Sweden and Finland.

Thus, the meteorological analyses and modelling both support the following picture: polar stratospheric ice clouds were predominantly formed above Greenland's east coast by vertically-propagating mountain waves. Due to the presence of a tropospheric anticyclone between Greenland and Scandinavia the stratospheric isentropes were elevated as well. Thus, the ice particles approximately maintained their temperature or warmed slightly on their way to Scandinavia. Stratospheric temperature fluctuations due to the inertia-gravity

waves over the Atlantic might even have led to additional cooling in regions of $T < T_{ICE}$. Finally, the observed air mass above Sodankylä was composed of solid aerosols with layers of remnants of the ice layer formed over Greenland.

In summary, in the Arctic winter of 2004/2005 ice PSCs and Antarctic-like water vapour dehydration and rehydration could be detected by the backscatter sondes and the frostpoint hygrometer launched at Sodankylä. Meteorological analyses suggest a long-lasting formation of ice particles by mountain-wave induced temperature fluctuations locally over the east coast of Greenland as the cause for the exceptional event in the Arctic stratospheric vortex.

5.4. PSC and water vapour measurements in the long-term perspective

The PSC measurements studied here were made in the years 1994–2006. In order to put this period into a long-term perspective and link this to the study of long-term changes of ozone analysed in the first part of the thesis, radiosonde measurements from the years 1965–2006 were used. Radiosondes measuring temperature profiles in the stratosphere have been flown from Sodankylä on a regular basis twice per 24 hours; the dataset thus allows one to calculate estimates of PSC occurrence based on $T<T_{NAT}$. Monthly statistics are shown in Figure 32. It can be seen that the frequency of PSC existence temperatures has increased since the beginning of the 1990s. This tendency is in line with the results of observed ozone decrease shown in the first part of the thesis.

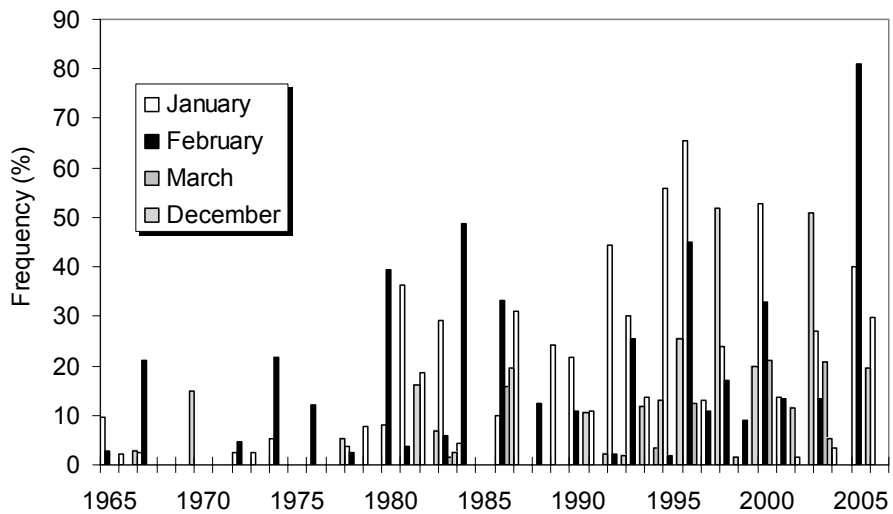

Figure 32. Occurrence of radiosonde temperatures below T_{NAT} at 50 hPa over northern Finland since 1965, grouped by months.

In order to obtain an estimate of the frequency of gravity wave events over northern Scandinavia, data have been analysed using the radiosonde record starting in the winter of 1984/1985. Cases of strong low-level wind (> 10 m/s) were selected together with a wind direction across the Scandinavian mountain range (between 255 and 345 degrees); the results are shown in Figure 33. It may be noted that, in many cases, the month of the highest frequency of potential wave events is also characterized by the highest frequency of observed temperatures sufficient for PSC formation, e.g. January 1996 and December 1997. However, here the main uncertainties arise from the fact that in some winters, e.g. 1996/1997, the lowest temperatures may occur at altitudes higher than that of balloon burst.

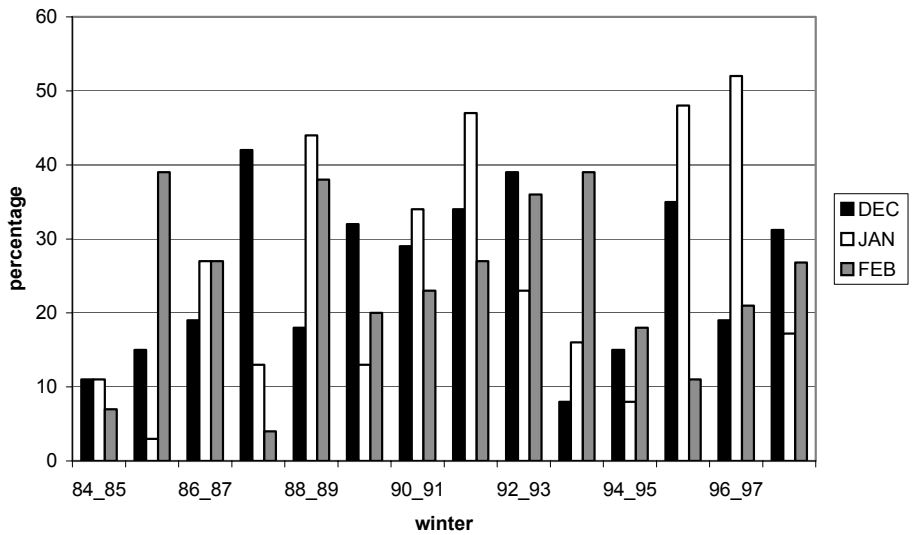

Figure 33. Occurrence of favorable conditions for orographic waves over northern Scandinavia.

At Sodankylä both aerosol-profiling instruments (the lidar and the sondes) were deployed during cold events when PSCs were expected according to stratospheric forecasts. In addition, temperature profiles from regular radiosondes, available every 12 hours, were used to plan the balloon-borne instrument launches. According to regular radiosonde profiles, there have been 1–3 events each winter when the temperature has been below the water ice threshold (Figure 34). As a summary of all observations, the ice particle layers were 0.5–1.5 km in vertical extent, their lowest altitude being 21.5 km and highest 27 km. The peak aerosol backscatter ratio at 532 nm (lidar observations) was generally

30 or greater, with an aerosol depolarization around 10%. According to the profiles from aerosol backscatter sondes, the peak backscatter ratio in the 940 nm channel varied between 100 and 350 in layers having a local temperature 0.5–3 K below the water ice threshold.

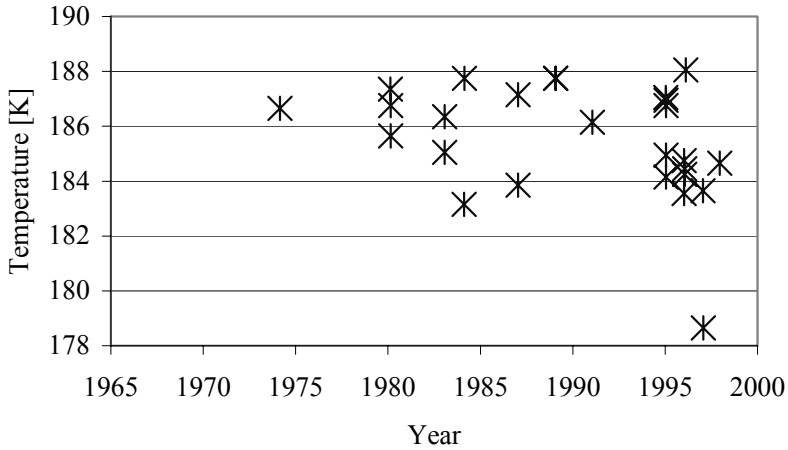

Figure 34. Radiosonde observations of temperatures below T_{ICE} over northern Finland since 1965.

Lidar and balloon-borne observations performed in northern Finland provide evidence of the occurrence of PSC type II during the very cold events in the Arctic stratosphere. According to long-term radiosonde data, these events occur 1 to 3 times every winter. Strong wavelike structures in the temperature profiles measured by radiosonde are a common feature in all these cases. It is likely that mesoscale processes like orographic gravity waves cause the observed temperature anomalies. The occurrence of favourable conditions for the propagation of gravity waves into the stratosphere over northern Scandinavia was calculated from long-term radiosonde data, showing a variability between 3 and 52 percent per month.

Both large-scale and small-scale disturbances can be detected from radiosonde profiles [e.g., *Shutts et al.*, 1998]. In the winter of 1998/1999, the multiple sonde technique proposed by *Shutts et al.* [1994] was tested at Sodankylä. For this purpose two ground receivers were installed: a DigiCora MW15 and a MARWIN MW12 by Vaisala, while an additional MicroCora receiver was used as a backup system, although without the Loran-C wind-finding system. All radiosondes were RS-80 by Vaisala, the balloon type being the Totex CR350 and, on some occasions during the early part of the campaign period, the CR1200. During multiple launches, balloons of the same type were filled with different amounts of gas in order to adjust the relative spacing of the sonde trajectories. An example of a multiple sonde launch is shown in Figure 35.

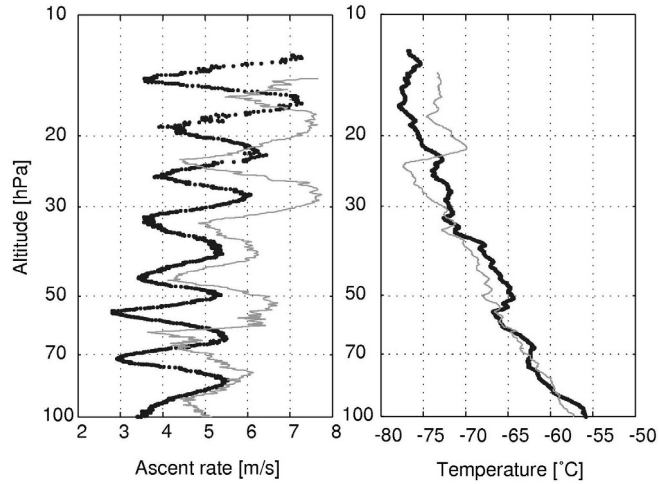

Figure 35. Radiosonde profiles of ascent rate and temperature of two quasi-simultaneous balloon launches from Sodankylä (67.4º N, 26.6º E) on February 1, 1999 at 06:29 (thick dotted line) and 06:47 (thin line).

As the second balloon, launched 18 minutes later, was adjusted for a higher ascent rate, it reached the 50 hPa surface almost simultaneously with the first sonde, but at a different horizontal location. The temperature as well as the ascent rate profile shows wavelike disturbances above 100 hPa. The origin for the gravity waves in this case was a strong shear in the jet stream at about 200 hPa. In the ascent rate, the peak-to-peak amplitude is about 3 m/s and, in the temperature sounding, amplitudes of maximum 7 K were recorded. In both soundings the vertical wavelength was about 2 km.

Within this thesis work, an analysis of synoptic-scale and mesoscale processes was made for each observed ice PSC event. It was found that, in general, the ice PSC observations during years of a weak and disturbed vortex were associated with mesoscale effects, in the presence of low temperatures on a synoptic scale however. Only in 1995/1996 were synoptic-scale temperatures over Scandinavia sufficient to explain the observed particle layers. Except for this one case, there are similarities in the location of tropospheric pressure systems during observed ice PSC events: generally, deep low-pressure systems travel north-easterly over the Norwegian Sea. In all studied cases, a blocking high pressure system over Scotland controlled the storm tracks that led to strong westerly winds throughout the troposphere in northern Scandinavia. In the wintertime stratosphere, westerlies prevail, so that in these cases the directional wind shear is small between the stratosphere and troposphere. These flow conditions favour the excitation and propagation of gravity waves with their

source in the lower troposphere as discussed in *Dörnbrack et al*. [1999]. In conclusion, the cases considered show that ice PSCs above northern Finland occur mainly under meteorological conditions that are favourable for mountain wave propagation up to stratospheric levels. The Scandinavian mountain range produces inertial gravity waves that lead to significant vertical displacements some hundreds of kilometres downstream. The case study for January 2005 shows that the source of the gravity wave observed over Scandinavia can alternatively be the Greenland mountains.

PSC formation depends on the amount of available water vapour. Stratospheric water vapour sondes have been flown at Sodankylä during every Arctic winter since 2002/2003. In Figure 36 the results are presented, grouped according to whether they are inside- or outside-vortex measurements. The outside-vortex measurements represent the typical mid-latitude water vapour mixing ratio distribution, with values typically between 4–5 ppmv in the lower stratosphere. The inside-vortex water vapour mixing ratio is between 5 and 7 ppmv, according to these measurements. In theory, one might expect higher water vapour values if sampling high-latitude water vapour due to transport through the large-scale stratospheric circulation. One of the important questions is whether or not stratospheric water vapour is increasing, as is seen from mid-latitude measurements. If such a trend exists in the polar stratosphere, it would mean further cooling of the lower stratosphere and a larger potential for the formation of polar stratospheric clouds. All this would lead to a delay in the recovery of the level of polar stratospheric ozone. These first years of water vapour sonde observations in the Arctic are therefore important material for future trend studies.

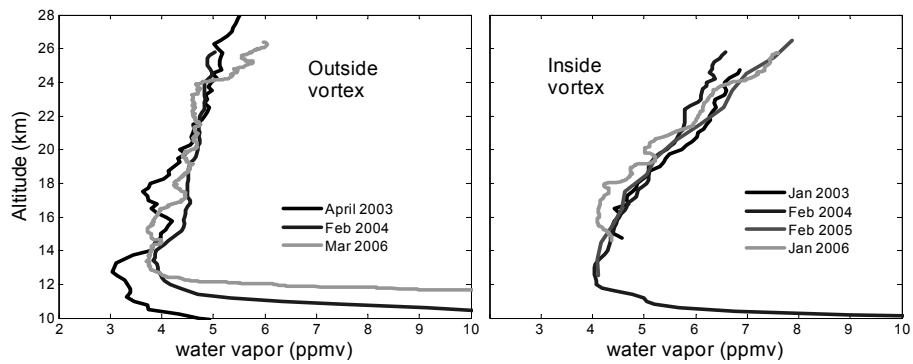

Figure 36. Profiles of stratospheric water vapour inside and outside the Arctic vortex as measured by balloon-borne instruments launched at Sodankylä during the Arctic winters of 2002/2003–2005/2006.

6. CONCLUSIONS

In both the stratosphere and the troposphere, the largest long-term changes in ozone profiles have occurred in the late winter/spring period (January-April), the period of greatest interannual variability. For the time-period 1989–1996 there are significant negative trends in the stratosphere in January–April of -3.2 ± 1.0%/year at altitudes between 150 and 40 hPa, with a smaller decrease in the 40–10 hPa layer of -1.9 ± 1.1 %/year. However, trends since then are positive: 4.9 ± 2.6 %/year between the tropopause and 150 hPa, 3.3 ± 2.0 %/year for 150–40 hPa and 1.6 ± 1.2 %/year at higher levels (40–10 hPa).

In order to explain the ozone trends and interannual changes, a multilinear regression model was applied to the ensemble ozonesonde data. A model using four explanatory variables in the stratosphere (average tropopause height, the calculated volume of polar stratospheric clouds adjusted by the effective equivalent stratospheric chlorine (EESC), the 100 hPa eddy heat flux averaged over 45–70º N, and the mean aerosol backscatter in the 200–100 hPa range) was able to explain 65% – 95%, depending on altitude, of the observed variance throughout the stratosphere in January-April. These proxies account for the changes in the synoptic-scale dynamical processes, the vortex ozone depletion, the ozone transport through the residual circulation, and the Mt. Pinatubo aerosol effect, respectively.

When the seasonal ozone profiles were reconstructed using the proxy time series, the reconstructed profiles agreed to within 5% with those observed in the winter-spring period, except for the winters 1989 and 2003, where the dynamical variance within the period January-April was too large. The March ozone profiles for 1989 and 2003 were also reconstructed and showed much less disagreement between the model and the observed ozone anomalies. No a priori information about the expected altitude ranges of the explanatory variables were used in the fit, and it was therefore remarkable that the multilinear regression yields altitude distributions for the coefficients that are in reasonably good agreement with the dynamical and chemical considerations. Quantitatively, in the case of the volume of polar stratospheric clouds or the vortex ozone loss proxy, the ozone depletion potential obtained from the multilinear regression analysis is 2.2 DU/10^6 km^3, a value close to that reported by *Rex et al.* [2004].

The model suggests that, in the stratosphere, the observed negative trends prior to 1996–1997 can be attributed to the combined effect of chemical and dynamical changes, while the observed increase since then is primarily due to the dynamical influences in the model.

In the troposphere, positive trends are found in all seasons. The trend in the January-April season for 1989–2003 is 1.1 ± 0.2%/year, while in the May – August period it is 0.7 ± 0.2%/year, and in the September–December period it is 0.6 ± 0.2%/year. In the explanatory regression model the tropopause altitude

term was replaced by the Arctic oscillation term, which provided the main contribution to the tropospheric ozone trends and interannual variability during January–April (65% of the explained variability in the troposphere). A possible reason is that the Arctic Oscillation regulates the transport of ozone and its precursors from industrialized regions towards the pole. It may also modulate stratosphere-troposphere exchange. The model explains up to 70–80% of the variability in the troposphere in the winter/spring season, and the trends of the model residuals become insignificant throughout the troposphere.

Ozonesondes have the benefit of high vertical resolution and are independent of solar light. They are the only source of internally coherent (after known corrections) long-term winter ozone data in the Arctic. According to the ensemble dataset obtained from the Arctic ozone soundings over the period 1989–2003, the largest negative deviations of total ozone occurred in January-April 1996 and 1997. This differs from mid-latitudes, where the largest negative deviations are found in 1993 [*WMO*, 2003]. Strong negative anomalies in total ozone have also been observed in the recent winters of 2000, 2003 and 2005; rapid Arctic ozone losses are predicted to occur in the future, because significant concentrations of ozone-depleting substances will remain in the atmosphere for several decades, and global climate change may cool the stratosphere further [*WMO*, 2003]. The results also suggest that a possible major volcanic eruption would have a strong impact on stratospheric ozone levels over the Arctic for at least for 1–2 years after the eruption. Continued ozonesonde measurements will help to detect stratospheric ozone recovery in high latitudes as a result of the reductions in ozone-depleting substances outlined in the Montreal Protocol.

The ozonesonde data have been homogenized using the results of a series of dual and multiple ozonesonde flights performed at Sodankylä (Finland) to characterize the influence of the concentration of the sensing solution used in the electrochemical concentration cell (ECC) sondes. These sonde flights at Sodankylä show that the use of a 1% potassium iodide (KI) sensing solution leads to a 2–8% difference, depending on altitude, between the ozone retrievals by the EN-SCI and SPC types of ECC ozonesondes. Another field experiment carried out at Sodankylä focused on the influence of thermistor positioning. The differences observed during the test flights were used in the present study to remove inhomogeneites related to changes in thermistor positioning. This correction was found to be about 3% in the stratosphere above 150 hPa and between 1 and 3% below the 150 hPa level, decreasing linearly with decreasing altitude in the troposphere.

The Sodankylä Total Ozone Intercomparison and Validation Campaign in March -April 2006 provided an excellent opportunity to assess the performance of the currently-used ozonesonde systems. During the campaign period the use of a 0.5% KI sensing solution for EN-SCI sondes led to relatively small differences (on average –0.8 ± 1.5%) compared to the best total ozone estimate

from 5 Brewer instruments. A similar difference using the OMI measurements was 1.0 ± 2.0%. The campaign period was characterized by a large amount of short-term ozone variability (lowest ozone column 416 DU, highest 501 DU during the ozonesonde ascents, average total ozone 459 ± 24 DU) and strong horizontal gradients in ozone, which are likely to explain part of the observed scatter in the comparison data, especially during the first half of the campaign. Agreement with Lidar observations is found to be within 0–5% in the altitude range of 15–30 km, and 5–10% in the layer 30–35 km (altitude dependent range).

In addition, balloon sonde observations were compared to aircraft measurements in the winter of 1996/1997. The first-ever scientific campaign involving the M55 Geophysica stratospheric aircraft was conducted at Rovaniemi (Finland) and provided a unique opportunity to obtain high-resolution information on the ozone distribution in the vicinity of the Arctic stratospheric vortex. In this work the aircraft measurements are compared to the sonde measurements using the technique of mapping the observed ozone in potential vorticity/ potential temperature space. It is found that the average difference between the aircraft-borne and balloon-borne sensors was –5.7 ± 2.8% when measurements inside the polar vortex were considered.

As part of the polar stratospheric cloud (PSC) study, an analysis of synoptic-scale and mesoscale processes was made for each observed ice PSC event. It was found that in general the ice PSC observations during years of a weak and disturbed polar stratospheric vortex were associated with mesoscale effects, in the presence, however, of low temperatures on the synoptic scale. Only in 1995/1996 were synoptic-scale temperatures over Scandinavia sufficiently low to explain the observed particle layers. Apart from this particular case, there were similarities in the location of tropospheric pressure systems during observed ice PSC events: generally, low-pressure systems were located to the north of Scandinavia causing strong westerly winds throughout the troposphere. In the wintertime stratosphere, westerlies prevail, so that in these cases the directional wind shear is small between the stratosphere and the troposphere. These flow conditions favour the excitation and propagation of gravity waves having their source in the lower troposphere. Thus the cases considered show that ice PSCs above northern Finland occur mainly under meteorological conditions that are favourable for mountain-wave propagation up to stratospheric levels. The Scandinavian mountain range produces inertial gravity waves that lead to significant vertical displacements some hundreds of kilometres downstream. The case study for January 2005 shows that, alternatively, the source of the gravity waves observed over Scandinavia can be the Greenland mountains.

The in situ measurements of the PSCs were accompanied by in situ profile measurements of stratospheric water vapour. These measurements showed Antarctic-like water vapour depletion events at times when the temperature

dropped below the critical value of ice PSC formation temperatures. Significant water vapour dehydration was observed twice during the measurements; during the January 2005 observation, layers of increased water vapour were also observed. The latter can be explained by a rehydration process associated with the falling ice particles. The water vapour measurements in the Arctic stratosphere are also part of a new climatology program with the aim of detecting trends in stratospheric water vapour, which has a strong impact on the chemical and radiative properties of the lower stratosphere. Presently observations since 2002/2003 are available; these provide an insight into the interannual variability of the inside- and outside-vortex water vapour profiles depending on the location of the polar stratospheric vortex with respect to the measurement site at Sodankylä.

7. REFERENCES

Andersen, S. B., B. M. Knudsen (2002), The influence of vortex ozone depletion on Arctic ozone trends, *Geophys. Res. Lett.*, *29*, doi:10.1029/2001GL014595.

Bodeker, G. E., I. S. Boyd, and W. A. Matthews (1998), Trends and variability in vertical ozone and temperature profiles measured by ozonesondes at Lauder, New Zealand: 1986–1996, *J. Geophys. Res.*, *103*(D22), 28,661–28,681.

Borrmann, S., S. Solomon, J. E. Dye, D. Baumgardner, K. K. Kelly, K. R. Chan (1997), Heterogeneous reactions on stratospheric background aerosols, volcanic sulfuric acid droplets, and type I polar stratospheric clouds: Effects of temperature fluctuations and differences in particle phase, *J. Geophys. Res.,* 102(D3), 3639–3648, 10.1029/96JD02976.

Boyd, I., G. Bodeker, B. Connor, D. Swart, and E. Brinksma (1998), An assessment of ECC ozonesondes operated using 1% and 0.5% KI cathode solutions at Lauder, New Zealand, *Geophys. Res. Lett.*, *25*(13), 2409–2412.

Brönnimann, S., J. Luterbacher, C. Schmutz, H. Wanner, and J. Staehelin (2000), Variability of total ozone at Arosa, Switzerland, since 1931 related to atmospheric circulation indices, *Geophys. Res. Lett.*, *27*, 2213–2216, doi:10.1029/1999GL011057.

Brunner, D., J. Staehelin, J. A. Maeder, I. Wohltmann, and G. E. Bodeker (2006), Variability and trends in total and vertically resolved stratospheric ozone, *Atmos. Chem. Phys. Discuss.*, *6*, 6317–6368.

Carslaw, K., B. Luo, S. Clegg, T. Peter, P. Brimblecombe and P. Crutzen (1994), Stratospheric aerosol growth and HNO_3 gas phase depletion from coupled HNO_3 and water uptake by liquid particles, *Geophys. Res. Lett.,* 21*,* 2479–2482.

Carslaw, K. S., B. Luo, T. Peter (1995), An analytic expression for the composition of aqueous HNO3 - H2SO4 stratospheric aerosols including gas phase removal of HNO3, Geophys. Res. Lett., 22(14), 1877–1880, 10.1029/95GL01668.

Carslaw, K. S., Peter T. and Clegg S.L. (1997), Modelling the composition of liquid stratospheric aerosols, *Review of Geophysics*, 37, 125–154.

Carslaw, K. S. and Peter T. (1997), Uncertainties in reactive uptake coefficients for solid stratospheric particles-1. Surface chemistry, *Geophys. Res. Lett.,* 24, 1743–1746.

Carslaw, K. S., M. Wirth, A. Tsias, et al. (1998), Increased stratospheric ozone depletion due to mountain-induced atmospheric waves, *Nature*, 391, 675–678

Carslaw, K. S., M. Wirth, A. Tsias, B. P. Luo, A. Dörnbrack, M. Leutbecher, H. Volkert, W. Renger, J. T. Bachmeister, T. Peter (1998), Particle microphysics and chemistry in remotely observed mountain polar stratospheric clouds, *J. Geophys. Res.,* 103(D5), 5785–5796, 10.1029/97JD03626.

Carslaw, K.S., Peter T., Bacmeister J.T., Eckermann S.D. (1999), Widespread solid particle formation by mountain waves in the Arctic stratosphere, *J. Geophys. Res.*, 104, 1827–1836.

Chipperfield, M. P. et al., 3D CTM Calculations for Arctic Winter 1996/97, Proceedings of the IV Europ. Workshop on Stratos. Ozone, Germany, 1997.

Christensen, T., Knudsen, B., Streibel, M., Andersen, S., Benesova, A., Braathen, G., Claude, H., Davies, J., De Backer, H., Dier, H., Dorokhov, V., Gerding, M., Gil, M., Henchoz, B., Kelder, H., Kivi, R., Kyro, E., Litynska, Z., Moore, D., Peters, G., Skrivankova, P., Stubi, R., Turunen, T., Vaughan, G., Viatte, P., Vik, A., Gathen, P.

and Zaitcev, I. (2005), Vortex-averaged Arctic ozone depletion in the winter 2002/2003, *Atmospheric Chemistry and Physics*, Vol. 5, pp 131–138.

Coy, L., E. R. Nash, and P. A. Newman (1997), Meteorolgy of the polar vortex: Spring 1997, *Geophys. Res. Lett,* 24*,* 2693–2696.

Del Guasta, M. Morandi, L. Stefanutti, S. Balestri, E. Kyrö, M.Rummukainen, R. Kivi, V. Rizi, F. Masci, B. Stein, C. Wedekind, B.Mielke, F. Immler, R. Matthey, V. Mitev, M. Douard (1998), Lidar Observation of Spherical particles in a 65 deg cirrus observed above Sodankyla, *J. Aerosol Science*, Vol. 29, No. 3, 357–374.

Deuber B., A. Haefele, D. G. Feist, L. Martin, N. Kämpfer, G. E. Nedoluha, V. Yushkov, S. Khaykin, R. Kivi, H. Vömel (2005), Middle Atmospheric Water Vapour Radiometer (MIAWARA): Validation and first results of the LAPBIAT Upper Tropospheric Lower Stratospheric Water Vapour Validation Project (LAUTLOS-WAVVAP) campaign, *J. Geophys. Res.,* 110, D13306, doi:10.1029/2004JD005543.

Dibb, J. E., R. W. Talbot, E. Scheuer, G. Seid, L. DeBell, B. Lefer, and B. Ridley (2003), Stratospheric influence on the northern North American free troposphere during TOPSE: 7Be as a stratospheric tracer, *J. Geophys. Res.*, *108*(D4), 8363, doi:10.1029/2001JD001347.

Dobson, G. M. B., and D. N. Harrison (1926), Measurements of the amount of ozone in the Earth's atmosphere and its reaction to other geophysical conditions, *Proc. R. Soc. London, Ser. A*, *110*, 660–693.

Dörnbrack, A., M. Leutbecher, R. Kivi, and E. Kyrö (1999), Mountain wave induced record low stratospheric temperatures above Northern Scandinavia, *Tellus*, 51A, p. 951–963.

Dörnbrack, A., M. Leutbecher (2001), Relevance of mountain waves for the formation of polar stratospheric clouds over Scandinavia: A 20 year climatology, *J. Geophys. Res*., 106(D2), 1583–1594, 10.1029/2000JD900250.

Dörnbrack, A., M. Leutbecher, J. Reichardt, A. Behrendt, K.-P. Müller, G. Baumgarten (2001), Relevance of mountain wave cooling for the formation of polar stratospheric clouds over Scandinavia: Mesoscale dynamics and observations for January 1997, *J. Geophys. Res.*, 106(D2), 1569–1582, 10.1029/2000JD900194.

Dye, J. E., Baumgardner D., Gandrud B. W., Kawa S. R., Kelly K. K., Loewenstein M., Ferry G.V., Chan K. R., and Gary B. L. (1992), Particle size distributions in Arctic polar stratospheric clouds, growth and freezing of sulfuric acid droplets, and implications for cloud formation, *J. Geophys. Res.,* 97, 8015–8034.

Enell, C.-F., Å. Steen, T. Wagner, U. Fries, K. Pfeilsticker, U. Platt, K.-H. Fricke (1999), Occurrence of polar stratospheric clouds at Kiruna, *Ann. Geophysicae*, 17, 1457–1462.

EN-SCI Corporation (1996), *Instruction Manual, Model 1Z ECC-O3-Sondes*, Boulder, Colo.

Farman, J. C., B. G. Gardiner, and J. D. Shanklin (1985), Large losses of total ozone in the Antarctica reveal seasonal ClO_x/NO_x interaction, *Nature*, *315*, 201–210.

Fioletov, V. E., J. B. Kerr, D. I. Wardle, J. Davies, E. W. Hare, C. T. McElroy, and D. W. Tarasick (1997), Long-term ozone decline over the Canadian Arctic to early 1997 from ground-based and balloon observations, *Geophys. Res. Lett.*, *24(22)*, 2705–2708, doi:10.1029/97GL52829.

Fioletov, V. E., G. E. Bodeker, A. J. Miller, R. D. McPeters, and R. Stolarski (2002), Global and zonal total ozone variations estimated from ground-based and satellite measurements: 1964–2000, *J. Geophys. Res.*, *107*, 4647, doi:10.1029/2001JD001350.

Fortuin, J., and H. Kelder (1998), An ozone climatology based on ozonesonde and satellite measurements, *J. Geophys. Res.*, *103*, 31,709–31,734.

Fusco, A. C., and M. L. Salby (1999), Interannual variations of total ozone and their relationship to variations of planetary wave activity, *J. Clim.*, *12*, 1619–1629.

Fusco, A. C., and J. A. Logan (2003), Analysis of 1970–1995 trends in tropospheric ozone at Northern Hemisphere midlatitudes with the GEOS-CHEM model, *J. Geophys. Res.*, *108*(D15), 4449, doi:10.1029/2002JD002742.

Georgiadis T., F. Ravegnany, L. Stefanutti, V. Yushkov, A. Oulanovsky, and N. Lechenu (1997), Some results of in situ ozone measurements with fast ozone analyser (FOZAN) on board high-altitude aircraft GEOPHYSICA during APE, Proceedings of the IV Europ. Workshop on Stratos. Ozone, Germany.

Hadjinicolaou, P., A. Jrrar, J. A. Pyle, and L. Bishop (2002), The dynamically driven long-term trend in stratospheric ozone over northern middle latitudes, *Q. J. R. Meteorol. Soc*, *128*, 1393–1412.

Hadjinicolaou, P., J. Pyle, and N. Harris (2005), The recent turnaround in stratospheric ozone over northern middle latitudes: a dynamical modelling perspective, *Geophys. Res. Lett.*, *32*, L12821, doi:10.1029/2005GL022476.

Hanson, D., and K. Mauersberger (1988), Laboratory studies of the nitric acid trihydrate: implications for the south polar stratosphere, *Geophys. Res. Lett.,* 15*,* 855–858.

Herman, R. L., K. Drdla, J. R. Spackman, D. F. Hurst, P. J. Popp, C. R. Webster, P. A. Romashkin, J. W. Elkins, E. M. Weinstock, G. C. T. B. W. Gandrud, M. R. Schoeberl, H. Jost, E. L. Atlas, and T. P. Bui (2002), Hydration, dehydration, and the total hydrogen budget of the 1999/2000 winter arctic stratosphere, *J. Geophys. Res.*, *108*(D5), 8320, doi:10.1029/2001JD001257.

Hoinka, K. P., H. Claude, and U. Köhler (1996), On the correlation between tropopause pressure and ozone above central europe, *Geophys. Res. Lett.*, *23*, 1753–1756.

Hoiskar, B.A.K., Dahlback, A., Vaughan, G., Braathen, G., Goutail, F., Pommereau, J.-P. and Kivi, R. (1997), Interpretation of ozone measurements by ground-based visible spectroscopy — a study of the seasonal dependence of airmass factors for ozone based on climatology data. *J. Quant. Spectrosc. Radiat. Transfer*, 57, p. 569–579.

Hoor, P., Gurk, C., Brunner, D., Hegglin, M. I., Wernli, H., and Fischer, H. (2004), Seasonality and extent of extratropical TST derived from in-situ CO measurements during SPURT, *Atmos. Chem. Phys*., 4, 1427–1442.

Houghton, J., Y. Ding, D. Griggs, M. Noguer, P. van der Linden, X. Dai, K. Maskell, and C. Johnson (Eds.) (2001), *Climate Change 2001: The Scientific Basis*, 881 pp., Cambridge University Press, Cambridge, United Kingdom and New York, NY, USA.

Jiménez C., H. C. Pumphrey, I. A. MacKenzie, G. L. Manney, M. L. Santee, M. J. Schwartz, R. S. Harwood, J. W. Waters (2006), EOS MLS observations of dehydration in the 2004–2005 polar winters, *Geophys. Res. Lett.,* 33, L16806, doi:10.1029/2006GL025926.

Johnson, B. J., S. J. Oltmans, H. Vömel, H. G. J. Smit, T. Deshler, and C. Kröger (2002), Electrochemical concentration cell (ECC) ozonesonde pump efficiency measurements and tests on the sensitivity to ozone of buffered and unbuffered ECC sensor cathode solutions, *J. Geophys. Res.,* 107(D19), 4393, doi:10.1029/2001JD000557.

Kärcher, B., and U. Lohmann (2002), A parameterization of cirrus cloud formation: Homogeneous freezing of supercooled aerosols, *J. Geophys. Res.*, *107*, 4010, doi:10.1029/2001JD000470.

Karpetchko, A., E. Kyrö, and B. M. Knudsen (2005), Arctic and Antarctic polar vortices 1957–2002 as seen from the ERA-40 reanalyses, *J. Geophys. Res.*, *110*(D21), D21109, doi:10.1029/2005JD006113.

Karpechko, A., A. Lukyanov, E. Kyro, S. Khaikin, L. Korshunov, R. Kivi and H. Vömel (2007), The water vapour distribution in the Arctic lowermost stratosphere during LAUTLOS campaign and related transport processes including stratospheretroposphere exchange, *Atmos. Chem. Phys*., 7, 107–119, 2007.

Kawa, S. R., K. D. W. Fahey, J. C. Wilson, M. R. Schoeberl, A. R. Douglass, R. S. Stolarski, E. L. Woodbridge, H. Jonsson, L. R. Lait, P. A. Newman, M. H. Proffitt, D. E. Anderson, M. Loewenstein, K. R. Chan, C. R. Webster, R. D. May, K. K. Kelly, (1993), Interpretation of NO_x/NO_y observations from AASE-II using a model of chemistry along trajectories, *Geophys. Res. Lett.,* 20, 2507–2510.

Keesee, R. G., (1989), Nucleation and particle formation in the upper atmosphere, *J. Geophys. Res.,* 94, 14683–14692.

Kirk-Davidoff, D. B., Hintsa, E. J., Anderson, J. G., and Keith, D. W. (1999), The effect of climate change on ozone depletion through changes in stratospheric water vapour, *Nature*, 402, 399–401.

Kivi, R., E. Kyrö, A. R. MacKenzie, V. V. Rudakov, V. V. Khattatov, M. P. Chipperfield, A. M. Lee, G. O. Braathen, H. Gernandt, I. S. Mikkelsen, and M. Molyneux (1998a), APE/POLECAT transport studies: ozonesondes during APE, Proc. 4th Europ. Workshop on Polar Strat.Ozone, 201–204.

Kivi, R., E. Kyrö, C. Wedekind, L.Rontu, A. Dörnbrack, B. Stein, H. Wille, V. Mitev, R. Matthey, J. Rosen, N. Kjome, V. Rizi, G. Redaelli, B. Lazzarotto, B. Calpini, M. Del Guasta, M. Morandi, L. Stefanutti, P. Agostini, A. Antonelli, M. Rummukainen, T. Turunen, J. Karhu (1998b), SAONAS activities at Sodankylä in winter 1996/1997. Proc. 4th Europ. Workshop on Polar Strat. Ozone, 135–138.

Kivi, R., E. Kyrö, T. Turunen, T. Ulich, and E. Turunen (1999a), Atmospheric trends above Finland. Part II. Troposphere and stratosphere, *Geophysica*, 35, p.71–85.

Kivi R, E. Kyrö, and T. Turunen (1999b), Long-term meteorological monitoring activities at Sodankylä and trends of the recent decade, In: Proc. of Annual Conf. of Geophys. Soc. of Finland, 95–100.

Kivi, R., E. Kyrö, L. Rontu, A. Dörnbrack, M. Müller, C. Wedekind, H.Wille, B. Stein, V. Rizi, G. Redaelli, V. Mitev, R. Matthey, J. Rosen, L.Stefanutti, and M. Del Guasta (1999c), On occurrence of type II PSCs over Northern Finland as observed by Lidar and balloon-borne sondes. In: Mesoscale processes in the stratosphere, 143–147.

Kivi, R., A. Dörnbrack, E. Kyrö, V. Mitev, V. Rizi, and M. Müller (2000a), Ice PSCs above northern Finland: Observations and mesoscale meteorological model simulations, Proc. of the Quadrennial Ozone Symposium, Hokkaido University, Sapporo, 481–482.

Kivi, R., E. Kyrö, A. Dörnbrack, M. Müller, H. Wille, B. Stein, V. Mitev, R. Matthey, L. Stefanutti, M. Del Guasta, and V. Rizi (2000b), Observations of stratospheric temperatures, ozone and aerosols above northern Finland in the winter of 1998/99, Proc. 5th European Workshop on Stratospheric Ozone, St. Jean de Luz, 1999 (N. R. P. Harris, M. Guirlet and G. T. Amanatidis, eds), 169–172.

Kivi, R., E. Kyrö, A. Dörnbrack, T. Birner (2001), Observations of vertically thick polar stratospheric clouds and record low temperature in the Arctic vortex, *Geophys. Res. Lett*., 28 (19), 3661–3664, 10.1029/2001GL013187.

Kivi, R., E. Kyrö, and A. Dörnbrack (2002a), Polar stratospheric cloud and ozone observations in northern Finland during the recent winters, In Proceedings: 2nd AMAP International Symp. on Environmental Pollution of the Arctic, Oslo.

Kivi, R., E. Kyrö, and T. Turunen (2002b), Ozone and temperature observations at Sodankylä, In Proceedings: 2nd AMAP International Symposium on Environmental Pollution of the Arctic, Arctic Monitoring and Assesment Programme AMAP, Oslo, Norway.

Kivi, R., E. Kyrö, A.Dörnbrack, and T. Birner (2003), Polar stratospheric cloud observations in northern Finland during the recent winters, In: Proc. Sixth European Symposium on Stratospheric Ozone (N. R. P. Harris, G. T. Amanatidis, J. G. Levine, eds.), 245–249.

Kivi, R., E. Kyrö, and T. Turunen (2004a), Stratospheric ozone observations at Sodankylä during 1989–2003, in Ozone, Volume 1, Proc. of the Quadrennial Ozone Symposium, Ed. by Chr. Zerefos, University of Athens, Greece, 377–378.

Kivi, R., Kyrö, E., Dörnbrack, A. (2004b), Observations of polar stratospheric clouds at Sodankylä, Finland, in Ozone, Volume 2, Proc. of the Quadrennial Ozone Symposium, Ed. by Chr. Zerefos, University of Athens, Greece, 982–983.

Kivi, R., E. Kyrö, T. Turunen, N. R. P. Harris, P. von der Gathen, M. Rex, S. B. Andersen, I. Wohltmann (2007a), Ozonesonde observations in the Arctic during 1989–2003: ozone variability and trends in the lower stratosphere and free troposphere, *J. Geophys. Res*., 112, D08306, doi:10.1029/2006JD007271.

Kivi, R. et al. (2007b), Ice PSCs and stratospheric dehydration above Sodankylä, submitted to *Geophys. Res. Lett.*

Kivi, R. et al. (2007c), Ozonesonde observations during the Sodankylä Total Ozone Intercomparison and Validation Campaign (SAUNA), to be submitted to *J. Geophys. Res*.

Knudsen, B.M., and G.D. Carver (1994), Accurancy of the isentropic trajectories calculated for the EASOE campaign, *Geophys. Res. Lett.,* 21, 1199–1202.

Knudsen, B. M., N. Larsen, I. S. Mikkelsen, J.-J. Morcrette, G. O. Braathen, E. Kyrö, H. Fast, H. Gernandt, H. Kanzawa, H. Nakane, V. Dorokhov, V. Yushkov, G. Hansen, M. Gil, R. J. Shearman (1998), Ozone depletion in and below the Arctic vortex for 1997, *Geophys. Res. Lett.,* 25(5), 627–630, 10.1029/98GL00300.

Knudsen, B. M, S. B. Andersen (2001), Longitudinal variation in springtime ozone trends, *Nature*, 413, 699 – 700.

Knudsen, B. M., N. R. P. Harris, S. B. Andersen, B. Christiansen, N. Larsen, M. Rex, B. Naujokat (2004), Extrapolating future Arctic ozone losses, *Atmos. Chem. Phys.*, 4, 1849–1856.

Komhyr, W. D. (1969), Electrochemical concentration cells for gas analysis, *Ann. Geophys*., 25, 203–210.

Komhyr, W. D. (1986), Operations handbook — Ozone measurements to 40-km altitude with model 4A electrochemical concentration cell (ECC) ozonesondes (used with 1680 MHz radiosondes), Silver Spring, Md.

Komhyr, W. D., R. A. Barnes, G. Brothers, J. A. Lathrop, and D. P. Opperman (1995), Electrochemical concentration cell ozonesonde performance evaluation during STOIC 1989, *J. Geophys. Res.*, 100, 9231–9244.

Koop, T., U. M. Biermann, W. Raber, B. P. Luo, P. J. Crutzen, T. Peter (1995), Do stratospheric aerosol droplets freeze above the ice frost point, Geophys. Res. Lett., 22(8), 917–920, 10.1029/95GL00814.

Koop, T., K. S. Carslaw and T. Peter (1997), Thermodynamic stability and phase transition of PSC particles, *Geophys. Res. Lett*., 24, 2199–2202.

Koop, T., B. Luo, A. Tsias and T. Peter (2000), Water activity as the determinant for homogeneous ice nucleation in aqueous solutions, *Nature*, *406*, 611–614.

Kyrö, E., et al. (1992), Analysis of the ozone soundings made during first quarter of 1989 in the Arctic, *J. Geophys. Res.*, *97*, 8083–8091.

Kyrö, E., R. Kivi, T. Turunen, H. Aulamo, V.. Rudakov, V. Khattatov, A. R. MacKenzie, M. P. Chipperfield, A. M. Lee, L. Stefanutti, and F. Ravegnani (2000a), Ozone measurements during the Airborne Polar Experiment: aircraft instrument validation; isentropic trends; and hemispheric fields prior to the 1997 Arctic ozone depletion, *J. Geophys. Res*, 105, 14599–14611.

Kyrö, E., R. Kivi, H. Aulamo and J. Damski (2000b), Changes in Arctic Polar Vortex, *Proc. of the Quadrennial Ozone Symposium*, Hokkaido University, Sapporo.

Kyrö, E., T. Turunen, R. Kivi, V. Antikainen, and K. Pienimäki (1998), EEC ozonesonde performance tests, Proc. 4th Europ. Workshop on Polar Strat. Ozone, 692–695.

Laaksonen, A., and M. Kulmala, (1991), Homogeneous heteromolecular nucleation of sulphuric acid and water vapours in the stratospheric conditions: a theoretical study of the effect of hydrate interaction, *J. Aerosol Sci., 22*, 779–787.

Lait, L. R., M. R. Schoeberl, P. A. Newman, M. H. Proffitt, M. Loewnstein, J. R. Podolske, S. E. Strahan, K. R. Chan, B. Gary, J. J. Margitan, E. Browell, M. P. McCormic, and A. Torres (1990), Reconstruction of O_3 and N_2O fields from ER-2, DC-8, and balloon observations, *Geophys. Res. Lett.*, 17, 521–524.

Lait, L. R. (1994), An alternative form for potential vorticity, *J. Atmos. Sci.*, 51, 1754–1759.

Lait, L., Newman, P., Schoeberl, M., McGee, T., Twigg, L., Browell, E., Fenn, M., Grant, W., Butler, C., Bevilacqua, R., Davies, J., DeBacker, H., Andersen, S., Kyrö, E., Kivi, R., Gathen, P., Claude, H., Benesova, A., Skrivankova, P., Dorokhov, V., Zaitcev, I., Braathen, G., Gil, M., Litynska, Z., Moore, D. and Gerding, M. (2004), Non-coincident inter-instrument comparisons of ozone measurements using quasi-conservative coordinates, *Atmospheric Chemistry and Physics*, Vol. 4, 2345–2352.

Lamarque, J.-F., and P. G. Hess (2004), Arctic oscillation modulation of the northern hemisphere spring tropospheric ozone, *Geophys. Res. Lett.*, *31*, L06127, doi:10.1029/2003GL019116.

Larsen, N., B. M. Knudsen, J. M. Rosen, N. T. Kjome, R. Neuber, and E. Kyrö (1997), Temperature histories in liquid and solid polar stratospheric cloud formation, *J. Geophys. Res.*, *102*, 23505–23517.

Larsen, N., I. S. Mikkelsen, B. M. Knudsen, J. Schreiner, C. Voigt, K. Mauersberger, J. M. Rosen, and N. T. Kjome (2000), Comparison of chemical and optical in situ measurements of polar stratospheric cloud particles, *J. Geophys. Res.*, *105,* 1491–1502.

Larsen, N., Knudsen, B., Svendsen, S., Deshler, T., Rosen, J., Kivi, R., Weisser, C., Schreiner, J., Mauerberger, K., Cairo, F., Ovarlez, J., Oelhaf, H. and Spang, R. (2004), Formation of solid particles in synoptic-scale Arctic PSCs in early winter 2002/2003, *Atmospheric Chemistry and Physics*, Vol. 4, 2001–2013.

Leutbecher, M., and H. Volkert (2000), The propagation of mountain waves into the stratosphere: quantitative evaluation of three-dimensional simulations, *J. Atmos. Sci.*, *57*, 3090–3108.

Logan, J. A. (1985), Tropospheric ozone: seasonal behavior, trends and anthropogenic influence, *J. Geophys. Res.*, *90*(10), 463–482.

Logan, J. A. (1994), Trends in the vertical distribution of ozone, an analysis of ozonesonde data, *J. Geophys. Res.*, *99*(25), 25553–25585.

Logan, J. A., et al. (1999), Trends in the vertical distribution of ozone: A comparison of two analyses of ozonesonde data, *J. Geophys. Res.*, *104*(D21), 26373–26400, doi:10.1029/1999JD900300.

Luo, B., T. Peter, P. Crutzen, (1994), Freezing of stratospheric aerosol droplets, *Geophys. Res. Lett.,* 21, 1447–1450, 10.1029/93GL03076.

Ma, J., D. W. Waugh, A. R. Douglass, S. R. Kawa, P. A.Newman, S. Pawson, R. Stolarski, and S. J. Lin (2004), Interannual variability of stratospheric trace gases: The role of extratropical wave driving, *Q. J. R. Meteorol. Soc.*, *130*, 2459–2474.

MacKenzie, A. R., M. Kulmala, A. Laaksonen, T. Vesala, On the theories of type 1 polar stratospheric cloud formation (1995), *J. Geophys. Res.,* 100(D6), 11275–11288, 10.1029/95JD00699.

Manney, G. L., M. L. Santee, L. Froidevaux, K. Hoppel, N. J. Livesey, and J. W. Waters (2006), EOS MLS observations of ozone loss in the 2004–2005 Arctic winter, *Geophys. Res. Lett.*, *33*, L04802, doi:10.1029/2005GL024494.

Manney, G.L., et al. (1994), On the motion of air through the stratospheric polar vortex, *J. Atmos. Science,* 52, 3049–3068.

Marenco, A., H. Gouget, P. Nedelec, and J.-P. Pages (1994), Evidence of a long-term increase in tropospheric ozone from Pic du Midi data series: Consequences: positive radiative forcing, *J. Geophys. Res.*, *99*(16), 617–632.

Marti, J., and K. Mauersberger (1993), A survey and new measurements of ice vapour pressure at temperatures between 170 and 250 k, *Geophys. Res. Lett.*, *20*, 363–366.

Matthey, R., et al. (1997), Depolarisation/backscatter lidar for stratospheric studies, *SPIE*, *3104, Lidar Atmospheric Monitoring, 16–18 June 1997*, Munich, FRG, 2–11.

Maturilli M., A. Dörnbrack (2006), Polar stratospheric ice cloud above Spitsbergen, *J. Geophys. Res.*, 111, D18210, doi:10.1029/2005JD006967.

McGee, T. J., Whiteman, D., Ferrare, R., Butler, J. J., and Burris, J. F.(1991), STROZ LITE: Stratospheric ozone lidar experiment, *Opt. Eng.,* 30, 31–39.

McGee, T. J., Gross, M. R., Ferrare, R., Heaps, W., and Singh, U. N. (1993), Raman DIAL measurements of stratospheric ozone in the presence of volcanic aerosols, *Geophys. Res. Lett.,* 20, 955–958.

McGee, T., Newman, P., Gross, M., Singh, U., Godin, S., Lacoste, S., and Megie, G. (1994), Correlation of ozone loss with the presence of volcanic aerosols, *Geophys. Res. Lett.,* 21, 2 801– 2 801.

McGee, T. J., Ferrare, R. A., Whiteman, D. N., Butler, J. J., Burris, J. F., and Owens, M. A. (1995a), Lidar measurements of stratospheric ozone during the STOIC campaign, *J. Geophys. Res*., 100, 9255–9262.

McGee, T. J., Gross, M. T., Singh, U. N., Butler, J. J., and Kimvilakani, P. E. (1995b), Improved stratospheric ozone lidar, *Opt. Eng.,* 34, 1421–1430.

McPeters, R. D., G. J. Labow, and B. J. Johnson (1997), A satellite-derived ozone climatology for balloonsonde estimation of total column ozone, *J. Geophys. Res.*, *102*(D7), 8875–8886, doi:96JD02977.

McPeters R. D., G. J. Labow, J. A. Logan (2007), Ozone climatological profiles for satellite retrieval algorithms, *J. Geophys. Res.,* 112, D05308, doi:10.1029/2005JD006823.

Meilinger, S. K., T. Koop, B. P. Luo, T. Huthwelker, K. S. Carslaw, U. Krieger, P. J. Crutzen, T. Peter (1995), Size-dependent stratospheric droplet composition in lee wave temperature fluctuations and their potential role in PSC freezing, *Geophys. Res. Lett*., 22(22), 3031–3034, 10.1029/95GL03056.

Milton, J. S., and J. Arnold (1995), *Introduction to probability and statistics*, 3 ed., McGraw Hill, New York.

Mitev, V., R. Matthey, I. Grigorov, R. Kivi, E. Kyrö, M. Morandi, F. Castagnoli, M. DelGuasta, B. Stein, C. Wedekind, V. Rizi, P. Agostini (1999), Rayleigh backscatter lidar measurement of stratospheric temperature above Sodankyla - Finland, In: 5th Europ. Workshop on Polar Strat. Ozone, European Commission.

Morris, G.A., et al. (1995), Trajectory mapping and applications to data from Upper Atmosphere Research Satellite, *J. Geophys. Res.,* 100, 16491–16505.

Müller, M., B. Stein, C. Wedekind, H. Wille, L. Wöste, R. Kivi, E. Kyrö, V. Rizi, G. Redaelli, V. Mitev, and R. Matthey (1998), Case study on Lidar observed Ice PSC over Northern Finland. In Proceedings: European Workshop on Mesoscale Processes in the Stratosphere, Bad Tölz, Germany, 8–11 November.

Müller, M., R. Neuber, G. Beyerle, E. Kyrö, R. Kivi, L. Wöste (2001), Non-uniform PSC occurrence within the Arctic polar vortex, *Geophys. Res. Lett.,* 28(22), 4175–4178, 10.1029/2001GL013799.

Murphy, D. M., and T. Koop (2005), Review of the vapour pressures of ice and supercooled water for atmospheric applications, *Q. J. R. Met. Soc.*, *131*, 1539–1565.

Nedoluha, G. E., R. M. Bevilacqua, and K. W. Hoppel (2002), POAM III measurements of dehydration in the antarctic and comparison with the arctic, *J. Geophys. Res.*, *107*, doi:10.1029/2001JD001184.

Neter, J., M. H. Kutner, C. J. Nachtsheim, and W. Wasserman (1996), *Applied Linear Statistical models*, 4 ed., McGraw Hill.

Newman, P. A., and E. R. Nash (2000), Quantifying the wave driving of the stratosphere, *105,* 12,485–12,497.

Newman, P. A., E. R. Nash, S. R. Kawa, S. A. Montzka, and S. M. Schauffler (2006), When will the Antarctic ozone hole recover?, *Geophys. Res. Lett.*, *33*, L12814, doi:10.1029/2005GL025232.

Oltmans, S. (1981), Surface ozone measurements in clean air, *J. Geophys. Res.*, *86*, 1174–1180.

Oltmans, S. J. (1985), Measurements of water vapour in the stratosphere with a frost point hygrometer, in *Proc. 1985 International Symposium on Moisture and Humidity*, pp. 251–258, Instrument Society of America, Washington, D. C.

Oltmans, S. J., et al. (1998), Trends of ozone in the troposphere, *Geophys. Res. Lett.*, *25*(2), 139–142, doi:10.1029/97GL03505.

Peter, T. (1997), Microphysics and heterogeneous chemistry of polar stratospheric clouds. *Annu. Rev. Phys. Chem.*, *48,* 785–822.

Randel, W. J., and F. Wu (1999), Cooling of the Arctic and Antarctic polar stratospheres due to ozone depletion, *Journal of Climate*, *12*, 1467–1479.

Randel, W. J., F. Wu, and R. Stolarski (2002), Changes in column ozone correlated with the stratospheric ep flux, *J. Meteorol. Soc. Japan*, *80*(4B), 849–862.

Rao, T. N., S. Kirkwood, J. Arvelius, P. von der Gathen, and R. Kivi (2003), Climatology of UTLS ozone and the ratio of ozone and potential vorticity over northern Europe, *J. Geophys. Res.*, *108* (D22), 4703, doi:10.1029/2003JD003860.

Reid, S., A. Tuck, and G. Kiladis (2000), On the changing abundance of ozone minima at northern midlatitudes, *J. Geophys. Res.*, *105*, 12,169–12,180.

Rex, M., et al. (1997), Prolonged stratospheric ozone loss in the 1995–96 arctic winter, *Nature*, *389*, 835–838.

Rex, M., R. J. Salawitch, P. von der Gathen, N. R. P. Harris, M. P. Chipperfield, and B. Naujokat (2004), Arctic ozone loss and climate change, *Geophys. Res. Lett.*, *31*, L04116, doi:10.1029/2003GL018844.

Rizi, V., Redaelli, R., Visconti, G., Wedekind, C., Stein, B., Wille, H., Mielke, B., Rairoux, P., Woste, L., Del Guasta M., Morandi, Castagnoli, F., Balestri, S., Stefanutti, L., Matthey, R., Mitev, Douard, M., Wolf, J.-P., Kyrö, E., Rummukainen, M., Kivi, R. (1999), Trajectory studies of PSC lidar observations at Sodankylä (Finland) during SESAME: comparison with box model results of particle evolution. *J. Atm. Chem*., Vol 32, 165–181.

Rosen, J. M., and N. T. Kjome (1991), Backscattersonde: A new instrument for atmospheric aerosol research, *Appl. Opt.*, *30*, 1552–1561.

Rosen, J. M., N. T. Kjome, N. Larsen, B. M. Knudsen, E. Kyrö, R. Kivi, J. Karhu, R. Neuber, I. Beninga (1997), Polar stratospheric cloud threshold temperatures in the 1995–1996 arctic vortex, *J. Geophys. Res*., 102(D23), 28195–28202, 10.1029/97JD02701.

Rummukainen, M., Laurila, T. and Kivi, R. (1996), Yearly Cycle of Lower Tropospheric Ozone North of the Arctic Circle, *Atm. Env*., vol 30, 1875–1885.

Schoeberl, M. R., L. R. Lait, P. A. Newman, and J. E. Rosenfeld (1992), The structure of polar vortex, *J. Geophys. Res.*, 97, 7859–7882.

Schoeberl, M.R., et al. (1993), The evolution of ClO and NO along air parcel trajectories, *Geophys. Res. Lett.,* 20, 2511–2514.

Schoeberl, M.R., et al. (1995), Trajectory modelling, *Proc. International School of Physics, Enrico Fermi, course CXVI, ed. G. Fiocco and G. Visconti*, North Holland, New York, 289–305.

Schreiner, J, C. Voigt, A. Kohlmann, F. Arnold, K. Mauersberger, N. Larsen, (1999), Chemical Analysis of Polar Stratospheric Cloud Particles, *Science*, 283, 5404, 968 – 970 , 10.1126/science.283.5404.968.

Science Pump Corporation (1996), *Operator's Manual Model 6A ECC Ozonesonde*, Camden, N. J.

Simmonds, P., R. Derwent, A. Manning, and G. Spain (2004), Significant growth in surface ozone at Mace Head, Ireland, 1987–2003, *Atmospheric Environment*, *38*, 4769–4778.

Smit, H. G. J., M. Helten, W. Sträter, and D. Kley (2000), JOSIE 1996–1999: Evaluation of the performance of ecc-sondes under quasi-flight conditions in the environmental simulation chamber, in *Quadrennial Ozone Symposium,* Sapporo*,* Japan, pp. 141–142.

Smit, H., and W. Sträter (2004), JOSIE-2000, Jülich Ozonesonde Intercomparison Experiment 2000, the 2000 WMO international intercomparison of operating procedures for ECC-ozonesondes at the environmental simulation facility at Jülich, *Tech. Rep. 1225*, World Meteorological Organization, Geneva.

Solomon, S. (1999), Stratospheric ozone depletion: A review of concepts and history, *Rev. Geophys.*, *37*, 275–316.

Solomon, S., R. W. Portman, R. R. Garcia, L. W. Thomason, L. R. Poole, and M. P. McCormack (1996), The role of aerosol variations in anthropogenic ozone depletion at northern midlatitudes, *J. Geophys. Res.*, *101*, 6713–6727, doi:10.1029/95JD03353.

Solomon, S. (1999), Stratospheric ozone depletion: a review of concepts and history, *Rev. Geophys. 37,* 275–316.

Sparling, L.C., et al. (1995), Trajectory modelling of emissions from lower stratospheric aircraft, *J. Geophys. Res.,* 100, 1427–1438.

Staehelin, J., N. Harris, C. Appenzeller, and J. Eberhard (2001), Ozone trends: A review, *Rev. Geophys.*, *39*, 231–290.

Stefanutti, L., L. Sokolov, A. R. MacKenzie, Th. Peter, V. Khattatov, and S. Balestri (1998), The M-55 Geophysica as a platform for the Airborne Polar Experiment, *J. Atmos. Ocean. Technol.,* 16, 1303–1312.

Stefanutti, L., A. R. MacKenzie, S. Balestri, V. Khattatov, G. Fiocco, E. Kyrö, T. Peter (1999), Airborne Polar Experiment-Polar Ozone, Leewaves, Chemistry, and Transport (APE-POLECAT): Rationale, road map and summary of measurements, *J. Geophys. Res.,* 104 (D19), 23941–23960, 10.1029/1998JD100078.

Stein, B., Wedekind, C., Wille, H., Immler, F., Müller, M., Wöste, L., del Guasta, M., Stefanutti, L., Antonelli, A., Agostini, P., Rizi, V., Redaelli, G., Mitev, V., Matthey, R., Kivi, R. and Kyrö, E. (1999), Optical classification, existence temperatures and coexistence of different PSC types, *J. Geophys. Res.*, 104, 23983–23993.

Steinbrecht, W., et al. (1996), NDSC intercomparison of stratospheric aerosol processing algorithms, *Selected Papers of the 18th Int. LASER RADAR conf., Berlin July 1996,* 501–504.

Steinbrecht, W., H. Claude, U. Köhler, and K. Hoinka (1998), Correlations between tropopause height and total ozone: Implications for long-term changes, *J. Geophys. Res.*, *103*, 19,183–19,192.

Suortti, T., Karhu, J., Kivi, R., Kyrö, E., Rosen, J., Kjome, N., Larsen, N., Neuber, R., Khattatov, V., Rudakov, V., Yushkov, V. and Nakane H. (2001), Evolution of the Artic stratospheric aerosol mixing ratio measured with balloon-borne aerosol backscatter sondes for years 1988–2000, *J. Geophys. Res.,* 106, 20759–20766.

Suortti, T. M., A. Kats, R. Kivi, N. Kämpfer, U. Leiterer, L. M. Miloshevich, R. Neuber, A. Paukkunen, P. Ruppert, H. Vömel, V. Yushkov (2007), Tropospheric comparisons of Vaisala radiosondes and balloon-borne chilled-mirror and Lyman-alpha hygrometers during LAUTLOS-WAVVAP experiment, *J. Atmos. Oceanic Technol*., accepted for publication.

Taalas, P., and E. Kyrö (1992), Two years of regular ozone soundings in the European Arctic, Sodankylä, *J. Geophys. Res.*, *97*, 8093–8098.

Tabazadeh, A., and O.B. Toon (1996), The presence of metastable HNO_3/H_2O solid phases in the stratosphere, *J. Geophys. Res.,* 101, 9071–9078.

Tabazadeh, A., Toon O.B., and Hamill P. (1995), Freezing behaviour of stratospheric sulfate aerosols inferred from trajectory studies, *Geophys. Res. Lett.,* 22 1725–1728.

Tabazadeh, A., Toon, O.B., Gary B. L., Bacmeister J. T., and Schoeberl M. R. (1996), Observational constraitns on the formation of Type Ia polar stratospheric clouds, *Geophys. Res. Lett.,* 23, 2109–2112.

Tarasick, D. W., J. B. Kerr, D. I. Wardle, J. Bellefleur, and J. Davies (1995), Tropospheric ozone trends over Canada: 1980–1993, *Geophys. Res. Lett.*, *22*, 409–412.

Tarasick, D. W., V. E. Fioletov, D. I. Wardle, J. B. Kerr, and J. Davies (2005), Changes in the vertical distribution of ozone over Canada from ozonesondes: 1980–2001, *J. Geophys. Res.*, *110*, D02304, doi:10.1029/2004JD004643.

Thompson A. M., et al. (2003), Southern Hemisphere Additional Ozonesondes (SHADOZ) 1998–2000 tropical ozone climatology 1. Comparison with Total Ozone Mapping Spectrometer (TOMS) and ground-based measurements, *J. Geophys. Res.*, 108(D2), 8238, doi:10.1029/2001JD000967.

Thompson, D. W. J., and J. M. Wallace (1998), The Arctic Oscillation signature in the wintertime geopotential height and temperature fields, *Geophys. Res. Lett.*, *25*, 1297–1300.

Thompson, D. W. J., J. M. Wallace, and G. C. Hegerl (2000), Annular modes in the extratropical circulation. Part II: Trends, *J. Climate*, *13*, 1018–1038.

Tsias, A., Prenni A. J., Carslaw K. S., Onash T.P., Luo B. P., Tolbert M. A., Peter T. (1997), Freezing of polar stratospheric clouds in orographically induced strong warming events, *Geophys. Res. Lett.,* 24, 2303–2306.

Uppala, S. M., et al. (2004), The ERA-40 ECMWF re-analysis, *Quart. J. R. Meteorol. Soc.*, *131*, 2961–3012, doi:10.1256/qj.04.176.

Vaughan, G., and J. D. Price (1991), On the relation between total ozone and meteorology, *Quart. J. R. Meteorol. Soc.*, *117*, 1281–1298.

Vingarzan, R. (2004), A review of surface ozone background levels and trends, *Atmospheric Environment*, *38*, 3431–3442.

Vömel, H., S. J. Oltmans, D. J. Hofmann, T. Deshler, J. M. Rosen, The evolution of the dehydration in the Antarctic stratospheric vortex (1995), *J. Geophys. Res.,* 100(D7), 13919–13926, 10.1029/95JD01000.

Vömel, H., M. Rummukainen, R. Kivi, J. Karhu, T. Turunen, E. Kyrö, J. M. Rosen, N. T. Kjome, and S. Oltmans (1997), Dehydration and sedimentation of ice particles in the Arctic stratospheric vortex, *Geophys. Res. Lett.*, *24,* 795–798.

Vömel, H., V. Yushkov, S. Khaykin, L. Korshunov, E. Kyro and R. Kivi (2007a), Intercomparisons of stratospheric water vapour sensors: FLASH-B and NOAA/CMDL frost point hygrometer, *J. Atmos. Oceanic Technol*., in press.

Vömel, H., H. Selkirk, L. Miloshevich, J. Valverde-Canossa, J. Valdés, E. Kyrö, R.Kivi, W. Stolz, G. Peng, J. A. Diaz, (2007b), Radiation Dry Bias of the Vaisala RS92 Humidity Sensor, *J. Atmos. Oceanic Technol*., in press.

Vömel, H., D. E. David, and K. Smith (2007c), Accuracy of tropospheric and stratospheric water vapor measurements by the cryogenic frost point hygrometer: Instrumental details and observations, *J. Geophys. Res.,* 112, D08305, doi:10.1029/2006JD007224.

Von der Gathen, P., et al. (1995), Observational evidence for chemical ozone depletion over the Arctic in winter 1991–92, *Nature*, *3752*, 131–134.

Wang, Y., D. Jacob, and J. Logan (1998), Global simulation of tropospheric O_3-NO_x-hydrocarbon chemistry, 3. Origin of tropospheric ozone and effects on non-methane hydrocarbons, *J. Geophys. Res.*, *103*(10), 757–768.

Weber, M., S. Dhomse, F. Wittrock, A. Richter, B.-M. Sinnhuber, and J. P. Burrows (2003), Dynamical control of NH and SH winter/spring total ozone from GOME observations in 1995–2002, *Geophys. Res. Lett.*, *30*(11), 1583, doi:10.1029/2002GL016799.

Weber, M., L. N. Lamsal, M. Coldewey-Egbers, K. Bramstedt, and J. P. Burrows (2005), Pole-to-pole validation of GOME WFDOAS total ozone with ground-based data, *Atmos. Chem. Phys.*, *5*, 1341–1355.

Weiss, A., J. Staehelin, C. Appenzeller, and N. R. P. Harris (2001), Chemical and dynamical contributions to ozone profile trends of the Payerne (Switzerland) balloon soundings, *J. Geophys. Res.*, *106*, 22685–22694, doi:10.1029/2000JD000106.

Wirth, M., A. Tsias, A. Dörnbrack, V. Weiß, K. S. Carslaw, M. Leutbecher, W. Renger, H. Volkert, T. Peter (1999), Model-guided Lagrangian observation and simulation of mountain polar stratospheric clouds, *J. Geophys. Res.,* 104(D19), 23971–23982, 10.1029/1998JD900095.

World Meteorological Organisation (WMO) (1957), *Definition of the thermal tropopause, Bull. Vol. 6*, World Meteorological Organization, Geneva, Switzerland.

World Meteorological Organisation (WMO) (1995), Scientific assessment of ozone depletion: 1994. World Meteorological Organization, Global ozone Research and Monitoring Project, *report No. 37*, World Meteorological Organization, Geneva.

World Meteorological Organisation (WMO) (1999), Scientific Assessment of Ozone depletion: 1998, Rep. no. 44, Global Ozone Research and Monitoring Project, Geneva.

World Meteorological Organisation (WMO) (2003), *Scientific assessment of ozone depletion: 2002*, Rep. 47, Global Ozone Research and Monitoring Project, Geneva, Switzerland.

World Meteorological Organisation (WMO) (2007), *Scientific assessment of ozone depletion: 2006*, Global Ozone Research and Monitoring Project, Geneva, Switzerland.

Wohltmann, I., M. Rex, D. Brunner, and J. Mäder (2005), Integrated equivalent latitude as a proxy for dynamical changes in ozone column, *Geophys. Res. Lett.*, *32*, L09811, 10.1029/2005GL022497.

Wohltmann, I., R. Lehmann, M. Rex, D. Brunner, and J. Mäder (2007), A process-oriented regression model for column ozone, *J. Geophys. Res.,* in press.

Zanis P., E. Maillard, J. Staehelin, C. Zerefos, E. Kosmidis, K. Tourpali, I. Wohltmann (2006), On the turnaround of stratospheric ozone trends deduced from the re-evaluated Umkehr record of Arosa, Switzerland, *J. Geophys. Res.,* 111, D22307, doi:10.1029/2005JD006886.

Zhang, R., P. J.Wooldridge and M. J. Molina (1993), Vapour pressure measurements for the $H_2SO_4/H_2O/HNO_3$ and $H_2SO_4/H_2O/HCl$ systems: incorporation of stratospheric acids into background sulfate aerosols, *J. Phys. Chem*., 97 8541–8548.

Zhao, J., R. P. Turco, O. B. Toon (1995), A model simulation of Pinatubo volcanic aerosols in the stratosphere, *J. Geophys. Res.,* 100(D4), 7315–7328, 10.1029/94JD03325, 1995.

Zängl, G. and K. P. Hoinka (2001), The tropopause in the polar regions, *Journal of Climate*, 14, 3117–3139.

8. ABSTRACT

Stratospheric ozone depletion has been one of the major issues of atmospheric research since the discovery of the Antarctic ozone hole. In the first place, long-term changes in ozone profiles are important to the Earth UV shield, and secondly they are of considerable climatic interest too. The latter is because ozone is also a greenhouse gas whose radiative forcing is depending on its vertical distribution. A decrease in stratospheric ozone leads to a cooling tendency, while an increase in tropospheric ozone leads to net positive radiative forcing. Tropospheric ozone also affects climate change indirectly, depending on the concentrations of nitrogen oxides, as it controls the oxidation capacity of the troposphere. Despite its importance, there are only a few regular measurement programs of ozone profiles in northern high latitudes that have sufficient length and measurement frequency for long-term data studies. One of the two existing long-term continuous measurement programs in the European sector of the Arctic is run at Sodankyä, Finland (67.4° N, 26.6° E).

The first part of the thesis is a study of the interannual and longer-term variations in ozone profiles over the Arctic from 1989 to 2003, using ozonesonde observations from seven northern high-latitude stations. The new datasets included here are those from the European sector of the Arctic. This part of the thesis is structured as follows: first the factors affecting ozone variability are discussed, and then the datasets are described; the next section gives an extensive summary of ozonesonde tests made during the thesis work, and intercomparisons with other instruments (ground-based, airborne and satellite-borne instruments). Finally, a statistical analysis of the ozonesonde data is presented based on the current knowledge of the factors affecting the ozone profiles in the Arctic. The second part of the thesis is closely related to the ozone analysis. Here in situ profile measurements of polar stratospheric clouds and water vapour are analysed, the main focus being on the observations of stratospheric ice clouds in the Arctic. These unique data were obtained by the author during the Arctic field campaigns in the years 1994–2006.

The ozonesonde data were homogenized using the results of a series of dual and multiple ozonesonde flights performed at Sodankylä to characterize the influence of the concentration of the sensing solution used in ECC sondes. These sonde flights at Sodankylä show that the use of a 1% KI sensing solution leads to a 2–8% difference, depending on the altitude, between ozone retrievals by the EN-SCI and SPC types of ECC ozonesondes. At the same time, a 0.5% KI solution in the case of the EN-SCI sondes yields on average a better than 2% agreement with the SPC sondes. Another field experiment carried out at Sodankylä focused on the influence of thermistor positioning. The differences observed during the test flights were used in the present study to remove inhomogeneites related to changes in thermistor positioning. This correction was found to be about 3% in the stratosphere above 150 hPa and between 1 and

3% below the 150 hPa level, decreasing linearly with decreasing altitude in the troposphere. During the Sodankylä Total Ozone Intercomparison and Validation Campaign, 33 ozonesondes were flown in the time-period of March 22- April 14, 2006 timed to coincide with the AURA satellite overpasses and Brewer direct sun measurements. The sondes reached an average altitude of 6 hPa, which allowed reliable total column estimation. The total ozone from the sondes was compared to the total ozone measurements based on five Brewer spectrophotometers operated at Sodankylä and the Ozone Monitoring Instrument (OMI) on board AURA satellite. In addition, direct comparison with an ozone lidar was carried out. It was found that the use of a 0.5% KI sensing solution for the EN-SCI sondes led on average to –0.8 ± 1.5% differences compared to the best ozone estimate from the Brewer spectrophotometers. A similar difference of 1.0 ± 2.0% was found using the OMI measurements. The total ozone derived from sondes depends on the method used to estimate the residual ozone. Climatological methods based on satellite climatologies or sonde climatology introduce a small negative bias of the order of 2–4% during anomalous time-periods such as March-April 2006. On average, for 15 years (1989–2003) of March–April data there is excellent agreement between the Brewer and sonde observations, if one applies local sonde climatology between 30 and 10 hPa supplemented by a climatological constant mixing ratio above 10 hPa to estimate the residual ozone. In addition to the ground-based and satellite-based comparisons, aircraft observations of stratospheric ozone were available during the winter of 1996/1997. Comparison with the aircraft observations showed a difference of 5.7 ± 2.8%, when observations inside the Arctic vortex were analyzed.

The quality-assessed and homogenized ozone measurements were analyzed with a statistical model. The statistical model study indicated that in both the stratosphere and troposphere the largest long-term changes have occurred in the late winter/spring period (January-April), the period of greatest interannual variability. For the time-period 1989–1996 there are significant negative trends in the stratosphere in January–April of –3.2 ± 1.0 %/year at altitudes between 150 and 40 hPa, with a smaller decrease in the 40–10 hPa layer of –1.9 ± 1.1 %/year. However, trends since then are positive: 4.9 ± 2.6 %/year between the tropopause and 150 hPa, 3.3 ± 2.0%/year for 150–40 hPa and 1.6 ± 1.2 %/year at higher levels (40–10 hPa). A model using four explanatory variables in the stratosphere (average tropopause height, the calculated volume of polar stratospheric clouds adjusted by the effective equivalent stratospheric chlorine (EESC), the 100 hPa eddy heat flux averaged over 45–70º N, and the mean aerosol backscatter in the 200–100 hPa range) was able to explain 65% – 95% of the observed variance, depending on the altitude, throughout the stratosphere in January-April. The proxies account for the changes in the synoptic-scale dynamical processes, the vortex ozone depletion, the ozone transport through residual circulation, and the Pinatubo aerosol effect, respectively. When the

seasonal ozone profiles were reconstructed using the proxy time series, the reconstructed profiles agreed to within 5% with the observed ones for the winter-spring period, except for the winters 1989 and 2003, when the dynamical variance over the period January–April was too large. The March ozone profiles for 1989 and 2003 were also reconstructed and showed much less disagreement between model and observed ozone anomalies. No a priori information about the expected altitude ranges of the explanatory variables was used in the fit, and it was therefore remarkable that the multilinear regression yields altitude distributions for the coefficients that are in reasonably good agreement with the dynamical and chemical considerations. Quantitatively, in the case of VPSC or the vortex ozone loss proxy, the ozone depletion potential obtained from the multilinear regression analysis is 2.2 DU/10^6 km^3, a value close to that reported by *Rex et al.* [2004]. The model suggests that, in the stratosphere, the observed negative trends prior to 1996–1997 can be attributed to the combined effect of chemical and dynamical changes, while the observed increase since then is primarily due to the dynamical influences in the model.

In the troposphere, positive trends are found in all seasons. The trend in Janury–April for 1989–2003 is 1.1 ± 0.2 %/year, while in May–August it is 0.7 ± 0.2 %/year and in September–December it is 0.6 ± 0.2 %/year. In the explanatory regression model the tropopause altitude term was replaced by the Arctic oscillation term, which provided the main contribution to the tropospheric ozone trends and interannual variability during January–April (65% of explained variability in the troposphere). A possible reason is that the Arctic Oscillation regulates the transport of ozone and its precursors from industrialized regions towards the pole. It may also modulate stratosphere-troposphere exchange. The model explains up to 70–80% of the variability in the troposphere in the winter/spring season, and the trends of the model residuals become insignificant throughout the troposphere. According to the ensemble dataset obtained from the Arctic ozone soundings over 1989–2003, the largest negative deviations of total ozone occurred in January–April 1996 and 1997. This differs from mid-latitudes, where largest negative deviations are found in 1993. Strong negative anomalies in total ozone were also observed in the recent winters of 2000, 2003 and 2005; rapid Arctic ozone losses are predicted to occur in the future, because significant concentrations of ozone-depleting substances will remain in the atmosphere for several decades, and global climate change may cool the stratosphere further. The results also suggest that a possible major volcanic eruption would have a strong impact on stratospheric ozone levels over the Arctic for at least 1–2 years after the eruption.

Within the PSC study, an analysis of synoptic-scale and mesoscale processes was made for each observed ice PSC event. It was found that, in general, the ice PSC observations during years of a weak and disturbed vortex were associated with the mesoscale effects, in the presence, however, of low temperatures on a synoptic-scale. Only in 1995/1996 were synoptic-scale temperatures over

Scandinavia sufficiently low to explain the observed particle layers. Apart from this particular case, there were similarities in the location of tropospheric pressure systems during observed ice PSC events: generally, low-pressure systems were located north of Scandinavia, causing strong westerly winds throughout the troposphere. In the wintertime stratosphere westerlies prevail, so that the directional wind shear is small between the stratosphere and the troposphere. These flow conditions favour the excitation and propagation of gravity waves with their source in the lower troposphere. Thus the cases considered show that ice PSCs above northern Finland occur mainly under meteorological conditions that are favourable for mountain-wave propagation up to stratospheric levels. The Scandinavian mountain range produces inertial gravity waves that lead to significant vertical displacements some hundreds of kilometres downstream. The case study from January 2005 shows that alternatively the source of the gravity wave observed over Scandinavia could have been the Greenland mountains.

PSC formation depends on the amount of available water vapour. At Sodankylä, the stratospheric water vapour sondes have been flown during each Arctic winter since 2002/2003. The results presented were grouped according whether the measurements were inside or outside the vortex, showing clear differences. The outside-vortex measurements represent the typical mid-latitude water vapour mixing ratio distribution, with values typically between 4–5 ppmv in the lower stratosphere. The inside-vortex water vapour mixing ratio, according to these measurements, is between 5 and 7 ppmv. One of the important questions is whether or not stratospheric water vapour is increasing, as is seen from mid-latitude measurements. If such a trend exists in the polar stratosphere, it would mean further cooling of the lower stratosphere and a larger potential for the formation of polar stratospheric clouds. All this would lead to a delay in the recovery of polar stratospheric ozone levels.

9. SUMMARY IN ESTONIAN

Osooni, polaarsete stratosfääripilvede ja veeauru vertikaalse jaotuse uurimine Arktikas

Antud töö eesmärgiks on osoonimuutuste uurimine arktilises piirkonnas. Kuna osoonivälju mõjutavad polaarsed stratosfääripilved ja veeauru jaotus stratosfääris, on lisatud ka vastavate mõõtmiste tulemused. Suur osa vaatlustulemustest on saadud Soomes Sodankyläs aastatel 1994–2006. Autor on osalenud kõigis Sodankyläs tehtud mõõtmistes nimetatud aastatel. Lisaks on osooniväljade uurimisel kasutatud andmeid teistest arktilistest jaamadest. Osoonisondide mõõtmiste aegridade uurimine pakub esmakordselt võimaluse selgitada osooniprofiili pikaajalisi muutusi arktilises troposfääris ja stratosfääris. Varem on seda tüüpi uuringuid tehtud Kanada jaamade andmetel, siin on esimest korda kaasatud andmed Euroopa sektorist. Osoonisondide andmestiku kasutamine eeldab instrumentide ja nende ettevalmistamise põhjalikku tundmist, kuna igas mõõtmises kasutatakse erinevat andurit. Kasutatavate instrumentide omaduste selgitamiseks on autor Sodankyläs teinud rea võrdlusvaatlusi ja samuti osalenud rahvusvahelistel välimõõtmistel. Tulemuseks on osoonisondide homogeniseeritud aegrida, mida on siin kasutatud trendiuuringus.

Vaatlusridade homogeniseerimise eeesmärgil on antud töö valmimise käigus kõigepealt tehtud arvukalt kaht tüüpi elektrokeemilise osoonisondi (EN-SCI ja SPC) võrdlusvaatlusi. Atmosfääris tehtud testide tulemusena on autor leidnud, et varem kasutusele võetud 1%-line kaaliumjodiidi (KI) lahus põhjustab 2–8% erinevuse eri sonditüüpide vahel sõltuvalt kõrgusest atmosfääris. Samal ajal annab EN-SCI andurite puhul suhteliselt parima tulemuse 0.5%-lise KI lahuse kasutamine. Samuti on autor uurinud teisi osooniandureid mõjutavaid tegureid, näiteks temperatuuri mõõtmist osoonipumbas, ja tuletanud empiirilised valemid nende tegurite arvestamiseks aegridade homogeniseerimise eesmärgil. Väga hea võimaluse osooniandurite omaduste uurimiseks atmosfäärimõõtmiste tingimustes pakkusid 22.3.–14.4.2006 Sodankyläs toimunud osooniandurite võrdlusmõõtmised. Lidarmõõtmistega võrreldes oli kooskõla kõrgustel 15–30 km parem kui 3%, kõrgustel 30–35 km küündisid erinevused 7%-ni. Osooni koguhulga erinevus maapealsete Breweri spektromeetri mõõtmistega võrreldes oli $-0.8 \pm 1.5\%$ ja Ozone Monitoring Instrument (OMI) satelliidivaatlustega võrreldes $1.0 \pm 2.0\%$. Sondimõõtmistega saadud summaarse osooni hulk sõltub meetodist, kuidas hinnata nn. jääkosooni hulka ülalpool sondi lennulage. Enamtuntud klimatoloogilised meetodid põhjustasid antud juhul 2–4% kõrvalekalde. 15 aasta märtsi-aprilli andmete analüüsi põhjal saab erinevatest meetoditest keskmiselt parima tulemuse mitmete aastate ulatuses, kui kasutada regionaalset klimatoloogiat 30 ja 10 hPa vahemikus ja konstantset segusuhet 10 hPa kõrgemal. Lisaks aastal 2006 tehtud võrdlusvaatlustele on kasutatud ka strato-

sfääris M55 Geophysica-nimelise teadusuuringuteks kohandatud lennuki pardalt tehtud vaatlusi talvel 1996/1997. Viimased erinesid sondimõõtmistest keskmiselt –5.7 ± 2.8%, kui analüüsida stratosfääri tsirkumpolaarse pöörise sees tehtud vaatlusi.

Kontrollitud ja homogeniseeritud vaatlusridasid kasutati statistilise mudeli arvutustes. Tulemuste põhjal on suurimad muutused stratosfääris leidnud aset jaanuaris–aprillis. Rõhunivoode vahemikus 150–40 hPa esines aastatel 1989–1996 negatiivne trend –3.2 ± 1.0% aastas ja 40–10 hPa vahemikus –1.9 ± 1.1% aastas. Siiski pärast seda oli trend positiivne: 4.9 ± 2.6% aastas tropopausi ja 150 hPa vahel, 3.3 ± 2.0% aastas kõrgustel 150–40 hPa and 1.6 ± 1.2% aastas kõrgemal atmosfääris (40–10 hPa). Stratosfääri mudel andis võimaluse põhjendada 65–95% varieeruvusest sõltuvalt kõrgusest. Mudel sisaldas järgmisi faktoreid: keskmine tropopausi kõrgus, "effective equivalent stratospheric chlorine" (EESC) mõjutusi arvestav polaarsete stratosfääri pilvede ruumala, 100 hPa häiriv soojusvoog ("eddy heat flux") keskmistatud üle 45–70ºN, aerosooli põhjustatud keskmine tagasihajumine kõrgusel 200–100 hPa. Need tegurid kirjeldavad osooni muutuste seisukohalt olulisi protsesse atmosfääris, milleks on sünoptilise mastaabiga meteoroloogilised protsessid, tsirkumpolaarse pöörise sisene osooni hajumine, osooni transport atmosfääri tsirkulatsiooni kaudu ja Pinatubo vulkaanipurske mõjutused. Antud mudel andis võimaluse rekonstrueerida keskmisi sesoonseid osooniprofiile erinevatel aastatel, enamikel juhtudel oli rekonstrueeritud ja vaadeldud profiilide erinevus väiksem kui 5%. Märtsis oli mudeliga arvutatud integreeritud stratosfääriosooni kadu 2.2 DU/10^6 km^3. Osooni vähenemine stratosfääris kuni aastateni 1996/1997 on seletatav keemiliste ja dünaamiliste tegurite koosmõjuna, hilisem kasv seletub peaasjalikult dünaamiliste teguritega.

Troposfääris esines kõigil aastaaegadel osooni kasvutrend. Jaanurist aprillini oli trend 1.1 ± 0.2% aastas, maist augustini 0.76 ± 0.2% aastas, septembrist detsembrini 0.6 ± 0.2% aastas. Troposfääri regressioonimudelis oli valitud tropopausi kõrguse asemel arktilise ostsillatsiooni (AO). Viimane andis suurima panuse jaanuari–aprilli muutlikkusesse (65% kogu varieeruvusest). Võimalik põhjus on see, et AO reguleerib osooni ja tema prekursorite transporti industrialiseeritud piirkondadest polaaralade suunas ja mõjutab ka stratosfääri-troposfääri vahetusprotsesse. Antud troposfääri mudel selgitab 70–80% osooni varieeruvusest talvel/kevadel.

Suurimad summaarse osoonihulga vähenemised esinesid jaanuaris-aprillis aastatel 1996 ja 1997. See erineb keskmiste laiuskraadide andmetest, kus miinimum on registreeritud 1993. aastal varasema Pinatubo vulkaanipurske tulemusena. Suured negatiivsed arktilise osooni anomaaliad on esinenud ka aastatel 2000, 2003 ja 2005. Samuti võib selliseid kõrvalekaldeid oodata lähematel aastatel, kuna antropogeenseid osooni lagundavaid Cl ja Br ühendeid esineb stratosfääris ohtralt ka lähikümnenditel ja globaalne kliimamuutus võib põhjus-

tada stratosfääri jätkuvat jahtumist. Samuti näitavad mudelarvutused, et suurtel vulkaanipursetel on märgatav mõju arktilistele osooniväljadele.

Stratosfääri jahtumine võib põhjustada polaarsete stratosfääripilvede (PSC) sagedasemat esinemist. Nendel stratosfääri pilvedel (tuntud ka pärlmutterpilvede nime all) on tähtis roll osooni lagundamisel nn. heterogeensete protsesside kaudu. Pilvede moodustumine eeldab madalaid temperatuure ja samuti piisavat veeaurusisaldust. Pilvede optilisi omadusi on antud töös uuritud nn. tagasihajumissondi ja aerosoolilidari abil. Erilist tähelepanu on pühendatud meteorologilistele tingimustele, mis võimaldavad lokaalseid miinimumtemperatuure arktilises stratosfääris. Selliseid tingimusi on esinenud keskmiselt 1–3 korda talve jooksul ka nendel puhkudel, kui arktiline stratosfäär on olnud ebastabiilne kogu talve lõikes. Erinevate juhtumite põhjal on leitud, et stratosfääri jääpilvede moodustumine on tõenäoline, kui orograafilised lained põhjustavad stratosfääri lokaalset külmenemist. Orograafiliste lainete mõjutajaks võivad Põhja-Euroopas olla Skandinaavia mäed ja mõnel juhul isegi Gröönimaa. Lisaks temperatuurile mõjutab PSC moodustumist ka veeaurusisaldus. Stratosfääri veeaurusisalduse mõõtmine on keeruline väga väikeste veeaurukoguste tõttu. Antud töö käigus on autor osalenud uue veeaururõhu anduri väljatöötamisel. Eesmärgiks on regulaarsed mõõtmised mitmete aastate lõikes. Lisaks arktiliste protsesside uurimisele võimaldab see stratosfääri veeauru pikaajalise mõõtmisi. Kui ka Arktikas stratosfääri veeauru hulk kasvab nagu keskmistel laiuskraadidel tehtud vaatlused näitavad, toob see endaga pikemas perspektiivis kaasa polaarsete stratosfääripilvede sagedama esinemise ja aeglustab arktiliste osooniväljade olukorra paranemist.

10. ACKNOWLEDGEMENTS

I am very grateful to Prof. Esko Kyrö and Dr. Kalju Eerme for supervision, for scientific discussions and for their comments on the work presented in the thesis. I also wish to thank the staff of the Environmental Physics Institute at the University of Tartu for many years of cooperation, and for advice and practical help during my Ph.D. studies. I have received vital support especially from Prof. Rein Rõõm, Dr. Hanno Ohvril, Prof. Hannes Tammet, Dr. Piia Post and Aleksandra Linnas during my studies at the University.

I am also very grateful to my research colleagues at FMI, Juha Karhu, Timo Turunen, Kaisa Lakkala, Tuomo Suortti, Aleksei Karpechko and Pauli Heikkinen for providing a lot of support, ideas and practical help related to measurements and data analysis during the long period of work at the FMI. I also wish to thank Prof. Jouni Pulliainen, Osmo Aulamo and Timo Sukuvaara for their continuous support to my thesis work at the institute.

I wish to thank Dr. Andreas Dörnbrack at the DLR for our long-term cooperation, and many ideas, scientific discussions and advice related to stratospheric and tropospheric meteorology. I also wish to thank Dr. Holger Vömel at the University of Colorado for our long-term cooperation and for his continuous support for the frostpoint hygrometer measurements at Sodankylä. I am grateful to Prof. J. Rosen and N. Kjome at the University of Wyoming for more than 12 years of cooperation and for making the backscatter sonde program possible. Special thanks are due to Dr. C. Wedekind, Dr. B. Stein, H. Wille (FUB), Dr. M. Maturilli (FUB, now at AWI), Dr. V. Mitev, Dr. R. Matthey (Observatory of Neuchâtel), Dr. L Stefanutti, Dr. M. del Guasta (CNR-IROE), Dr. V. Rizi (University of L'Aquila) and Dr. B. Lazzarotto (EPFL/DGR) for their contribution to lidar activities at Sodankylä. Dr. Neil Harris at the University of Cambridge, Dr. Peter von der Gathen at AWI, Dr. Bryan Johnson, Dr. Samuel Oltmans at NOAA, Dr. Rene Stübi at the MeteoSwiss, Dr. Bojan Bojkov and Dr. Richard McPeters at NASA are gratefully acknowledged for the scientific discussions related to the ozonesondes.

I would like to thank M. Weber for providing the GOME data, P. Newman and L. Lait for providing the access to the EESC model, and B. Knudsen for helpful suggestions. I further thank the National Oceanic and Atmospheric Administration for providing the proxy data and the World Ozone and Ultraviolet Radiation Data Centre for providing part of the ozonesonde measurements used in the study. I am also very grateful to Robin King for his extensive work to improve the English in my thesis and for valuable comments on the content of the work presented here. Special thanks are due to Aive Maasalu for the layout and final corrections.

Finally, I would like to thank my family for the patience, encouragement and the support thay have shown for my work.

This work has been supported by the FMI, the University of Tartu, the EC DG Research through the CANDIDOZ (EVK2-CT-2001-00024), QUOBI (EVK2-CT-2001-00129) and SCOUT-O3 projects and by the Finnish Academy. The backscattersonde program was partially supported by the U. S. National Science Foundation under grant OPP-9423285.

11. CURRICULUM VITAE

RIGEL KIVI

Nationality:	Estonian
Date of birth:	October 24, 1961
Personal status:	Married, two children
Address:	Institute of Environmental Physics, University of Tartu, Ülikooli 18, 50090, Tartu
Phone:	(+372) 737 5550
Fax:	(+372) 737 5556
E-mail:	rigel.kivi@fmi.fi

Education

1970–1980	Tallinn Secondary School No. 21
1980–1985	University of Tartu, Faculty of Physics and Chemistry
1998–2006	University of Tartu, Institute of Environmental Physics

Employment

1985–1990	Tartu Observatory, Tõravere
1990–1994	FMI, meteorologist
1994–present	FMI, research scientist, senior research scientist, head of the research group in FMI-ARC

Scientific work

Main research topics: measurements of stratospheric and tropospheric ozone, polar stratospheric cloud and stratospheric water vapour profiles.

12. ELULUGU

RIGEL KIVI

Rahvus:	Eesti
Sünniaeg:	24.10.1961
Perekonnaseis:	abielus, kaks last
Aadress:	Keskkonnafüüsika instituut, Tartu Ülikool, Ülikooli 18, 50090, Tartu
Telefon:	(+372) 737 5550
Faks:	(+372) 737 5556
E-post:	rigel.kivi@fmi.fi

Hariduskäik

1970–1980	Tallinna 21. Keskkool
1980–1985	Tartu Ülikool, füüsika-keemiateaduskond, geofüüsika eriala
1998–2006	Tartu Ülikool, keskkonnafüüsika instituut, doktorantuur

Teenistuskäik

1985–1990	Tartu Observatoorium, Tõravere
1990–1994	FMI, meteoroloog
1994–tänaseni	FMI, teadur, vanemteadur, rühma juht

Teadustegevus

Peamised töösuunad: stratosfääri ja troposfääri osooni, polaarsete stratosfääri pilvede ja stratosfääri veeauru kõrgusjaotuse mõõtmised.

DISSERTATIONES GEOPHYSICALES UNIVERSITATIS TARTUENSIS

1. **Andres Kuusk.** The hot-spot effect in plant canopy reflectance. Tartu, 1991.
2. **Tiit Nilson.** Radiative transfer in non-homogeneous plant canopies. Tartu, 1991.
3. **Helgi Arst.** Atmosfääri ja mere kiirguskarakteristikud looduskeskkonna seisundi informaatoritena (vene keeles). Tartu, 1991.
4. **Juha Sarkkula.** Measuring and modelling water currents and quality as a part of decision making process for water pollution control. Tartu, 1992.
5. **Piia Post.** On the two radiatively effective cloud parameters. Tartu, 1993.
6. **Aadu Mirme.** Electric aerosol spectrometry. Tartu, 1994.
7. **Aare Luts.** Mathematical simulation of the evolutions of air ions. Tartu, 1995.
8. **Tiit Kutser.** Estimation of water quality in turbid inland and coastal waters by passive optical remote sensing. Tartu, 1997.
9. **Ülle Kikas.** Atmospheric aerosol in the Baltic region. Tartu, 1998.
10. **Tarmo Kõuts.** Processes of deep water renewal in the Baltic sea. Tartu, 1999.
11. **Anu Reinart.** Underwater light field characteristics in different types of Estonian and Finnish lakes. Tartu, 2000.
12. **Marko Kaasik.** Parameterisation of atmospheric boundary layer in the numerical model of air pollution transport. Tartu, 2000.
13. **Janek Laanearu.** Topographically constrained deep-water flows in channels. Tartu, 2001.
14. **Urmas Raudsepp.** Wind-driven circulation in the gulf of Riga. Tartu, 2001.
15. **Urmas Hõrrak.** Air ion mobility spectrum at a rural area. Tartu, 2001.
16. **Marko Vana.** Formation and evolution of atmospheric aerosol size spectrum by the occurrence of nucleation burst events in the atmospheric boundary layer; transport of the climatically active particulate air pollution. Tartu, 2002.
17. **Veljo Kimmel.** Analysis of methods of air quality assessment. Applications in Estonia. Tartu, 2002.
18. **Oleg Okulov.** Variability of atmospheric transparency and precipitable water in Estonia. Tartu, 2003.
19. **Aarne Männik.** Implementation and validation of the nonhydrostatic adiabatic core of the numerical weather prediction model hirlam. Tartu, 2003.
20. **Matti Mõttus.** Shortwave solar radiation field inside willow canopy. Tartu, 2004.
21. **Kalev Rannat.** Long weakly nonlinear waves in geophysical applications. Tartu, 2007.